

การเลือกขอลเวชันและพลวัตของไอออนลิเทียมในสารละลายผสมของน้ำและ  
แอมโมเนีย : การจำลองพลวัตเชิงโมเลกุลบนพื้นฐานของวิธีโอเนียม-เอ็กซ์เอล



นางสาวพิไลลักษณ์ กาบบาลี

วิทยานิพนธ์นี้เป็นส่วนหนึ่งของการศึกษาตามหลักสูตรปริญญาวิทยาศาสตรดุษฎีบัณฑิต  
สาขาวิชาเคมี  
มหาวิทยาลัยเทคโนโลยีสุรนารี  
ปีการศึกษา 2557

**PREFERENTIAL SOLVATION AND DYNAMICS OF Li<sup>+</sup>  
IN AQUEOUS AMMONIA SOLUTION: AN ONIOM-XS  
MD SIMULATIONS STUDY**

**Pilailuk Kabbalee**



**A Thesis Submitted in Partial Fulfillment of the Requirements for the  
Degree of Doctor of Philosophy in Chemistry  
Suranaree University of Technology  
Academic Year 2014**

**PREFERENTIAL SOLVATION AND DYNAMICS OF Li<sup>+</sup> IN  
AQUEOUS AMMONIA SOLUTION: AN ONIOM-XS MD  
SIMULATIONS STUDY**

Suranaree University of Technology has approved this thesis submitted in partial fulfillment of the requirements for the Degree of Doctor of Philosophy.

Thesis Examining Committee

---

(Assoc. Prof. Dr. Jatuporn Wittayakun)

Chairperson

---

(Assoc. Prof. Dr. Anan Tongraar)

Member (Thesis Advisor)

---

(Prof. Dr. Kritsana Sagarik)

Member

---

(Asst. Prof. Dr. Kunwadee Rangsiwatananon)

Member

---

(Assoc. Prof. Dr. Chinapong Kritayakornupong)

Member

---

(Prof. Dr. Sukit Limpijumnong)

Vice Rector for Academic Affairs  
and Innovation

---

(Assoc. Prof. Dr. Prapun Manyum)

Dean of Institute of Science

ฟีโลลักษณะ กาบบาลี : การเลือกซอลเวชันและพลวัตของไอออนลิเทียมในสารละลายผสม  
ของน้ำและแอมโมเนีย : การจำลองพลวัตเชิงโมเลกุลบนพื้นฐานของวิธีไอเนียม-เอ็กซ์เอส  
(PREFERENTIAL SOLVATION AND DYNAMICS OF  $\text{Li}^+$  IN AQUEOUS  
AMMONIA SOLUTION : AN ONIOM-XS MD SIMULATIONS STUDY)  
อาจารย์ที่ปรึกษา : รองศาสตราจารย์ ดร.อนันต์ ทองระอา, 111 หน้า.

เทคนิคการจำลองพลวัตเชิงโมเลกุล (MD) ที่ผสมผสานกลศาสตร์ควอนตัมและกลศาสตร์  
โมเลกุล (QM/MM) บนพื้นฐานของวิธีไอเนียม-เอ็กซ์เอส (เรียกชื่อโดยย่อว่า ONIOM-XS MD) ได้  
ถูกนำมาประยุกต์เพื่อศึกษาการเลือกซอลเวชันและพลวัตของไอออนลิเทียมในสารละลายผสม  
ของน้ำและแอมโมเนีย การศึกษานี้แบ่งออกเป็นสองส่วน ส่วนที่หนึ่ง การจำลอง ONIOM-XS MD  
จะถูกดำเนินการโดยใช้โปรโตคอล เช่นเดียวกับการจำลอง QM/MM MD แบบดั้งเดิม เมื่อทำการ  
เปรียบเทียบกับผลการศึกษาที่ได้จากการจำลอง QM/MM MD แบบดั้งเดิม (ซึ่งทำนายว่าซอลเวชัน  
ชั้นแรกและชั้นที่สองของไอออนลิเทียมจะประกอบด้วยโมเลกุลน้ำเท่านั้นโดยเกิดสารเชิงซ้อน  
 $\text{Li}^+[(\text{H}_2\text{O})_4][(\text{H}_2\text{O})_4]$ ) พบว่าการจำลอง ONIOM-XS MD ให้ผลการศึกษาที่แตกต่าง กล่าวคือ  
ชี้ให้เห็นว่าไอออนลิเทียมสามารถที่จะเหนี่ยวนำทั้งน้ำและแอมโมเนียเพื่อเกิดสารเชิงซ้อนในรูป  
ของ  $\text{Li}^+[(\text{H}_2\text{O})_3\text{NH}_3][(\text{H}_2\text{O})_{11}(\text{NH}_3)_3]$  โดยไอออนลิเทียมจะแสดงความสามารถในการสร้าง  
โครงสร้างที่ไม่แข็งแรงมากนักและซอลเวชันชั้นแรกจะมีความยืดหยุ่นโดยอาจเกิดสารเชิงซ้อน  
หลายแบบสลับไปมา อาทิ  $\text{Li}^+(\text{H}_2\text{O})_4$ ,  $\text{Li}^+(\text{H}_2\text{O})_3\text{NH}_3$  และ  $\text{Li}^+(\text{H}_2\text{O})_2(\text{NH}_3)_2$  นอกจากนี้ ยังพบว่า  
การเกิดซอลเวชันชั้นที่สองไม่ค่อยชัดเจน ซึ่งชี้ให้เห็นว่า ไอออนลิเทียมมีอิทธิพลกับลิแกนด์ในชั้นนี้  
ไม่มากนัก ผลการศึกษาที่แตกต่างกันนี้ ยืนยันให้เห็นถึงความสำคัญของการประยุกต์เทคนิคการ  
จำลอง ONIOM-XS MD สำหรับการศึกษาระบบนี้ ในส่วนที่สอง ได้ทำการจำลอง ONIOM-XS  
MD อีกชุดหนึ่งโดยมีการเปลี่ยนแปลงชนิดเบสิสเซตจากเดิมที่เป็นชนิด DZV มาเป็นชนิด DZP  
พบว่า ผลการศึกษาที่ได้ค่อนข้างคล้ายกัน ชี้ให้เห็นว่า ผลของการใช้เบสิสเซตชนิด DZP ที่รวม  
ฟังก์ชันโพลาไรซ์ไม่มีผลต่อการเลือกซอลเวชันและพลวัตของไอออนลิเทียมในสารละลายผสมของ  
น้ำและแอมโมเนีย นั่นคือ หากพิจารณาในเรื่องการประหยัดเวลาสำหรับการจำลอง ONIOM-XS  
MD การใช้เบสิสเซตชนิด DZV ก็น่าจะเพียงพอสำหรับการศึกษาระบบนี้

สาขาวิชาเคมี  
ปีการศึกษา 2557

ลายมือชื่อนักศึกษา \_\_\_\_\_  
ลายมือชื่ออาจารย์ที่ปรึกษา \_\_\_\_\_

PILAILUK KABBALEE : PREFERENTIAL SOLVATION AND  
DYNAMICS OF  $\text{Li}^+$  IN AQUEOUS AMMONIA SOLUTION : AN ONIOM-  
XS MD SIMULATIONS STUDY. THESIS ADVISOR : ASSOC. PROF.  
ANAN TONGRAAR, Ph.D. 111 PP.

#### LITHIUM ION/ QM/MM/ ONIOM-XS

A sophisticated quantum mechanics/molecular mechanics (QM/MM) molecular dynamics (MD) technique based on the ONIOM-XS method, called the ONIOM-XS MD, has been applied for studying the preferential solvation and dynamics of  $\text{Li}^+$  in aqueous ammonia solution. This work was divided into 2 parts. In part I, an ONIOM-XS MD simulation was performed with the same simulation protocol as employed in a recent conventional QM/MM MD study. As compared to the conventional QM/MM MD results, which predicted that the first and second solvation shells of  $\text{Li}^+$  consist exclusively of water molecules with the arrangement of the  $\text{Li}^+[(\text{H}_2\text{O})_4][(\text{H}_2\text{O})_4]$  type, the ONIOM-XS MD simulation clearly indicate that this ion can order both water and ammonia molecules to form a favorable  $\text{Li}^+[(\text{H}_2\text{O})_3\text{NH}_3][(\text{H}_2\text{O})_{11}(\text{NH}_3)_3]$  configuration. Regarding the ONIOM-XS MD simulation, it was observed that the “structure-making” ability of  $\text{Li}^+$  is not too strong and that the first solvation shell of  $\text{Li}^+$  is somewhat flexible in that different 4-fold coordinated species, such as  $\text{Li}^+(\text{H}_2\text{O})_4$ ,  $\text{Li}^+(\text{H}_2\text{O})_3\text{NH}_3$  and  $\text{Li}^+(\text{H}_2\text{O})_2(\text{NH}_3)_2$ , could be converted back and forth. In addition, it was revealed that the second solvation shell of  $\text{Li}^+$  is less structured, indicating a small influence of  $\text{Li}^+$  in ordering the ligand molecules in this shell. These observed discrepancies clearly confirm the important

treatment of the ONIOM-XS MD technique in obtaining more detailed descriptions of such a condensed-phase system. In part II, another ONIOM-XS MD simulation has been performed in which a significant change is made by using a larger DZP basis set, *i.e.*, instead of the DZV basis set employed in part I. It was observed that the results obtained by the ONIOM-XS MD simulations using the DZV and DZP basis sets are rather similar. This implies that the effect of polarization function is marginal (negligible) for this particular system, *i.e.*, the DZV basis set is considered as a promising choice in situations where the computational facilities are very limited.



School of Chemistry

Student's Signature\_\_\_\_\_

Academic Year 2014

Advisor's Signature\_\_\_\_\_

## ACKNOWLEDGEMENTS

I wish to express my deep gratitude to all of people who gave me the possibility to complete this thesis. First of all, most of credits in this thesis should justifiably go to my advisor, Assoc. Prof. Dr. Anan Tongraar, for his guidance, valuable suggestions, kindness and encouragement throughout the course of my graduate. I would like to thank Prof. Dr. Kritsana Sagarik and all lecturers at School of Chemistry, Institute of Science, Suranaree University of Technology (SUT), for their encouragement and help. I would like to thank all committee members for their time and useful comments and suggestions. Furthermore, I am thankful to Prof. Dr. Jiali Gao for his kindness and sincere suggestions for my research work and life when I visited at the University of Minnesota, United States of America. I would also like to thank my colleagues in Professor Gao's group for their help, giving me the wonderful experiences.

I would like to acknowledge the financial support from the Thailand Research Fund (TRF) through the Royal Golden Jubilee (RGJ) Ph.D. program (Grant No. PHD/0156/2551), and Suranaree University of Technology (SUT).

Finally, I would like to express my deepest gratitude to my parents for their unconditional love, wonderful encouragement and all supports.

Pilailuk Kabbalee

# CONTENTS

	<b>Page</b>
ABSTRACT IN THAI.....	I
ABSTRACT IN ENGLISH .....	II
ACKNOWLEDGEMENTS.....	IV
CONTENTS.....	V
LIST OF TABLES .....	VIII
LIST OF FIGURES .....	IX
LIST OF ABBREVIATIONS.....	XII
<b>CHAPTER</b>	
<b>I INTRODUCTION.....</b>	<b>1</b>
1.1 Literature review .....	1
1.2 Research objectives.....	8
1.3 Scope and limitation of the study.....	9
1.4 References .....	10
<b>II QUANTUM CHEMISTRY.....</b>	<b>17</b>
2.1 Introduction to quantum chemistry .....	17
2.2 Schrödinger equation .....	17
2.3 Born-Oppenheimer approximation .....	20
2.4 Molecular orbital theory.....	22
2.5 The LCAO-MO method and basis set .....	24

## CONTENTS (Continued)

	<b>Page</b>
2.6 Basis set superposition error .....	29
2.7 The variation method .....	30
2.8 Hartree-Forck self-consistent field method.....	32
2.9 Electron correlation.....	37
2.10 Density functional theory.....	38
2.11 Many body perturbation theory.....	40
2.12 References.....	43
<b>III MOLECULAR DYNAMICS SIMULATIONS.....</b>	<b>46</b>
3.1 Introduction to computer simulation.....	46
3.2 Molecular dynamics (MD) simulation.....	48
3.3 Statistical mechanics.....	50
3.4 Intermolecular interactions.....	52
3.5 Effective potentials.....	53
3.6 Time integration algorithms.....	55
3.6.1 Verlet algorithm.....	55
3.6.2 Predictor-corrector algorithm.....	57
3.7 Periodic boundary conditions.....	59
3.8 Cut-off and potential at cut-off.....	61
3.9 Neighbor lists.....	62
3.10 Long-range interactions.....	63

## CONTENTS (Continued)

	<b>Page</b>
3.11 Temperature scaling.....	64
3.12 Conventional <i>ab initio</i> QM/MM MD technique.....	65
3.13 ONIOM-XS MD technique.....	67
3.14 Simulation details.....	70
3.15 References.....	73
<b>IV RESULTS AND DISCUSSION.....</b>	<b>75</b>
4.1 Preferential solvation and dynamics of Li <sup>+</sup> in aqueous ammonia solution: New insights through an ONIOM-XS MD simulation (Part I).....	76
4.2 The effect of polarization function on the preferential solvation and dynamics of Li <sup>+</sup> in aqueous ammonia solution (Part II) .....	90
4.3 References.....	95
<b>V CONCLUSION.....</b>	<b>100</b>
<b>APPENDICES .....</b>	<b>102</b>
APPENDIX A THEORETICAL OBSERVATIONS.....	103
APPENDIX B LIST OF PRESENTATIONS.....	105
APPENDIX C PUBLICATION .....	106
<b>CURRICULUM VITAE.....</b>	<b>111</b>

## LIST OF TABLES

Table	Page
4.1 Mean residence times (MRTs) of solvated ligands and of pure solvents, as obtained by the conventional QM/MM and ONIOM-XS MD simulations .....	89
4.2 Mean residence times (MRTs) of solvated ligands, as obtained by the ONIOM-XS MD simulations using the DZV and DZP basis sets .....	95
A.1 Comparison of some structural parameters for $\text{Li}^+$ solvation in aqueous ammonia solution.....	103
A.2 Optimized geometries and stabilization energies of $\text{Li}^+(\text{H}_2\text{O})_m(\text{NH}_3)_n$ complexes, where $m + n = 4$ , as obtained by various QM methods and basis sets .....	104

## LIST OF FIGURES

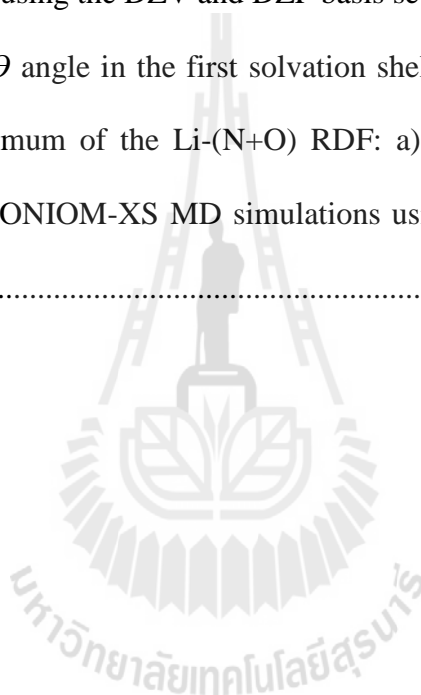
<b>Figure</b>	<b>Page</b>
2.1 The STO $\exp(-\alpha r)$ and GTO for 1s orbital $\exp(-\alpha r^2)$ .....	26
2.2 The STO-3G basis set representing the desired STO.....	27
3.1 Simulations as a bridge between (a) microscopic and macroscopic, and (b) theory and experiment. ....	47
3.2 The MD scheme .....	49
3.3 Schematic representation of the idea of periodic boundary conditions.....	60
3.4 Verlet neighbor list.....	62
3.5 System's partition.....	65
3.6 Schematic diagram of the ONIOM-XS MD technique.....	68
3.7 Stabilization energies of different $\text{Li}^+(\text{H}_2\text{O})_m(\text{NH}_3)_n$ complexes, where $m + n = 4$ , as obtained by various QM levels of accuracy using a) 6-311++G(d,p), b) DZP and c) DZV basis sets, respectively.. .....	71
3.8 Optimized Li-O distances of different $\text{Li}^+(\text{H}_2\text{O})_m(\text{NH}_3)_n$ complexes, where $m + n = 4$ , as obtained by various QM levels of accuracy using a) 6-311++G(d,p), b) DZP and c) DZV basis sets, respectively.. .....	72
3.9 Optimized Li-N distances of different $\text{Li}^+(\text{H}_2\text{O})_m(\text{NH}_3)_n$ complexes, where $m + n = 4$ , as obtained by various QM levels of accuracy using a) 6-311++G(d,p), b) DZP and c) DZV basis sets, respectively.. .....	73

## LIST OF FIGURES (Continued)

<b>Figure</b>	<b>Page</b>
4.1 a) Li-(N+O), b) Li-O and c) Li-N radial distribution functions and their corresponding integration numbers, as obtained by the conventional QM/MM and ONIOM-XS MD simulations.....	79
4.2 Coordination number distributions, calculated up to first minimum of the Li <sup>+</sup> -ligand RDFs: a) Li <sup>+</sup> -(H <sub>2</sub> O-NH <sub>3</sub> ), b) Li <sup>+</sup> -H <sub>2</sub> O and c) Li <sup>+</sup> -NH <sub>3</sub> .....	81
4.3 Distributions of a) O-Li-N, b) O-Li-O and c) N-Li-N angles, calculated up to first minimum of the Li-(N+O) RDF. ....	82
4.4 Distributions of $\theta$ angle in the first solvation shell of Li <sup>+</sup> , calculated up to the first minimum of the Li-(N+O) RDF: a) H <sub>2</sub> O and b) NH <sub>3</sub> .....	83
4.5 Time dependence of Li-O (top) and Li-N (down) distances, as obtained from the 40 ps of the ONIOM-XS MD simulation .....	85
4.6 Distributions of the number of first-shell ligands: a) H <sub>2</sub> O-NH <sub>3</sub> , b) H <sub>2</sub> O and c) NH <sub>3</sub> , calculated up to first minimum of the Li-(N+O) RDF.....	86
4.7 a) Li-(N+O), b) Li-O and c) Li-N radial distribution functions and their corresponding integration numbers, as obtained by the ONIOM-XS MD simulations using the DZV and DZP basis sets.....	91
4.8 Coordination number distributions, calculated up to first minimum of the Li <sup>+</sup> -ligand RDFs: a) Li <sup>+</sup> -(H <sub>2</sub> O+NH <sub>3</sub> ), b) Li <sup>+</sup> -(H <sub>2</sub> O) and c) Li <sup>+</sup> -(NH <sub>3</sub> ), as obtained by the ONIOM-XS MD simulations using the DZV and DZP basis sets.....	92

## LIST OF FIGURES (Continued)

<b>Figure</b>	<b>Page</b>
4.9 Distributions of a) O-Li-N, b) O-Li-O and N-Li-N angles, calculated up to first minimum of the Li-(N+O) RDFs, as obtained by the ONIOM-XS MD simulations using the DZV and DZP basis sets .....	93
4.10 Distribution of $\theta$ angle in the first solvation shell of $\text{Li}^+$ , calculated up to the first minimum of the Li-(N+O) RDF: a) $\text{H}_2\text{O}$ and b) $\text{NH}_3$ , as obtained by the ONIOM-XS MD simulations using the DZV and DZP basis sets .....	94



## LIST OF ABBREVIATIONS

ADF	=	Angular distribution function
au	=	Atomic unit
Aug-cc-pVDZ	=	Additional diffuse basis function and correlation consistent polarized valence double zeta
B3LYP	=	Becke three-parameter hybrid functional combined with Lee-Yang-Parr correlation function
BJH	=	Flexible water model developed by Bopp, Jancsó and Heinzinger
BLYP	=	Becke hybrid functional combined with Lee-Yang-Parr correlation function
BO	=	Born-Oppenheimer
BOMD	=	Born-Oppenheimer molecular dynamics
BSSE	=	Basis set superposition error
CC	=	Coupled cluster
CCSD	=	Coupled cluster calculations using both single and double substitutions from Hartree-Fock determinant
CF2	=	Central force model version 2
CN	=	Coordination number
CND	=	Coordination number distribution
CP-MD	=	Car-Parrinello molecular dynamics
CPU	=	Central processing unit

**LIST OF ABBREVIATIONS (Continued)**

$D$	=	Self-diffusion coefficient
DFT	=	Density functional theory
DZP	=	Double zeta polarization
DZV	=	Double zeta valence
$e$	=	Electron charge
$E_{tot}$	=	Total interaction energy
$E_{MM}$	=	Interactions within MM region
$E_{QM-MM}$	=	Interactions between QM and MM regions
ECP	=	Effective core potential
<i>etc</i>	=	et cetera
$F_i$	=	Force acting on each particle
$F_{MM}$	=	MM force
$F_{QM}$	=	QM force
fs	=	Femtosecond
FT-IR	=	Fourier transform infrared spectroscopy
GGA	=	Generalized gradient approximation
GTO	=	Gaussian-type orbital
$\hat{H}$	=	Hamiltonian operator
HB	=	Hydrogen bond
HF	=	Hartree-Fock

**LIST OF ABBREVIATIONS (Continued)**

IR	=	Infrared spectroscopy
kcal/mol	=	Kilocalorie per mole
$l$	=	Number of particles in the switching layer
LCAO-MO	=	Linear combination of atomic orbitals to molecular orbitals
$m$	=	Mass
MC	=	Monte Carlo
MD	=	Molecular dynamics
$m_e$	=	Mass of electron
$m_k$	=	Mass of nucleus
MO	=	Molecular orbital
MP2	=	Second-order Møller-Plesset
MRT	=	Mean residence times
$n_1$	=	Number of particle in the QM sphere
$n_2$	=	Number of particle in the MM region
ND	=	Neutron diffraction
$N_{ex}$	=	Number of exchange events
NMR	=	Nuclear magnetic resonance
NVE	=	Microcanonical ensemble
NVT	=	Canonical ensemble

**LIST OF ABBREVIATIONS (Continued)**

ONIOM	=	Own N-layered Integrated molecular Orbital and molecular Mechanics
ONIOM-XS	=	An extension of the ONIOM method for molecular simulation in condensed phase
ps	=	Picosecond
QCDF	=	Quasi-component distribution functions
QM/MM	=	Quantum mechanics/molecular mechanics
QMSTAT	=	Quantum mechanics/statistical mechanics
$r_0$	=	Distance characterizing the end of QM region
$r_1$	=	Distance characterizing the start of QM region
$r_{ab}$	=	Distance between particles $a$ and $b$
RDF	=	Radial distribution function
RHF	=	Restricted Hartree-Fock
$r_{max}$	=	First maximum of RDF peak
$r_{min}$	=	First minimum of RDF peak
SCF	=	Self-consistent field
$S_m(r)$	=	Smoothing function
SPC/E	=	Simple point charge effective pair water model
STO	=	Slater-type orbital
$t^*$	=	Time for observing the number of exchange ligand

## LIST OF ABBREVIATIONS (Continued)

TIP4P	=	Four-point transferable intermolecular potential
TIP5P	=	Five-point transferable intermolecular potential
$t_{\text{sim}}$	=	Simulation time
UHF	=	Unrestricted open-shell Hartree-Fock
V	=	Potential field
XAS	=	X-ray absorption spectroscopy
XD	=	X-ray diffraction
XES	=	X-ray emission spectroscopy
Z	=	Atomic number
$\mu$	=	Chemical potential
$\mu\text{VT}$	=	Grand canonical ensemble
$\Phi$	=	Trial function
$\Psi$	=	Wavefunction
$(\Psi_{QM}   \hat{H}   \Psi_{QM})$	=	Interaction within QM region
h	=	Planck's constant
$^{\circ}$	=	Degree
$\tau_{H_2O}$	=	MRT of water molecules
$\tau_{NH_3}$	=	MRT of ammonia molecules
$\chi(x)$	=	Spin orbital

**LIST OF ABBREVIATIONS (Continued)**

$\nabla^2$  = Laplacian operator



# CHAPTER I

## INTRODUCTION

### 1.1 Literature review

Characteristics of ions solvated in mixed solvents have been a topic of special interest for scientists since such detailed knowledge is essential for understanding the role of these ions in chemical and biological processes. (Vizoso and Rode, 1996; Sajeevkumar and Singh, 1996; Pranowo and Rode, 2001; Gutmann, 2008). Under the environment of multiple solvent species, the ability of ions to preferentially order the solvent components surrounding them, *i.e.*, to form their specific solvation complexes, depends on the strength of binding energy between the ions and the solvent molecules. Such phenomenon is usually discussed in terms of preferential solvation (Gill and Cheema, 1983; Tongraar and Rode, 2007). With regard to the principle of hard and soft acids and bases (*HSAB*) (Schwarzenbach and Baur 1956; Ahrland, Chatt and Davies, 1958; Beerbower and Jensen, 1983; Pearson, 1993, 1995; Komorowski, 1993), “hard acids” will prefer to coordinate to “hard bases” and “soft acids” will prefer to coordinate to “soft bases”. In this respect, “hard acids” refer to species with small size, high positive charge, strongly solvated and low electronegativity, while “hard bases” refer to those species with small size, strongly solvated, highly electronegativity and weakly polarizable. For example,  $\text{Li}^+$  and  $\text{Na}^+$  can be considered as “hard acids”, where the  $\text{Li}^+$  is harder than  $\text{Na}^+$ . Likewise,  $\text{H}_2\text{O}$  and  $\text{NH}_3$  can be classified as “hard bases”, where the  $\text{H}_2\text{O}$  is regarded as a harder one

when compared to  $\text{NH}_3$ . Consequently, when  $\text{Li}^+$  is dissolved in  $\text{H}_2\text{O-NH}_3$  mixture, it could be expected that  $\text{Li}^+$  should preferably bind to the harder  $\text{H}_2\text{O}$  over the softer  $\text{NH}_3$ .

Detailed knowledge with respect to preferential solvation phenomena can be obtained by both experiments, such as FT-Raman, infrared (IR) and visible spectroscopy, X-ray, neutron diffractions and NMR measurements (Qiao, Luan, Fang, Zhou, Yao, Wang, Li, Chen and Tian, 2008; Kamińska-Piotrowicz and Stangret, 1995, 1998; Petrov, Wiessner, Fiebig and Staerk, 1995; Qiao, Luan, Fang, Zhou, Yao, Wang, Li, Chen and Tian, 2008; Sajeevkumar and Singh, 1996), and theoretical investigations, in particular Monte Carlo (MC) and molecular dynamics (MD) simulations (Pranowo and Rode, 2001; Rode and Tanabe, 1988; Vizoso and Rode, 1996). In experiments, there is no single technique that can provide comprehensive results of systems under investigation. For example, it is known that the techniques of X-ray and neutron diffraction are only useful in providing structural details, while the IR and Raman techniques are instead employed in order to obtain dynamics information.

In conjunction with experiments, results from computer simulations can provide valuable complementary information not accessible to experimental approaches, both in the characterization of ion–solvent complexes and in the specific mechanism of the involved interactions. Especially for the detailed descriptions at molecular level, computer simulations can be seen as the elegant tools since it is known that experiments often lead to ambiguous results due to the limitations of their experimental techniques (Magina, Licheri, Pascgina and Piccaluga, 1988; Hewish, Neilson and Enderby, 1982; Howell and Neilson, 1996). In this respect, it should be

realized that a comparison between experiments and theories is not straightforward since most of the experimental methods for structural analysis have to be carried out with solutions of relatively high concentrations, while most of the computer simulations have been performed for very dilute solutions. By means of MC and MD simulations, system's interactions derived by means of *ab initio* quantum mechanical calculations are recognized as most suitable treatment for multiple molecular interactions. However, the performance of *ab initio* calculations for a condensed-phase system consisting of a large number of particles is too time-consuming. Thus, most of the previous MC and MD simulations on the preferential ion solvation had relied on classical molecular mechanical (MM) force fields (Pranowo and Rode, 2001; Rode and Tanabe, 1988; Vizoso and Rode, 1996). In this respect, the potential functions employed for describing inter- and intramolecular interactions of interacting atoms or molecules are constructed by fitting analytical formula to sets of experimental data or to *ab initio* energy surface calculations, most of which are based on pairwise additive approximations. During the past decades, a number of simulations based on pairwise additive approximations can yield reasonable results for the energetic data and the structural and dynamical properties of many molecular systems. However, the importance of non-additive contributions for a correct description of the intermolecular interactions has often been demonstrated (Beaumont, Chihara and Morrison, 1961; Ermakova, Solca, Huber and Marx, 1995; Clementi, Kistenmacher, Kołos and Romano, 1980; Curtiss, Woods, Halley, Hautman and Rahman, 1987; Lybrand and Kollman, 1985). In particular for strongly interacting systems, like ion-containing solutions, it has been demonstrated that the non-additive contributions always play a significant role and that the neglect of these terms results

in wrong geometrical arrangements and coordination numbers (Probst, Spohr, Heinzinger and Bopp, 1991; Ortega-Blake, Novaro, Les and Rybak, 1982; Lybrand and Kollman, 1985; Clementi, Kistenmacher, Kolos and Romano, 1980; Curtiss, Halley, Hautman and Rahman, 1987; Bernal-Uruchurtu and Ortega-Blake, 1995).

Nowadays, as a consequence of the rapid development in computer capacity and performance, more sophisticated and accurate simulation techniques incorporating quantum mechanical algorithms have become accessible. For example, a well-known Car–Parrinello MD (CP-MD) technique has been established for the study of condensed phase systems (Car and Parrinello, 1985; Tuckerman, Marx, Klein and Parrinello, 1997). By the CP-MD technique, all interactions in the system are described by means of *ab initio* calculations, most of which are relied on density functional theory (DFT). However, some limitations of the CP-MD technique come from the use of simple generalized gradient approximation (GGA) functionals, such as BLYP and PBE, and of the relatively small system size. For example, with regard to recent CP-MD simulations of liquid water, it has been demonstrated that some properties of the liquid water are quite sensitive to the density functionals chosen, *i.e.*, several of them were found to overestimate the water–water interactions (Vande Vondele, Mohamed, Krack, Hutter, Sprik and Parrinello, 2005; Yoo, Zeng and Xantheas, 2009). In this respect, some dynamics properties of water obtained from those CP-MD simulations, such as self-diffusion coefficients, showed significantly smaller value than that of experimental data, *i.e.*, implying that the liquid water simulated by the CP-MD technique under ambient condition is super-cooled or glassy (Lee and Tuckerman, 2007).

Besides the CP-MD technique, an alternative approach is to apply a so-called combined quantum mechanics/molecular mechanics (QM/MM) MD technique, which has been successfully applied for studying numerous condensed-phase systems (Kerdcharoen, Liedl and Rode, 1996; Tongraar, Liedl and Rode, 1997, 1998; Marini, Liedl and Rode, 1999; Kerdcharoen and Rode; 2000; Rode, Schwenk and Tongraar, 2004). This technique treats the active-site region, *i.e.* the solvation shell around the ion, quantum mechanically, while the environment consisting of further solvent molecules is described by MM potentials. By this scheme, the complicated many body contributions as well as the polarization effects, at least within the solvation sphere of the ion, can be reliably included.

With regard to the QM/MM MD technique, however, there are some unsolved problems that undermine the validity of this approach. For example, according to the conventional QM/MM MD scheme, a smoothing function is applied only for the exchanging particles that are crossing the QM/MM boundary. Such treatment is not realistic since an immediate exchange of particles between the QM and MM regions also affects the forces acting on the remaining QM particles. In addition, the conventional QM/MM framework cannot clearly define the energy expression during the solvent exchange process (Kerdcharoen and Morokuma, 2002; 2003). To solve these problems, a more sophisticated QM/MM MD technique based on ONIOM-XS method (which will be abbreviated throughout this work as “ONIOM-XS MD”) has been proposed (Kerdcharoen and Morokuma, 2002). The ONIOM method, originally developed by Morokuma *et al.* (Svensson, Humbel, Froese, Mutsubara, Sieber and Morokuma, 1996), can handle not only the QM + MM combinations (which is implemented in the conventional QM/MM scheme), but also the QM + QM

combinations. Recently, the ONIOM-XS MD technique has been successfully applied to the systems of  $\text{Li}^+$  and  $\text{Ca}^{2+}$  in liquid ammonia (Kerdcharoen and Morokuma, 2002, 2003),  $\text{K}^+$  and  $\text{Ca}^{2+}$  in aqueous solution (Wanprakhon, Tongraar and Kerdcharoen, 2011) as well as liquid water (Thaomola, Tongraar and Kerdcharoen, 2012). Especially for the cases of  $\text{K}^+$  and  $\text{Ca}^{2+}$  in aqueous solution, the ONIOM-XS MD simulations have provided more reliable data on the structure and dynamics of these two hydrated ions, *i.e.*, compared to the results obtained by the conventional QM/MM MD scheme (Wanprakhon, Tongraar and Kerdcharoen, 2011).

In the present study, the ONIOM-XS MD technique will be applied for studying the preferential solvation of  $\text{Li}^+$  in aqueous ammonia solution. Simple ion, like  $\text{Li}^+$ , is well-known for widespread and diverse effects, both in animals and plant (Birch and Phillips, 1991; Williams, Gershon and Shopsin, 1973). The characteristics of  $\text{Li}^+$  solvated in aqueous ammonia solution have been studied by means of classical MC (Kheawsrikul, Hannongbua, Kokpol and Rode, 1989) and MD (Tongraar and Rode, 1999) simulations using MM force fields, which revealed an octahedral arrangement for the first solvation shell of  $\text{Li}^+$  with different water to ammonia ratios of 4:2 and 3:3, respectively. With regard to the earlier MC and MD results, however, it has been demonstrated that the effects of many-body contributions, which are neglected in the construction of pair potentials, are significant and are not negligible, especially for the systems of strong ion-ligand interactions (Tongraar and Rode, 1999). Consequently, a more accurate Born-Oppenheimer *ab initio* QM/MM MD simulation (Tongraar and Rode, 1999) has been carried out for this system, showing that the average coordination number of  $\text{Li}^+$  is 4, consisting of 3 water and one ammonia ligands. The QM/MM MD results clearly demonstrated the failure of

pairwise additive approximations in describing such systems, *i.e.*, leading to wrong prediction for the coordination number and ligand composition of the solvated ion. According to the earlier QM/MM MD work, however, a relatively small QM region was employed, *i.e.*, corresponding to the size of first solvation shell of the ion. In this sense, the interactions of particles beyond the defined QM region (*i.e.*, those in the second solvation shell, which are described by means of pairwise additive approximations) may have a strong influence on the ligand preference and thus on the composition of the solvated ion. This leads to an important question whether the quality of pair potentials is sufficient to correctly describe the second solvation shell of  $\text{Li}^+$ . Later, an extended *ab initio* QM/MM MD simulation has been performed (Tongraar and Rode, 2008), in which the QM size was enlarged to 4.2 Å radius (*i.e.*, compared to the value of 3.4 Å employed in the earlier QM/MM MD study). Interestingly, the use of larger QM region had led to a clear water preference with an arrangement of  $\text{Li}^+[(\text{H}_2\text{O})_4][(\text{H}_2\text{O})_4]$  type, compared to the preferred  $\text{Li}^+[(\text{H}_2\text{O})_3\text{NH}_3][(\text{H}_2\text{O})_4(\text{NH}_3)_2]$  structure obtained by the previous QM/MM MD simulation using a small QM region not comprising the second solvation shell. These observed discrepancies clearly demonstrate the importance of QM treatment of the second shell of this solvated ion. Recently, CP-MD simulations have been performed for the system of  $\text{Li}^+$  in binary liquid mixture of water and ammonia (Pratihari and Chandra, 2011), revealing that  $\text{Li}^+$  is preferentially solvated by water and that the coordination number of  $\text{Li}^+$  is mostly four in its first solvation shell. A comparison of the structural parameters for  $\text{Li}^+$  in aqueous ammonia solutions, as obtained by various simulation techniques, is given in Table A.1.

Regarding the recent CP-MD and QM/MM MD simulations, which provided similar details (*i.e.*, the coordination number of 4 and the preference for water molecules as ligands) for the first solvation shell of  $\text{Li}^+$ , these two techniques, as mentioned earlier, still have their technical limitations. In particular, the observed preference for only water molecules as ligands in the first solvation shell of  $\text{Li}^+$  is questionable. In gas phase, HF calculations using DZP basis set show that the strength of ion-ammonia interactions is somewhat higher than that of ion-water interactions, *i.e.*, of the values of  $-41.25$  and  $-37.11$   $\text{kcal.mol}^{-1}$ , respectively. In this work, therefore, a more sophisticated ONIOM-XS MD technique will be applied for studying the preferential solvation of  $\text{Li}^+$  in aqueous ammonia solution. The results obtained by the ONIOM-XS MD simulations can be expected to provide more detailed descriptions on the preferential solvation and dynamics of the  $\text{Li}^+$  ion in such solvent mixture, leading to further understanding the role of this ion in chemical and biological processes.

## 1.2 Research objectives

1. To apply the high-level ONIOM-XS MD technique for studying the preferential solvation and dynamics of  $\text{Li}^+$  in aqueous ammonia solution. The results obtained by the ONIOM-XS MD simulation was compared to those derived by the conventional QM/MM and CP-MD frameworks.
2. To study the sensitivity of the basis sets (DZV and DZP) employed in the ONIOM-XS MD simulations of  $\text{Li}^+$  in aqueous ammonia solution.

### 1.3 Scope and limitation of the study

In this work, the investigations were divided into two parts. In the first part, an ONIOM-XS MD simulation was performed with the same simulation protocol as reported in the recent conventional QM/MM MD simulation using enlarged QM region (Tongraar and Rode, 2008). The objective was to compare the ONIOM-XS MD results with those obtained by the conventional QM/MM MD study. In this respect, the observed differences between the conventional QM/MM and ONIOM-XS MD simulations was compared and discussed with respect to the validity of the conventional QM/MM MD scheme for describing the properties of such system. For the second part of this work, another ONIOM-XS MD simulation, with the same simulation conditions as employed in part I, was performed. A significant change was made by using a larger DZP basis set, *i.e.*, instead of the DZV. The objective of this part was to investigate the effect of polarization function on the preferential solvation and dynamics of  $\text{Li}^+$  in aqueous ammonia solution.

Structural properties of the solvated  $\text{Li}^+$  will be characterized through a set of radial distribution functions (RDFs) and their running integration numbers, together with detailed analyses on angular distribution functions (ADFs) and orientations of water and ammonia molecules surrounding the ion. The dynamics details was analyzed by means of mean residence times (MRTs) of solvent molecule as well as of solvent exchange processes at the ion.

## 1.4 References

- Adams, D. J., Adams, E. M. and Hills, G. J. (1979). The computer simulation of polar liquids. **Molecular Physics**. 38: 387-400.
- Ahrland, S., Chatt, J. and Davies, N. R. (1958). The relative affinities of ligand atoms for acceptor molecules and ions. **Quarterly Reviews, Chemical Society**. 12: 265-276.
- Beaumont, R. H., Chihara, H. and Morrison, J. A. (1961). Thermodynamic properties of Krypton. Vibrational and other properties of solid Argon and solid Krypton. **Proceedings of the Physical Society**. 78: 1462.
- Beerbower, A. and Jensen, W. (1983). The HSAB principle and extended solubility theory. **Inorganica Chimica Acta**. 75: 193-197.
- Birch, N. J. and Phillips, J. D. (1991). Lithium and medicine: Inorganic pharmacology. **Academics Press**. 36: 49-68.
- Bernal-Uruchurtu, M. I. and Ortega-Blake, I. (1995). A refined Monte Carlo study of  $Mg^{2+}$  and  $Ca^{2+}$  hydration. **The Journal of Chemical Physics**. 103: 1588-1598.
- Car, R. and Parrinello, M. (1985). Unified approach for molecular dynamics and density-functional theory. **Physical Review Letters**. 55: 2471-2474.
- Clementi, E., Kistenmacher, H., Kolos, W. and Romano, S. (1980). Non-additivity in water-ion-water interactions. **Theoretica Chimica Acta**. 55: 257-266.
- Cook, J. L., Hunter, C. A., Low, C. M. R., Perez-Velasco, A. and Vinter, J. G. (2008). Preferential solvation and hydrogen bonding in mixed solvents. **Angewandte Chemie International Edition**. 47: 6275-6277.

- Curtiss, L. A., Woods Halley, J., Hautman, J. and Rahman, A. (1986). Nonadditivity of *ab initio* pair potentials for molecular dynamics of multivalent transition metal ions in water. **The Journal of Chemical Physics**. 86: 2319-2327.
- Ermakova, E., Solca, J., Huber, H. and Marx, D. (1995). Many-body and quantum effects in the radial distribution function of liquid neon and argon. **Chemical Physics Letters**. 246: 204-208.
- Gill, D. S. and Cheema, J. S. (1983). Preferential solvation of ions in mixed solvents. **Zeitschrift für Physikalische Chemie**. 134: 205-214.
- Gutmann, V. (1978). The Donor-acceptor approach to molecular interactions. **Plenum Press**: New York., USA. 91: 134-136.
- Hewish, N. A., Neilson, G. W. and Enderby, J. E. (1982). Environment of  $\text{Ca}^{2+}$  ions in aqueous solvent. **Nature**. 297: 138-139.
- Howell, I. and Neilson, G. W. (1996).  $\text{Li}^+$  hydration in concentrated aqueous solution. **Journal of Physics Condensed Matter**. 8: 4455-4463.
- Kamińska-Piotrowicz, E. and Stangret, J. (1995). Spectroscopy studies of preferential hydration of Co(II), Ni(II), Cu(II) and Zn(II) ions in acetonitrile-water mixtures. **Journal of Molecular Structure**. 344: 69-76.
- Kamińska-Piotrowicz, E. and Stangret, J. (1998). VIS spectroscopy studies of pseudooctahedral solvation complexes of cobalt(II) ion in mixed solvents. **Journal of Molecular Structure**. 440: 131-139.
- Kerdcharoen, T., Liedl, K. R. and Rode, B. M. (1996). A QM/MM simulation method applied to the solution of  $\text{Li}^+$  in liquid ammonia. **Chemical Physics**. 211: 313-323.

- Kerdcharoen, T. and Morokuma, K. (2002). ONIOM-XS: An extension of the ONIOM method for molecular simulation in condensed phase. **Chemical Physics Letters**. 355: 257-262.
- Kerdcharoen, T. and Morokuma, K. (2003). Combined quantum mechanics and molecular mechanics simulation of  $\text{Ca}^{2+}$  /ammonia solution based on the ONIOM-XS method: Octahedral coordination and implication to biology. **The Journal of Chemical Physics**. 118: 8856-8862.
- Kerdcharoen, T. and Rode, B. M. (2000). What is the solvation number of  $\text{Na}^+$  in ammonia? An *ab initio* QM/MM molecular dynamics study. **The Journal of Physical Chemistry A**. 104: 7073-7078.
- Kheawsrikul, S., Hannongbua, S. V., Kokpol, S. U. and Rode, B. M. (1989). A Monte Carlo study on preferential solvation of lithium (I) in aqueous ammonia. **Journal of the Chemical Society**. 85: 643-649.
- Komorowski, L. (1993). Structure and bonding. **Springer-Verlag**. Berlin-Heidelberg, Germany. 80: 45.
- Lee, H. S. and Tuckerman, M. E. (2007). Dynamical properties of liquid water from *ab initio* molecular dynamics performed in the complete basis set limit. **The Journal of Chemical Physics**. 126: 164501-164516.
- Lybrand, T. P. and Kollman, P. A. (1985). Water-water and water-ion potential functions including terms for many body effects. **The Journal of Chemical Physics**. 83: 2923-2933.
- Magini, M., Licheri, G., Paschina, G., Piccaluga, G. and Pinna, G. (1988). X-ray diffraction of ions in aqueous solutions: Hydration and complex formation. **CRC Press**, Boca- Raton, FL.

- Marini, G. W., Liedl, K. R. and Rode, B. M. (1999). Investigation of  $\text{Cu}^{2+}$  hydration and the Jahn–Teller effect in solution by QM/MM Monte Carlo simulations. **The Journal of Physical Chemistry A**. 103: 11387-11393.
- Ortega-Blake, I., Novaro, O., Les, A. and Rybak, S. (1982). A molecular orbital study of the hydration of ions. The role of nonadditive effects in the hydration shells around  $\text{Mg}^{2+}$  and  $\text{Ca}^{2+}$ . **The Journal of Chemical Physics**. 76: 5405-5413.
- Pearson, R. (1993). Chemical hardness: A historical introduction. **Springer-Verlag**. Berlin-Heidelberg, Germany. 80: 1-10.
- Pearson, R. G. (1995). The HSAB Principle more quantitative aspects. **Inorganica Chimica Acta**. 240: 93-98.
- Petrov, N. K., Wiessner, A., Fiebig, T. and Staerk, H. (1995). Study of preferential solvation in binary solvent mixtures by the spectro-streak picosecond technique. **Chemical Physics Letters**. 241: 127-132.
- Pranowo, H. D. and Rode, B. M. (2001). Preferential  $\text{Cu}^{2+}$  solvation in aqueous ammonia solution of various concentrations. **Chemical Physics**. 263: 1-6.
- Pratihari, S. and Chandra, A. (2011). A first principles molecular dynamics study of lithium atom solvation in binary liquid mixture of water and ammonia: Structural, electronic, and dynamical properties. **The Journal of Chemical Physics**. 134: 024519.
- Probst, M. M., Spohr, E., Heinzinger, K. and Bopp, P. (1991). A molecular dynamics simulation of an aqueous beryllium chloride solution. **Molecular Simulation**. 7: 43-57.
- Qiao, H., Luan, H., Fang, X., Zhou, Z., Yao, W., Wang, X., Li, J., Chen, C. and Tian, Y. (2008). FT-Raman spectroscopic and density functional theory studies on

- ion preferential solvation and ion association of lithium tetrafluoroborate in 4-methoxymethyl ethylene carbonate-based mixed solvents. **Journal of Molecular Structure.** 878: 185-191.
- Rode, B. M., Schwenk, C. F. and Tongraar, A. (2004). Structure and dynamics of hydrated ions - new insights through quantum mechanical simulations. **Journal of Molecular Liquids.** 110: 105-122.
- Rode, B. M. and Tanabe, Y. (1988). Simulation of preferential cation solvation in aqueous ammonia. **Journal of the Chemical Society.** 84: 1779-1788.
- Sajeevkumar, V. A. and Singh, S. (1996). Infrared spectral studies on preferential solvation of lithium ions in binary mixtures of acetonitrile and dimethyl formamide. **Journal of Molecular Structure.** 382: 101-110.
- Schwarzenbach, G. and Baur, R. (1956). Metallkomplexe mit Polyaminen XI: Mit cis- und trans-1,2-Diaminocyclohexan. **Helvetica Chimica Acta.** 39: 722-728.
- Stace, A. J. (1984). Preferential solvation of hydrogen ions in mixed water-amine ion clusters. **Journal of the American Chemical Society.** 106: 2306-2315.
- Thaomola, S., Tongraar, A. and Kerdcharoen, T. (2012). Insights into the structure and dynamics of liquid water: A comparative study of conventional QM/MM and ONIOM-XS MD simulations. **Journal of Molecular Liquids.** 174: 26-33.
- Tongraar, A., Liedl, K. R. and Rode, B. M. (1997). Solvation of  $\text{Ca}^{2+}$  in water studied by Born–Oppenheimer *ab initio* QM/MM dynamics. **The Journal of Physical Chemistry A.** 101: 6299-6309.
- Tongraar, A., Liedl, K. R. and Rode, B. M. (1998). Born–Oppenheimer *ab initio* QM/MM dynamics simulations of  $\text{Na}^+$  and  $\text{K}^+$  in water: From structure

- making to structure breaking effects. **The Journal of Physical Chemistry A.** 102: 10340-10347.
- Tongraar, A. and Rode, B. M. (1999). Preferential solvation of  $\text{Li}^+$  in 18.45 aqueous ammonia: A Born–Oppenheimer *ab initio* quantum mechanics/molecular mechanics MD simulation. **The Journal of Physical Chemistry A.** 103: 8524-8527.
- Tongraar, A. and Rode, B. M. (2007). Preferential solvation and dynamics of ions solvated in mixed solvents: Insights from QM/MM MD simulation approach. **American Institute of Physics.** 963:928-931.
- Tongraar, A. and Rode, B. M. (2008). The role of second shell quantum effects on the preferential solvation of  $\text{Li}^+$  in aqueous ammonia: An extended *ab initio* QM/MM MD simulation with enlarged QM region. **Chemical Physics Letters.** 466: 61-64.
- Tuckerman, M. E., Marx, D., Klein, M. L. and Parrinello, M. (1997). On the quantum nature of the shared proton in hydrogen bonds. **Science** 275: 817-820.
- Vande Vondele, J., Mohamed, F., Krack, M., Hutter, J., Sprik, M. and Parrinello, M. (2005). The influence of temperature and density functional models in *ab initio* molecular dynamics simulation of liquid water. **The Journal of Chemical Physics.** 122: 014515-014516.
- Vizoso, S. and Rode, B. M. (1996). Preferential solvation study: Solvation of sodium chloride in water-hydroxylamine mixtures. **Chemical Physics.** 213: 77-93.
- Wanprakhon, S., Tongraar, A. and Kerdcharoen, T. (2011). Hydration structure and dynamics of  $\text{K}^+$  and  $\text{Ca}^{2+}$  in aqueous solution: Comparison of conventional

QM/MM and ONIOM-XS MD simulations. **Chemical Physics Letters**. 517: 171-175.

William, R. J. P. (1971) Bio-inorganic Chemistry. **American Chemical Society**. 100: 1-41.

Yoo, S., Zeng, X. C. and Xantheas, S. S. (2009). On the phase diagram of water with density functional theory potentials: The melting temperature of ice  $I_h$  with the Perdew--Burke--Ernzerhof and Becke--Lee--Yang--Parr functionals. **The Journal of Chemical Physics**. 130: 221102-221104.



# CHAPTER II

## QUANTUM CHEMISTRY

### 2.1 Introduction to quantum chemistry

Quantum chemistry is based on quantum mechanical principles. The theory of quantum mechanics originated in the beginning of 20<sup>th</sup> century as a result of the failure of classical mechanics to correctly describe the black-body radiation or photoelectric effects and some unexplainable phenomena of very small particles, for example, electrons, atoms and molecules. In quantum chemistry, a fundamental behavior of matter at molecular scale can be described through the understanding of the electron behavior. In this respect, a wavefunction, which can be obtained by solving the *Schrödinger equation* (Schrödinger, 1926), is an essential tool of quantum chemistry for describing the properties of matter in terms of energies and positions of the nuclei and electrons. The applications of quantum chemistry include solving many chemical problems, particularly understanding of chemical bonding, spectral phenomena, molecular reactivity and various other fundamental chemical problems.

### 2.2 Schrödinger equation

In quantum chemistry, the complete description of a wavefunction can be given through the solution of the Schrödinger equation, which describing the atom system. Schrödinger obtained an equation by taking the classical time-independent

wavefunction equation and substituting *de Broglie's relation* for  $\lambda$ . The classical three-dimensional wave equation can be written as

$$\nabla^2\Psi = -\left(\frac{2\pi}{\lambda}\right)^2\Psi, \quad (2.1)$$

where  $\nabla$  is the Laplacian operator ( $\nabla \equiv \frac{\partial}{\partial x} + \frac{\partial}{\partial y} + \frac{\partial}{\partial z}$ ) and  $\Psi$  is the wave function describing the displacement at any point along the wave. Schrödinger substituted the *de Broglie* wavelength,  $\lambda$ , in terms of energy to adapt the classical wave equation to particle waves ( $\lambda = \frac{h}{\sqrt{2m(E-V)}}$ ). The Schrödinger equation is then given by

$$\nabla^2\Psi = -\left(\frac{8\pi^2m}{h^2}\right)(E-V)\Psi. \quad (2.2)$$

This equation can be rearranged in a series of algebraic step to a more convenient form of

$$\left[ \left(\frac{-h^2}{8\pi^2m}\right)\nabla^2 + V \right]\Psi = E\Psi, \quad (2.3)$$

which is known as *Schrödinger's time-independent* wave equation for a single particle of the mass ( $m$ ) moving in the three-dimensional potential field ( $V$ ). The left-hand side of the equation is called the *Hamiltonian operator* ( $\hat{H}$ ),

$$\hat{H} \equiv \left[ \left( \frac{-\hbar^2}{8\pi^2 m} \right) \nabla^2 + V \right], \quad (2.4)$$

which will be substituted in Schrödinger equation,

$$\hat{H}\Psi = E\Psi, \quad (2.5)$$

where  $\psi$  is then called an eigenfunction and  $E$  an eigenvalue.

The equation (2.5) can be further simplified since the *Born-Oppenheimer approximation* considers the nuclei wavefunction can be separated and the electron distribution depends only on the instantaneous positions of nuclei and not on their velocities. Therefore, an electronic Schrödinger equation can be obtained as

$$\hat{H}^{elec} \Psi^{elec} = E^{elec} \Psi^{elec}. \quad (2.6)$$

Hence, the Hamiltonian operator for an atom with  $k$  electrons can be written as

$$\hat{H}^{elec} = \underbrace{\left[ \left( \frac{-\hbar^2}{8\pi^2 m_e} \right) \sum_{i=1}^k \nabla_i^2 \right]}_{T_{\text{electron}}} - \underbrace{\sum_{i=1}^k \frac{Z}{r_i}}_{V_{\text{electron-nucleus}}} + \underbrace{\sum_{i=1}^{k-1} \sum_{j=i+1}^k \frac{1}{r_{ij}}}_{V_{\text{electron-electron}}}. \quad (2.7)$$

Within the Born-Oppenheimer approximation, the electronic Schrödinger equation can be solved at any given set of nuclei positions, thus  $T_{\text{nucleus}}$  is omitted. The Schrödinger equation for a multi-electron atom can be solved numerically. Although  $V_{\text{electron-electron}}$  cannot be included as an explicit term in the Hamiltonian, its effect on  $\Psi$  can be accounted by a mathematically simpler approach that each electron interacts with an average field of the nucleus and all other electrons (see self-consistent field

approximation in section 2.8). The Hamiltonian operator for a molecule with  $N$  atoms and  $k$  electrons is given by

$$\hat{H}^{elec} = \left[ \underbrace{\left( \frac{-h^2}{8\pi^2 m_e} \right) \sum_{i=1}^k \nabla_i^2}_{T_{\text{electron}}} - \underbrace{\sum_{j=1}^N \sum_{i=1}^k \frac{Z_j}{r_{ji}}}_{V_{\text{electron-nucleus}}} \right] + \underbrace{\sum_{i=1}^{k-1} \sum_{n=i+1}^k \frac{1}{r_{in}}}_{V_{\text{electron-electron}}} + \underbrace{\sum_{j=1}^{N-1} \sum_{m=j+1}^N \frac{Z_j Z_m}{R_{jm}}}_{V_{\text{nucleus-nucleus}}}, \quad (2.8)$$

where  $V_{\text{nucleus-nucleus}}$  is typically treated as a constant.

### 2.3 Born-Oppenheimer approximation

The Born-Oppenheimer approximation is a way to simplify the complicated Schrödinger equation for a molecule. The nucleus and electrons are attracted to each other with the same magnitude of electric charge, thus they exert the same force and momentum. While exerting the same kind of momentum, the nucleus, with a much larger mass in comparison to electron's mass, will have a very small velocity that is almost negligible. So we can consider the electrons as moving in the field of fixed nuclei, the nuclear kinetic energy is zero and their potential energy is merely a constant. Thus, from equation (2.8), the electronic Hamiltonian reduces to

$$\hat{H}^{elec} = \left[ \left( \frac{-h^2}{8\pi^2 m_e} \right) \sum_{i=1}^k \nabla_i^2 - \sum_{j=1}^N \sum_{i=1}^k \frac{Z_j}{r_{ji}} \right] + \sum_{i=1}^{k-1} \sum_{n=i+1}^k \frac{1}{r_{in}} = T_e + V_{ne} + V_{ee}. \quad (2.9)$$

The solution of the Schrödinger equation with  $\hat{H}_{elec}$  is the electronic wave function  $\Psi_{elec}$  and the electronic energy  $E_{elec}$ .

$$\hat{H}_{elec} \Psi_{elec} = E_{elec} \Psi_{elec}. \quad (2.10)$$

The total energy  $E_{tot}$  is then the sum of  $E_{elec}$  and the constant nuclear repulsion term  $E_{nuc}$ .

$$E_{tot} = E_{elec} + E_{nuc},$$

where

$$E_{nuc} = \sum_{j=1}^{N-1} \sum_{m=j+1}^N \frac{Z_j Z_m}{R_{jm}}. \quad (2.11)$$

When a system is in the state  $\Psi$ , the expectation value of the energy is given by

$$E[\Psi] = \frac{\langle \Psi | \hat{H} | \Psi \rangle}{\langle \Psi | \Psi \rangle},$$

where

$$\langle \Psi | \hat{H} | \Psi \rangle = \int \Psi^* \hat{H} \Psi d\bar{x}. \quad (2.12)$$

The Born-Oppenheimer can be applied to calculate the bond length and energy between molecules. By focusing on the specific separation between nucleus and

electron, their wavefunctions can be calculated. Thus, a molecule's energy in relationship with its bond length can be examined.

## 2.4 Molecular orbital theory

The molecular orbital (MO) theory is a method for determining molecular structure. A molecular orbital is a region in which an electron may be found in a molecule. The molecular orbital can be described by the wavefunction of the electron in a molecule, in particular a spatial distribution ( $|\psi_i(r)|^2$ ) of an electron and energy of up to two electrons within it. The complete wavefunction for an electron is termed a spin orbital ( $\chi$ ) which is the product of a molecular orbital ( $\psi$ ) and spin function ( $\alpha$  or  $\beta$ ). The wavefunction is simple product of spin orbital wavefunction for the description of an  $n$ -electron system, which can be written in the form of product of spin orbitals,

$$\Psi_{product} = \chi_1(1)\chi_2(2)\dots\chi_n(n), \quad (2.13)$$

where  $\chi_i(i)$  is the spin orbitals of electron  $i$ . However, such a wavefunction is unacceptable because it does not satisfy the property of antisymmetry. The multi-electron wavefunction must take into consideration the fact that electrons are indistinguishable, and therefore interchanging electron position assignments in a wavefunction cannot lead to a different wavefunction. To ensure the antisymmetry, the spin orbitals are arranged in a determinant wave function,

$$\Psi_{\text{det}} = \begin{vmatrix} \chi_1(1) & \chi_2(1) & \cdots & \chi_n(1) \\ \chi_1(2) & \chi_2(2) & \cdots & \chi_n(2) \\ \vdots & \vdots & \ddots & \vdots \\ \chi_1(n) & \chi_2(n) & \cdots & \chi_n(n) \end{vmatrix}. \quad (2.14)$$

The practical use in building up a determinant wavefunction is to choose a set of molecular orbitals,  $\psi_1, \psi_2, \psi_3, \dots, \psi_n$ , and then to assign electrons of  $\alpha$  and  $\beta$  spin to these orbitals. Exchanging any two rows of a determinant, a process which corresponds to exchanging two electrons changes the sign of the determinant and therefore directly leads to the antisymmetry property. If any two rows of a determinant are identical, which would correspond to two electron being assigned to the same spin orbital, then the determinant wavefunction in equation (2.14) vanishes if two columns are identical, which follows the *Pauli exclusion principle*. For some further properties of the molecular orbital wavefunctions, it is possible to force the orbitals to be *orthogonal* to each other,

$$\int \psi_i^* \psi_j dx dy dz = 0, \text{ for } i \neq j, \quad (2.15)$$

and molecular orbitals may be *normalized*,

$$\int \psi_i^* \psi_i dx dy dz = 1, \quad (2.16)$$

which corresponds to the requirement that the probability of finding the electron anywhere in the space is unity. Thus, the determinant wavefunction (equation (2.14)) may be normalized and full many-electron molecular orbital wavefunction, for

example, for the closed-shell ground state of a molecular with  $n$  (even) electrons, doubly occupying  $n/2$  orbitals, can be written as

$$\Psi = \frac{1}{\sqrt{n!}} \begin{vmatrix} \psi_1(1)\alpha(1) & \psi_1(1)\beta(1) & \psi_2(1)\alpha(1) & \cdots & \psi_{n/2}(1)\beta(1) \\ \psi_1(2)\alpha(2) & \psi_1(2)\beta(2) & \psi_2(2)\alpha(2) & \cdots & \psi_{n/2}(2)\beta(2) \\ \vdots & \vdots & \vdots & \ddots & \vdots \\ \psi_1(n)\alpha(n) & \psi_1(n)\beta(n) & \psi_2(n)\alpha(n) & \cdots & \psi_{n/2}(n)\beta(n) \end{vmatrix}. \quad (2.17)$$

An approximate wavefunction constructed from one electron orbital is often referred to as a *Slater determinant* (Slater, 1929).

## 2.5 The LCAO-MO method and basis set

A linear combination of atomic orbitals to molecular orbitals or LCAO-MO method is a quantum superposition of atomic orbitals, *i.e.*, a technique for calculating molecular orbitals in quantum chemistry. An initial assumption is that the number of the molecular orbitals,  $\psi$  is equal to the number of atomic orbitals included in the linear expansion. In this sense,  $n$  atomic orbitals combine to form  $n$  molecular orbitals, which can be numbered  $i = 1$  to  $n$  and which may not all be the same. The expression (linear expansion) for the  $i$ -th molecular orbital would be:

$$\psi_i = c_{1i}\phi_1 + c_{2i}\phi_2 + c_{3i}\phi_3 + \dots + c_{\mu i}\phi_\mu, \quad (2.18)$$

or

$$\psi_i = \sum_{\mu=1}^n c_{\mu i}\phi_\mu, \quad (2.19)$$

where  $c_{\mu i}$  are the molecular orbital expansion coefficients,  $n$  is the number of atomic basis function and the set of  $n$  function  $\phi_{\mu}$  is called *basis set*.

The common types of basis function, as also called *atomic orbital*, used in electronic structure calculations are Slater-type orbitals (STOs) (Slater, 1930) and Gaussian-type orbitals (GTOs) (Boys, 1950). The formalism of the STOs can be presented as

$$\phi_i(\zeta, n, l, m; r, \theta, \phi) = Nr^{n-1}e^{-\zeta r}Y_{lm}(\theta, \phi), \quad (2.20)$$

where  $n$ ,  $l$ , and  $m$  are quantum numbers referring to principal, angular momentum and magnetic, respectively.  $N$  is the normalization constant and  $\zeta$  is exponent. The  $r$ ,  $\theta$ , and  $\phi$  are spherical coordinates, and  $Y_{lm}$  is the angular momentum part. The STOs screening constants are calculated for small model molecules using rigorous self-consistent field methods, and then being generated for use with actual molecules of interest. The accuracy of STOs can be improved by combining two or more STOs (*i.e.*, with two different values of  $\zeta$ ) into a single one-electron wavefunction (double  $\zeta$  basis set).

However, the mathematical requirements for solving the integrals of the wave equation using STOs are very time-consuming. Gaussian-Type Orbitals (GTOs) are then introduced since they are mathematically simple than STOs, but less accurate (Boys, 1950). The GTO is expressed as

$$\phi_i(\alpha, l, m, n; x, y, z) = Ne^{-\alpha r^2}x^l y^m z^n, \quad (2.21)$$

where  $N$  is a normalization constant, and  $\alpha$  is exponent. The  $x$ ,  $y$ , and  $z$  are Cartesian coordinates. The  $l$ ,  $m$ , and  $n$  are now not quantum numbers but simply integral exponents at Cartesian coordinates and  $r^2 = x^2 + y^2 + z^2$ . The advantage of GTOs is that the product of two Gaussians at different centers is equivalent to a single Gaussian function centered at a point between the two centers. Therefore, the two-electron integral problem on three and four or more different atomic centers can be reduced to integrals over two different centers. However, the GTO gives an inferior representation of the orbitals at the atomic nuclei, which can be considered at 1s-orbital. A 1s-orbital of STO has a *cusp* at the atomic nucleus but a GTO does not, as shown in Figure 2.1. In this respect, the larger basis must be used to achieve the accuracy comparable to that obtained from STOs.

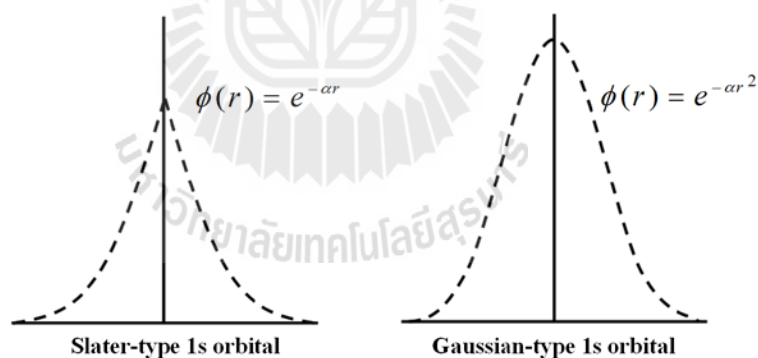


**Figure 2.1** The STO  $\exp(-\alpha r)$  and GTO for 1s orbital  $\exp(-\alpha r^2)$ .

The most important factor for creating the molecular orbital is the set of parameters applied to the basis function, called as *basis set*. The smallest number of function possible for constructing the molecular orbital is called a *minimum basis set*. The improvement of the basis set can be made by replacing two basis functions into each basis function in the minimal basis set, called as *double zeta* (DZ). The larger

basis set is a *triple zeta* (TZ), where three basis functions are used to represent each of the minimal basis sets. The compromise between the DZ and TZ basis sets is called a *split valence* (SV) basis set, in which each valence atomic orbital is represented by two basis functions while each core orbital is represented by a single basis function.

In 1969, Pople and coworkers (Hehre, Stewart and Pople, 1969) designed the basis set by expanding the STO in terms of  $n$  primitive Gaussians, called as STO- $n$ G basis set. The primitive Gaussian has been derived for  $n = 2-6$ . However, the STO-3G basis set is a widely used minimal basis set, as shown in Figure 2.2. The STO-3G basis set partially represents the *cusp* of s-type orbital at the atomic nuclei.

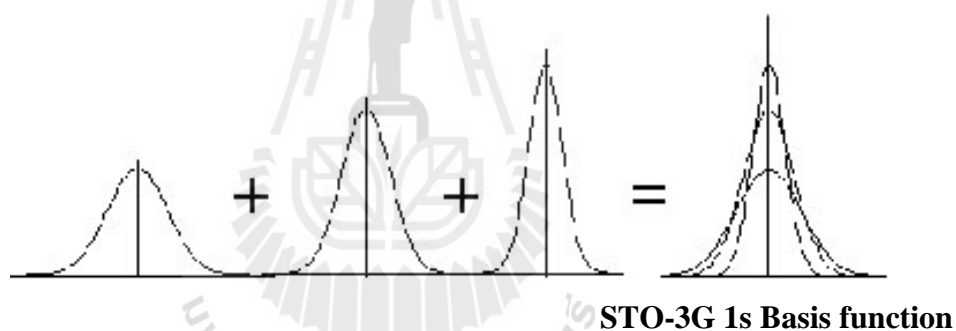


**Figure 2.2** The STO-3G basis set representing the desired STO.

Later, Pople and coworkers have applied the split valence for increasing flexibility in the basis set, which can be designed as  $k-nlmG$  basis set. The first parameter ( $k$ ) indicates the number of primitives used in the contracted core, while the two values ( $nl$ ) refer to a split valence, and three values ( $nlm$ ) refer to a triple split valence, such as 6-311G. For the triple split valence basis, the core orbitals are a contraction of six primitives and the valence split into three functions, represented by three, one and one primitive GTOs. The Pople's style basis sets may include diffuse

and/or polarization functions. The diffuse function can be denoted as + or ++ before the G, in which the first + indicates one set of diffuse s- and p-function adding on heavy atoms and the second + refer to the inclusion of diffuse s-function for hydrogen atom. The polarization function can be put after the G, which separates designation for heavy and hydrogen atoms. For example, 6-31+G(d) basis set refers to a split valence with additional diffuse sp-functions and a single d-type polarization function only on heavy atoms. The largest standard Pople style basis set is 6-311++G(3df,3pd). Additionally, the polarization function can be replaced with \* notation. For example, the 6-311G\* basis set is identical to 6-311G(d) and 6-311G\*\* basis set is identical to 6-311G(d,p).

Since several GTOs are often grouped together, the *contracted Gaussian function* has been applied to Dunning-Huzinaga (DZ) basis set (Dunning, 1970; Dunning, 1971; Huzinaga, 1965). The DZ basis set can be made by a contraction such as the (9s5p) primitive GTOs to [4s, 2p]. The contraction scheme is 6,1,1,1 for s-functions and 4,1 for the p-functions. In addition, the development of basis set by Dunning and coworker for recovering the correlation energy of the valence electrons is known as the *correlation consistent* (cc) basis sets. The general formulation can be written as cc-pVnZ, where  $n = D$  for double zeta, T for triple zeta, Q for quadruple zeta, and so on.

For the systems having a large number of core electrons elements, it is necessary to use a large number of basis functions for describing them. However, since the deep core electrons are not much important in a chemical sense, this leads to an approximation by replacing the core electrons with analytical functions, called as an *Effective Core Potential* (ECP) or *Pseudopotentials*. In practice, such basis set is

reasonably accurate and efficient, representing the combined nuclear-electronic core to the remaining electrons.

## 2.6 Basis set superposition error

When atomic basis sets are used to calculate molecular energies, particularly for weak interactions, an error occurs from the use of basis functions on improvement molecules (Davidson and Chakravorty, 1994). However, the energy difference obtained by such an approach will invariably be an overestimate of the true value. The discrepancy arise from a phenomenon known as “*Basis Set Superposition Error (BSSE)*” (Boys and Bernardi, 1970). The BSSE would be expected to be particularly significant when small, inadequate basis sets are used (*e.g.*, the minimal basis STO-*n*G basis sets) which do not provide for an adequate representation of the electron distribution far from the nuclei, particularly in the region where non covalent interactions are strongest. One way to estimate the basis set superposition error is via the *Counterpoise Procedure (CP)* of Boys and Bernardi in which the entire basis set is included in all calculations (Boys and Bernardi, 1970). Thus, in the general case;



$$\Delta E = E(AB) - [E(A) + E(B)]. \quad (2.23)$$

The calculation of the energy of the individual species A is performed in the presence of “*ghost*” orbitals of B; that is, without the nuclei or electrons of B. A similar calculation is performed for B using ghost orbitals on A. However, the counterpoise method will not provide effective improvement of the results if the atomic basis sets are very poor. The counterpoise procedure has been used as a

standard tool of theoretical chemistry although some researchers have raised serious doubts on the usefulness of this procedure (Schwenke and Truhlar, 1986; Schwenke and Truhlar, 1987). The counterpoise correction can be very reasonable for the estimation of weak electronic interaction energies with small basis sets at Hartree-Fock (HF) level of accuracy. However, this approach has failed for the estimation of strong electronic interaction energies even if with up to date basis sets, as demonstrated by a study of cyclic hydrogen fluoride trimer (Liedl, 1998). An alternative approach is to use a basis set in which the orbital exponents and contraction coefficients have been optimized for molecular calculations rather than for atoms. The relevance of the basis set superposition error and its dependence upon the basis set and the level of theory employed (*i.e.*, SCF or with electron correlation) remains a subject of much research.

## 2.7 The variation method

In general, the energy of the system can be calculated through the Schrödinger equation by operating the Hamiltonian operator on the wavefunction. One way that is popular is *variation method*, which is applied to determine the lowest energy, which represents the ground state of the system. However, the energy obtained will be higher than ground state.

The theory starts with a trial function  $\Phi$  of the electronic coordinates and is normalized, which can be written in terms of a linear combination of the wavefunction,

$$\Phi = \sum_i c_i \psi_i, \quad (2.24)$$

where the individual  $\psi_i$  and coefficients  $c_i$  are unknown. Then, the normality of  $\Phi$  imposes a constraint on the coefficient, deriving from

$$\begin{aligned}
 \int \Phi^2 dr = 1 &= \int \sum_i c_i \psi_i \sum_j c_j \psi_j dr \\
 &= \sum_{ij} c_i c_j \int \psi_i \psi_j dr \\
 &= \sum_{ij} c_i c_j \delta_{ij} \\
 &= \sum_i c_i^2.
 \end{aligned} \tag{2.25}$$

Then, considering the energy associated with the wavefunction  $\Phi$  as

$$\begin{aligned}
 \int \Phi \hat{H} \Phi dr = 1 &= \int \sum_i (c_i \psi_i) \hat{H} (\sum_j c_j \psi_j) dr \\
 &= \sum_{ij} c_i c_j \int \psi_i \hat{H} \psi_j dr \\
 &= \sum_{ij} c_i c_j E_j \delta_{ij} \\
 &= \sum_i c_i^2 E_i.
 \end{aligned} \tag{2.26}$$

After that, combining the results from equations (2.25) and (2.26), give

$$\int \Phi \hat{H} \Phi dr - E_0 \int \Phi^2 dr = \sum_i c_i^2 (E_i - E_0). \tag{2.27}$$

The coefficients have been assumed to be real number, thus,  $c_i^2$  and the result of  $(E_i - E_0)$  must be greater than or equal to zero. Therefore,

$$\int \Phi \hat{H} \Phi dr - E_0 \int \Phi^2 dr \geq 0, \quad (2.28)$$

Or

$$\frac{\int \Phi \hat{H} \Phi dr}{\int \Phi^2 dr} \geq E_0. \quad (2.29)$$

From equation (2.29), the quality of wavefunction for describing the ground state of a system can be defined by their associated energies as the better wavefunction could provide the lower energy. In addition, the guess of the trial wavefunction can be constructed in any manner, which determined the quality by the integral in equation (2.29).

## 2.8 Hartree-Fock self-consistent field method

Generally, the molecular orbital computational methods (*ab initio* and semiempirical) make use of the *Hartree-Fock* (HF) method to approximate the molecular wavefunction. The Hamiltonian considers each electron in the average field of all other electrons in the molecule. A single determinant wavefunction is substituted into the original electronic Schrödinger equation and after applying lots of algebra, it yields the HF equations. The resulting HF equations can be viewed as an alternative Schrödinger equation where the exact Hamiltonian has been replaced by an

approximation. By this scheme, the solution of wavefunction of many-electron system becomes to one-electron system. The Hamiltonian that describes this approximation is called the *Fock operator* and then the one-electron Hamiltonian operator is defined by

$$\hat{F}(1) = \hat{H}^{core}(1) + \sum_{a=1}^{N/2} (2\hat{J}_a(1) - \hat{K}_a(1)), \quad (2.30)$$

where  $\hat{H}^{core}(1)$  is the exact one-electron operator,

$$\hat{H}^{core}(1) = -\frac{1}{2}\nabla_1^2 - \sum_{a=1}^{N/2} \frac{Z_a}{r_{1a}}, \quad (2.31)$$

$\hat{J}_a$  and  $\hat{K}_a$  are coulomb integral and exchange integral operators, respectively,

$$\hat{J}_a(1)\phi_a(\chi_1) = \left( \int \phi_a^*(\chi_2) \frac{1}{r_{12}} \phi_a(\chi_2) d\chi_2 \right) \phi_a(\chi_1), \quad (2.32)$$

and

$$\hat{K}_a(1)\phi_a(\chi_1) = \left( \int \phi_a(\chi_2) \frac{1}{r_{12}} \phi_a^*(\chi_2) d\chi_2 \right) \phi_a(\chi_1). \quad (2.33)$$

The Fock operator and the exact Hamiltonian are different, *i.e.*, the coulomb operator has been replaced by an operator describing the interaction of each electron with the average field of all other electrons. In this respect, the expansion of the wavefunction in terms of basis functions from the application of LCAO-MO method

lead to a limitation of the accuracy of the *ab initio* HF approach since there is limited number of basis functions available. However, since the basis sets used in the calculations are finite, the energy will approach a limiting value. This limiting energy is called a *HF limit*. Moreover, the HF equation for atom can be solved by numerical integration. Nevertheless, complication arises when molecules are considered because there is more than one center. Thus, the HF equation can be written independently using *Roothaan-Hall equations*,

$$\sum_{v=1}^N (F_{\mu v} - \varepsilon_i S_{\mu v}) c_{v i} = 0, \quad \mu = 1, 2, 3, \dots, N, \quad (2.34)$$

with the normalization conditions,

$$\sum_{\mu=1}^N \sum_{v=1}^N c_{\mu i}^* S_{\mu v} c_{v i} = 1, \quad (2.35)$$

where  $\varepsilon_i$  is the one-electron energy of molecular orbital  $\psi_i$  and  $S_{\mu v}$  is the element of an  $N \times N$  matrix termed the overlap matrix.

$$S_{\mu v} = \int \phi_{\mu}^*(1) \phi_v(1) dx_1 dy_1 dz_1, \quad (2.36)$$

and  $F_{\mu v}$  is the element of another  $N \times N$  matrix, called the *Fock matrix*,

$$F_{\mu v} = H_{\mu v}^{core} + \sum_{\lambda=1}^N \sum_{\sigma=1}^N P_{\lambda \sigma} \left[ \langle \mu v | \lambda \sigma \rangle - \frac{1}{2} \langle \mu \lambda | v \sigma \rangle \right]. \quad (2.37)$$

In this expression,  $H_{\mu\nu}^{core}$  is a matrix representing the energy of a single electron in a field of “bare” nuclei. Its elements are

$$H_{\mu\nu}^{core} = \int \phi_{\mu}^*(1) \hat{H}^{core}(1) \phi_{\nu}(1) dx_1 dy_1 dz_1, \quad (2.38)$$

in which

$$\hat{H}^{core}(1) = -\frac{1}{2} \left( \frac{\partial^2}{\partial x_1^2} + \frac{\partial^2}{\partial y_1^2} + \frac{\partial^2}{\partial z_1^2} \right) - \sum_{A=1}^M \frac{Z_A}{r_{1A}}, \quad (2.39)$$

where  $Z_A$  is the atomic number of atom  $A$ , and summation is carried out over all atoms. The quantities  $\langle \mu\nu | \lambda\sigma \rangle$  and  $\langle \mu\lambda | \nu\sigma \rangle$  appearing in equation (2.27) are two-electron integrals,

$$\langle \mu\nu | \lambda\sigma \rangle = \iint \phi_{\mu}^*(1) \phi_{\nu}(1) \left( \frac{1}{r_{12}} \right) \phi_{\lambda}^*(2) \phi_{\sigma}(2) dx_1 dy_1 dz_1 dx_2 dy_2 dz_2, \quad (2.40)$$

and

$$\langle \mu\lambda | \nu\sigma \rangle = \iint \phi_{\mu}^*(1) \phi_{\lambda}(1) \left( \frac{1}{r_{12}} \right) \phi_{\nu}^*(2) \phi_{\sigma}(2) dx_1 dy_1 dz_1 dx_2 dy_2 dz_2, \quad (2.41)$$

which are multiplied by the elements of the one-electron density matrix,  $P_{\lambda\sigma}$ ,

$$P_{\lambda\sigma} = 2 \sum_{i=1}^{occ} c_{\lambda i}^* c_{\sigma i}. \quad (2.42)$$

The density matrix describes the electron density of the molecules. Thus, the criterion for judging convergence of the self-consistent, called as self-consistent field (SCF),

which refers to the density as well as to the energy because both have to be stationary at self-consistence. In equation (2.37), the summation occupies each molecular orbital, and the asterisk represents complex conjugation (required if the molecular orbitals are not the real functions). The electronic energy,  $E^{elec}$ , is now given by

$$E^{elec} = \frac{1}{2} \sum_{\mu=1}^N \sum_{\nu=1}^N P_{\mu\nu} (F_{\mu\nu} + H_{\mu\nu}^{core}), \quad (2.43)$$

and when adding the internuclear repulsion,

$$E^{nr} = \sum_A^N \sum_{B>A}^N \frac{Z_A Z_B}{R_{AB}}, \quad (2.44)$$

yields an expression for the total energy.

With regard to the two-electron integrals, the amount of atomic basis functions give rise to a major practical problem in the application of the *ab initio* HF method due to the computational requirement which is approximated to  $N^4/8$  for  $N$  basis functions. In fact, not only time consuming of the integral calculation, but also their storage on disk is practically impossible for large molecular systems. Consequently, the *Direct SCF methods* have become available, which reduce these problems significantly. By these approaches, the two-electron integrals are not stored but recalculated as required. This makes sense because the CPU of modern computers is very fast, while I/O operation takes quite long time. Secondly, only those integrals that are expected to have a significant value are actually calculated. With these tricks built into modern programs, the direct algorithms are actually faster than the conventional

one for systems of more than about 100 basis functions (depending on the particular computer).

Since *ab initio* quantum chemical methods are limited in their practical applicability because of their heavy demands of CPU time and storage space on disk or in computer memory, evaluation of the two-electron integrals for molecules with large number of electrons becomes computationally impractical. The *Semiempirical* HF methods have been developed to simplify these integrals that compensate for neglecting some of that time consuming mathematical terms. In general, the parameters used by semiempirical methods can be derived from experimental measurement or by performing *ab initio* calculations on model systems.

## 2.9 Electron correlation

The most significant drawback of HF method is that it fails to adequately represent electron correlation. In the self-consistent field method, the electrons are assumed to be moving in an average potential of the other electrons, and so the instantaneous position of an electron is not influenced by the presence of neighboring electron. In fact, the motions of electron are correlated and they tend to 'avoid' each other more than HF method would suggest, giving rise to a lower energy. The correlation energy is defined as the difference between the HF energy and the exact energy.

$$E_{exact} = E_{HF} + E_{correlation}. \quad (2.45)$$

Since the HF energy is always above the exact energy, the correlation energy is always negative,

$$E_{corr} < 0. \quad (2.46)$$

In addition, neglecting electron correlation can lead to some clearly anomalous results, especially as the dissociation limit is approached. As a consequence, the  $\Psi$  and  $E$  cannot be used to correctly predict atomic properties without somewhere accounting for electron correlation.

There are a number of way in which correlation effect can be incorporated into an *ab initio* molecular orbital calculation, such as Configuration interaction (CI) (Bauschlicher, Langhoff and Taylor, 1990), Many-body perturbation theory (MBPT) (Møller and Plesset, 1934), Couple cluster (CC) (Bartlett, 1989)) and electron density based methods such as density functional theory (DFT) (Jones and Gunnarrson, 1989).

## 2.10 Density functional theory

The structural and dynamical properties of molecules will be determined by electrons. For the treatment of system containing many atoms and many electrons, the *ab initio* methods are found to be very time-consuming. The *density functional theory* (DFT) is then used as an alternative approach, which takes into account the electron correlation using the concept of electron probability density. The DFT allows all of properties determined by the electron density,  $\rho(r)$ , which is the function of three variables:  $\rho(r) = \int(x, y, z)$ . The DFT was continuously developed. The major developments are as follows: Start with Thomas-Fermi model was introduced in 1920,

Hohenberg-Kohn proved the existent DFT (Hohenberg and Kohn, 1964), the Kohn-Sham (KS) scheme was proposed (Kohn and Sham, 1965), the DFT method was applied in molecular dynamic simulations (Car-Parrinello, 1985), Becke and LYP functional was developed (Becke, 1986; Becke, 1988; Lee, Yang and Parr, 1988) and in 1998 Walter Kohn received the Nobel prize for developing a complete DFT.

The DFT of Hohenberg, Kohn and Sham is based on the fact that the sum of the exchange and correlation energies of an electron can be calculated exactly only its density. By means of the Kohn-Sham method, the ground state electronic energy,  $E$ , can be written as

$$E = E_T + E_V + E_J + E_{XC}, \quad (2.47)$$

where  $E_T$ ,  $E_V$ ,  $E_J$  and  $E_{XC}$  refer to kinetic, potential (electron-nuclear interaction energy), Coulomb and the exchange/correlation energy, respectively. All components depend on the total electron density,  $\rho(r)$ , except ( $E_T$ ).

$$\rho(r) = 2 \sum_i^{\text{orbitals}} |\Psi_i(r_i)|^2. \quad (2.48)$$

Here,  $\Psi_i$  is called Kohn-Sham orbitals and the summation is carried out over pairs of electrons. Each energy components within the finite basis set can be written as

$$E_T = \sum_{\mu}^{\text{basisfunctions}} \sum_{\nu} \int \phi_{\mu}(r) \left[ -\frac{1}{2} \nabla^2 \right] \phi_{\nu}(r) dr, \quad (2.49)$$

$$E_V = \sum_{\mu}^{\text{basisfunctions}} \sum_{\nu} \rho_{\mu\nu} \sum_A \int \phi_{\mu}(r) \left| \frac{Z_A}{r-R_A} \right| \phi_{\nu}(r) dr, \quad (2.50)$$

$$E_J = \sum_{\mu}^{\text{basisfunctions}} \sum_{\nu} \sum_{\lambda} \sum_{\sigma} \rho_{\mu\nu} \rho_{\lambda\sigma} (\mu\nu|\lambda\sigma), \quad (2.51)$$

$$E_{XC} = \int f(\rho(r), \nabla\rho(r), \dots) dr, \quad (2.52)$$

where  $Z$  is the nuclear charge,  $r-R$  represents the distance between the electron and nucleus.  $f$  refers to exchange/correlation functional, which depends on the electron density and the gradient of the density.

In the local density approximation (LDA), the exchange-correlation can be defined as in the equation (2.52). To improve the exchange-correlation function, a non-local correction involving the gradient of  $\rho$  is added to the exchange-correlation energy. The LDA with gradient-corrections is called the generalized gradient approximation (GGA). The exchange-correlation functionals have been developed for use in DFT calculations, such as mPWPW19, B3LYP, MPW1K, PBE1PBE, BLYP, BP91 and PBE. The name of each function refers to the pairing of an exchange function and correlation function.

## 2.11 Many body perturbation theory

Møller and Plesset proposed an alternative way to tackle the problem of electron correlation (Møller and Plesset 1934). The method is based upon Rayleigh-Schrödinger perturbation theory, in which the “true” Hamiltonian operator  $\hat{H}$  is

expressed as the sum of a “zeroth-order” Hamiltonian  $\hat{H}_0$  (for which a set of molecular orbitals can be obtained) and perturbation,  $\hat{V}$  ;

$$\hat{H} = \hat{H}_0 + \hat{V} . \quad (2.53)$$

The eigenfunctions of the true Hamiltonian operator are  $\Psi_i$  with corresponding energy  $E_i$  . The eigenfunctions of the zeroth-order Hamiltonian are written  $\Psi_i^{(0)}$  with energy  $E_i^{(0)}$  . The ground state wavefunction is thus  $\Psi_0^{(0)}$  with energy  $E_0^{(0)}$  . To devise a scheme by which it is possible to gradually improve the eigenfunctions and eigenvalues of  $\hat{H}_0$  we can write the true Hamiltonian as follows;

$$\hat{H} = \hat{H}_0 + \lambda \hat{V} , \quad (2.54)$$

where  $\lambda$  is a parameter that can vary between 0 and 1, *i.e.*, when  $\lambda$  is zero then  $\hat{H}$  is equal to the zeroth-order Hamiltonian but when  $\lambda$  is one then  $\hat{H}$  equal its true value.

The eigenfunction  $\Psi_i$  and eigenvalues  $E_i$  of  $\hat{H}$  are then expressed in powers of  $\lambda$  ;

$$\Psi_i = \Psi_i^{(0)} + \lambda \Psi_i^{(1)} + \lambda^2 \Psi_i^{(2)} \dots = \sum_{n=0} \lambda^n \Psi_i^{(n)} , \quad (2.55)$$

$$E_i = E_i^{(0)} + \lambda E_i^{(1)} + \lambda^2 E_i^{(2)} \dots = \sum_{n=0} \lambda^n E_i^{(n)} , \quad (2.56)$$

$E_i^{(1)}$  is the first-order correction to the energy,  $E_i^{(2)}$  is the second-order correction and so on. These energies can be calculated from the eigenfunctions as follows;

$$E_i^{(0)} = \int \Psi_i^{(0)} \hat{H}_0 \Psi_i^{(0)} dr \quad (2.57)$$

$$E_i^{(1)} = \int \Psi_i^{(0)} \hat{V} \Psi_i^{(0)} dr \quad (2.58)$$

$$E_i^{(2)} = \int \Psi_i^{(0)} \hat{V} \Psi_i^{(1)} dr \quad (2.59)$$

$$E_i^{(3)} = \int \Psi_i^{(0)} \hat{V} \Psi_i^{(2)} dr. \quad (2.60)$$

The correction energy using second-order perturbation theory (MBPT(2)) is known as second-order Møller-Plesset perturbation theory (MP2). The correction energy of MP method can be written as

$$E_{corr} = E_0^{(2)} + E_0^{(3)} + E_0^{(4)} + \dots \quad (2.61)$$

The correction through  $E(2)$ , called MP2 correction, which considers the first term of the above equation as

$$E_0^{(2)} = \sum_i^{occupied} \sum_{j>i}^{virtual} \sum_a \sum_{b>a} \frac{\iint d\tau_1 d\tau_2 \chi_i(1) \chi_j(2) \left( \frac{1}{r_{12}} \right) [\chi_a(1) \chi_b(2) - \chi_b(1) \chi_a(2)]}{\epsilon_a + \epsilon_b - \epsilon_i - \epsilon_j}. \quad (2.62)$$

These integrals will be non-zero only for double excitations, according to the Brillouin theorem. Third- and fourth-order Møller-Plesset calculations (MP3 and MP4) are also available as standard options in many *ab initio* packages.

The advantage of many-body perturbation theory is that it is size independent, unlike configuration interaction interaction—even when a truncated expansion is used. However, Møller-Plesset perturbation theory is not variational and can sometimes give energies that are lower than the “true” energy. Møller-Plesset calculations are computationally intensive and so their use is often restricted to “single-point” calculations at geometry obtained from a lower level of theory. This is the most popular way to incorporate electron correlation in molecular quantum mechanical calculations, especially at the MP2 level. Moreover, the MP2 level of theory is more reliable than DFT. In practices, however, it’s quite time-consuming.

## 2.12 References

- Bartlett, R. J. (1989). Coupled-cluster approach to molecular structure and spectra: A step toward predictive quantum chemistry. **The Journal of Physical Chemistry**. 93: 1697-1708.
- Beck, A. D. (1986). Density-functional calculations of molecular-bond energies. **The Journal of Chemical Physics**. 84: 4524-4529.
- Beck, A. D. (1986). Density-functional exchange-energy approximation with correct asymptotic behavior. **Physical Review A**. 38: 3098-3100.
- Boys, S. F. (1950). Electronic wave functions. I. A general method of calculation for the stationary states of any molecular system. **Proceedings of the Royal Society of London. Series A. Mathematical and Physical Sciences**. 200: 542-554.
- Boys, S. F. and Bernardi, F. (1970). The calculation of small molecular interactions by the differences of separate total energies. Some procedures with reduced errors.

**Molecular Physics: An International Journal at the Interface Between Chemistry and Physics.** 19: 553-566.

- Davidson, E. R. and Chakravorty, S. J. (1994). A possible definition of basis set superposition error. **Chemical Physics Letters.** 217: 48-54.
- Dunning, T. H. J. (1970). Gaussian basis functions for use in molecular calculations. I. Contraction of (9s5p) atomic basis sets for the first-row atoms. **The Journal of Chemical Physics.** 53: 2823-2833.
- Dunning, T. H. J. (1971). Gaussian basis functions for use in molecular calculations. III. Contraction of (10s6p) atomic basis sets for the first-row atoms. **The Journal of Chemical Physics.** 55: 716-723.
- Hehre, W. J., Stewart, R. F. and Pople, J. A. (1969). Self-consistent molecular-orbital methods. I. Use of gaussian expansions of slater-type atomic orbitals. **The Journal of Chemical Physics.** 51: 2657-2664.
- Huzinaga, S. (1965). Gaussian-type functions for polyatomic systems. I. **The Journal of Chemical Physics.** 42: 1293-1302.
- Kohn, W. and Sham, L. J. (1965). Self-consistent equations including exchange and correlation effects. **Physical Review.** 140: A1133-A1138.
- Lee, C., Yang, W. and Parr, R. G. (1988). Development of the Colle-Salvetti correlation-energy formula into a functional of the electron density. **Physical Review B.** 37: 785-789.
- Liedl, K. R. (1998). Dangers of counterpoise corrected hypersurfaces. Advantages of basis set superposition improvement. **The Journal of Chemical Physics.** 108: 3199-3204.

- Møller, C. and Plesset, M. S. (1934). Note on an approximation treatment for many-electron systems. **Physical Review**. 46: 618-622.
- Schrödinger, E. (1926). Quantisierung als eigenwertproblem. **Annalen der Physik**. 385: 437-490.
- Schwenke, D. W. and Truhlar, D. G. (1986). Erratum: Systematic study of basis set superposition errors in the calculated interaction energy of two HF molecules. **The Journal of Chemical Physics**. 84: 4113-4113.
- Schwenke, D. W. and Truhlar, D. G. (1987). Erratum: Systematic study of basis set superposition errors in the calculated interaction energy of two HF molecules. **The Journal of Chemical Physics**. 86: 3760-3760.
- Sherrill, C. D. and Schaefer, H. F. (1999). The configuration interaction method: Advances in highly correlated approaches. **Advances in Quantum Chemistry**. (Vol. 34, pp. 143-269): Academic Press.
- Slater, J. C. (1930). Atomic shielding constants. **Physical Review**. 36: 57-64.

# CHAPTER III

## MOLECULAR DYNAMICS SIMULATIONS

### 3.1 Introduction to computer simulation

Computer simulations can provide microscopic details for understanding the properties of assemblies of molecules in terms of their structure and the microscopic interactions between them. This serves as a complement to conventional experiments, enabling us to learn something new, something that cannot be found out in other ways. The two main families of simulation technique are molecular dynamics (MD) and Monte Carlo (MC). Nowadays, there is a whole range of hybrid techniques which combine features from both. In general, the obvious advantage of MD over MC is that it gives a route to dynamical properties of the system, such as transport coefficients, time-dependent responses to perturbations, rheological properties and spectra.

Computer simulations act as a bridge (see Figure 3.1) between microscopic length and time scales and the macroscopic world of the laboratory, *i.e.*, starts with a guess at the interactions between molecules, and obtain 'exact' predictions of bulk properties. The predictions are "exact" in the sense that they can be made as accurate as require, subject to the limitations imposed by available computational facilities. At the same time, the hidden detail behind bulk measurements can be revealed. An example is the link between the diffusion coefficient and velocity autocorrelation function (the former is easy to measure experimentally, while the latter is much harder). In another sense, simulations act as a bridge between theory and experiment.

A theory can be tested by conducting a simulation using the same model, and the model can be tested by comparing with experimental results. We may also carry out computer simulations for systems that are difficult or impossible in the laboratory (for example, working at extremely high temperature or pressure).

Ultimately, in order to make direct comparisons with experimental measurements made on specific materials, a good model of molecular interactions is essential. The aim of so-called *ab initio* molecular dynamics is to reduce the amount of fitting and guesswork in the process to a minimum. On the other hand, regarding the phenomena of a rather generic nature, it is not necessary to have a perfectly realistic molecular model, *i.e.*, the one that contains the essential physics may be quite suitable.

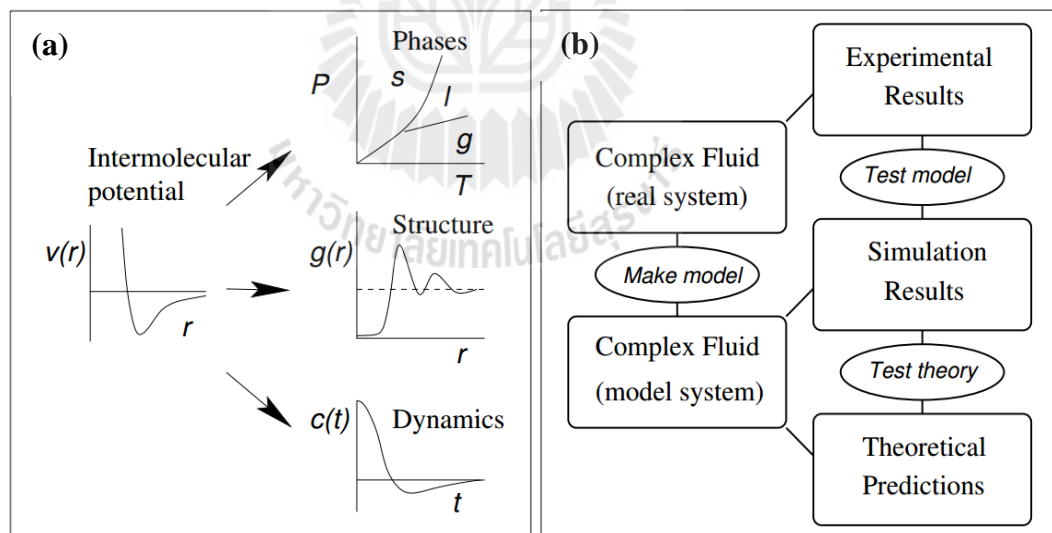


**Figure 3.1** Simulations as a bridge between (a) microscopic and macroscopic, and (b) theory and experiment.

### 3.2 Molecular dynamics (MD) simulation

In terms of computer simulations, the MD technique is a powerful tool. This technique is widely used for studying various molecular systems. The MD scheme is summarized in Figure 3.2. By the MD technique, Newton's equation of motion is employed, in which each particle in the system can be moved with respect to force from neighboring particles. The MD simulation starts with reading in the starting configurations, velocities, accelerations and forces. The starting configuration can be obtained either from experimental data such as from X-ray or random configuration. According to Newton's Equation of motion, since there is no time-dependent force that shall act in the system, the *time integration algorithms* will be used to obtain *time-dependent trajectories*, namely the knowledge of positions, velocities and accelerations of two successive time steps (small time interval). The energy of the system can be calculated using either molecular mechanics (MM) or QM method. Forces on each atom in the system can be derived from the energy with respect to change in the atom's position. These new forces will be used to obtain new configurations and the steps will be repeated until the system reaches equilibrium. Then, the coordinates, velocities, accelerations, forces and so on are collected for further structural and dynamical property calculations. In general, only positions and velocities are usually stored since most of the important and interesting properties can be obtained from these two quantities.

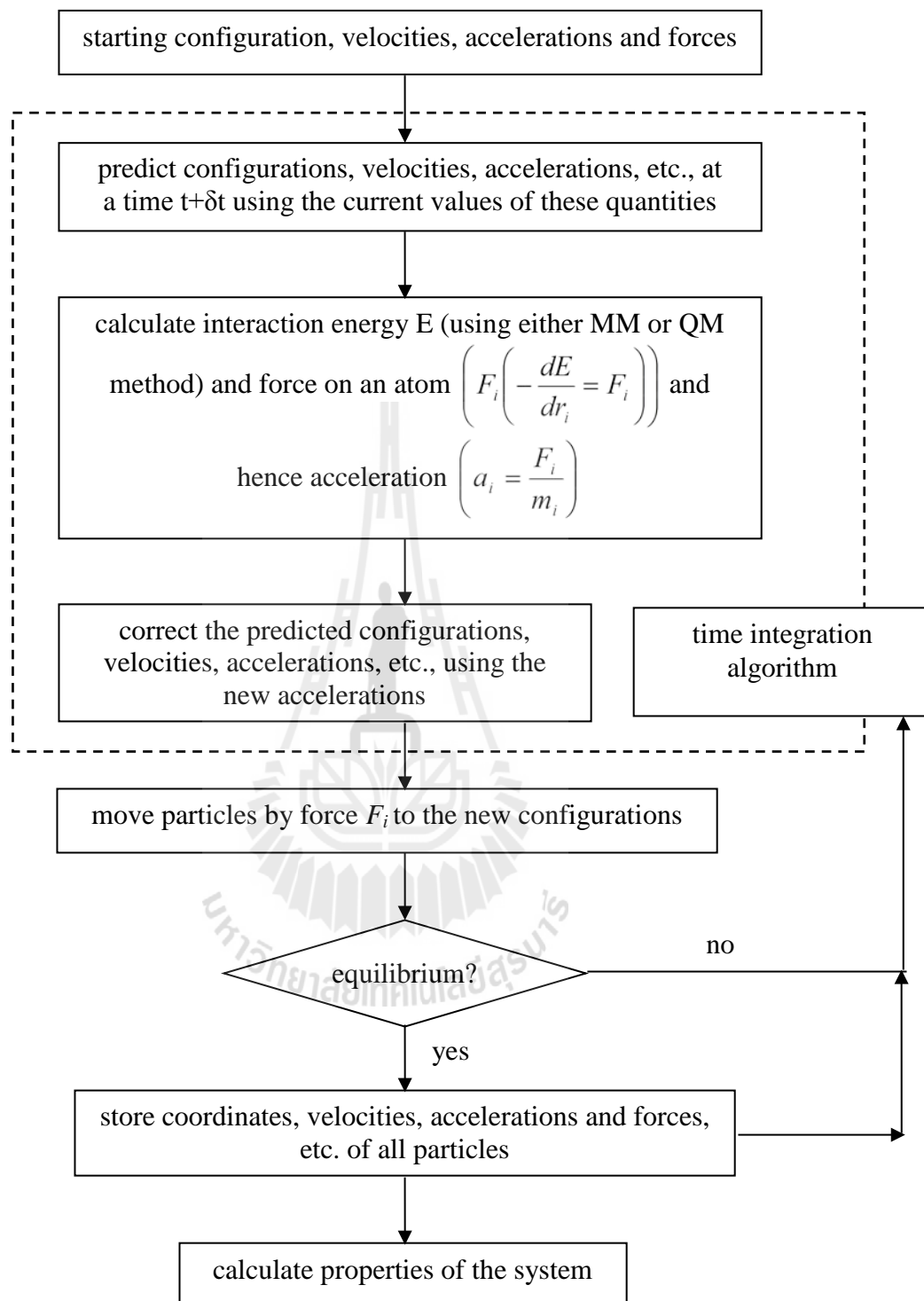


**Figure 3.2** The MD scheme.

### 3.3 Statistical mechanics

Generally, the results obtained by the MD simulation will provide information at microscopic level, including atomic positions and velocities. The conversion of microscopic information to macroscopic observables can be achieved by using statistical mechanics. The microscopic state of a system is defined by the atomic position,  $q$ , and momenta,  $p$ , which can also be considered as coordinates in a multidimensional space, called phase space. A single point in phase space, denoted by  $G$ , describes the state of the system. The collection of points in phase space is known as an ensemble.

An experiment is usually made on a macroscopic sample, which contains an extremely large number of atoms or molecules sampling a huge number of conformations. In statistical mechanics, averages corresponding to experimental observables are defined in terms of ensemble averages. An ensemble average is average taken over a number of replicas of the system considered simultaneously, which can be expressed as

$$\langle A \rangle_{ensemble} = \iint dp^N dr^N A(p^N, r^N) \rho(p^N, r^N), \quad (3.1)$$

where  $A(p^N, r^N)$  is the observable of interest and it is expressed as a function of the momenta,  $p$ , and the position,  $r$ , of the system. The integration is over all possible variables of  $r$  and  $p$ . The probability density of the ensemble is given by

$$\rho(p^N, r^N) = \frac{1}{Q} \exp \left[ -H \frac{(p^N, r^N)}{k_B T} \right], \quad (3.2)$$

where  $H$  is the Hamiltonian,  $T$  is the temperature,  $k_B$  is Boltzmann's constant and  $Q$  is the partition function,

$$Q = \iint (dp^N dr^N) \exp \left[ -H \frac{(p^N, r^N)}{k_B T} \right]. \quad (3.3)$$

This integral is extremely difficult to calculate since it must calculate all possible states of the system. By means of statistical mechanics, the experimental observable are defined in terms of time averages of property A that can be measured throughout infinite time, which can be expressed as

$$\langle A \rangle_{time} = \lim_{\tau \rightarrow \infty} \int_{t=0}^{\tau} A(p^N(t), r^N(t)) dt \approx \frac{1}{M} \sum_{i=1}^M A(p^N, r^N), \quad (3.4)$$

where  $\tau$  is the simulation time,  $M$  is the number of time steps in the simulation and  $A(p^N, r^N)$  is the instantaneous value of A.

The relationship between time averages and ensemble averages can be achieved using the Ergodic hypothesis, which states that the time averages equal the ensemble average, *i.e.*, the estimation of time average can be obtained over an enormous number of replicas of the system considered simultaneously,

$$\langle A \rangle_{time} = \langle A \rangle_{ensemble}. \quad (3.5)$$

In addition, the ensemble must be performed under some constraints, such as constant number of particles ( $N$ ), volume ( $V$ ), energy ( $E$ ), temperature ( $T$ ), chemical potential ( $\mu$ ), pressure ( $P$ ) and so on. For example, a simple ensemble is the *microcanonical ensemble*. This ensemble is a thermodynamically isolated system, where the  $N$ ,  $V$  and  $E$  are fixed throughout the simulation. The equilibrium states of  $NVE$  ensemble are characterized by the entropy. The development of  $NVE$  ensemble is the *canonical ensemble* ( $NVT$ ), in which the  $N$  and  $V$  are fixed and the ensemble has a well define temperature given by the temperature of the heat bath. The thermodynamic property derived from the  $NVT$  ensemble is Helmholtz free energy. The *grand canonical ensemble* ( $\mu VT$ ) is the extension of  $NVT$  ensemble which allows the energy exchange, but fixes the  $\mu$ ,  $V$  and  $T$ .

### 3.4 Intermolecular interactions

The calculation of the potential energy inevitably involves assumptions concerning the nature of attraction and repulsion between molecules. Intermolecular interaction is the result of both short- and long-range effects. Electrostatic, induction, and dispersion effects are examples of long range interactions. With regard to these terms, the energy of interaction is proportional to some inverse power of intermolecular separation. Electrostatic interactions result from the static charge distribution between molecules. This effect can be either attractive or repulsive and it is exclusively *pairwise additive approximation*. Induction effects are always attractive, resulting from the distortions caused by the molecular fields of neighboring molecules. However, the most important contribution is the attractive influence of

dispersion arising from instantaneous fluctuations caused by electron movement. Neither induction nor dispersion are pairwise additive approximation.

The short-range interactions are characterized by an exponential decay in the interaction energy with respect to intermolecular separation. At small intermolecular separations, there is a significant overlap of the molecular wave functions causing either intermolecular exchange or repulsion. These interactions are not pairwise additive. In general, it is possible to calculate the intermolecular interactions from first principles. In practice, however, the first principle or *ab initio* approach is confined to relatively simple systems. More commonly, the influence of intermolecular interaction is expressed by some types of intermolecular potential. The nature of intermolecular forces is discussed in greater detail (Stone, 1996).

### 3.5 Effective potentials

Before proceeding further, it is important to make the distinction between effective and true two-body potentials. Even though many potentials functionally pairwise (*i.e.*, they only require pair separation as inputs), they are often in reality “effective” potentials and it should not be confused with genuinely two-body potentials.

In general, the potential energy function is the total intermolecular interaction energy comprising all of the two-body, three-body, four-body up to  $N$ -body interactions,

$$V_{total} = \sum V(i, j) + \sum V(i, j, k) + \dots + \sum V(i, j, k, \dots, N). \quad (3.6)$$

However, most of earlier simulations had neglected the higher order interactions (three, four, ...,  $N$ -body), *i.e.*, these terms are assumed to converge rather slowly and the terms tend to have alternating signs (Kistenmacher, Popkie and Clementi, 1974). Therefore, the system's interactions are mostly relied on the summation of all two-body interactions,

$$V_{pair} = \sum_{i < j}^N v_{ij}(|r_i - r_j|), \quad (3.7)$$

where  $r_i$  and  $r_j$  are the position of species  $i$  and  $j$ , respectively. This is known as pairwise additive approximations.

Therefore, unless otherwise indicated, the potentials discussed should be treated as “effective.” In the past decades, a number of effective potentials have been developed (Maitland *et al.*, 1981) and applied to atoms. Historically, an empirical approach was used with the parameters of the potential being obtained from experimental data such as second virial coefficients, viscosities, molecular beam cross sections, etc. Conclusions regarding the accuracy of pair potential were made by comparing the properties predicted by the potential with experiment. In contrast, computer simulation permits the theoretical rigorous evaluation of the accuracy of intermolecular potentials. However, very few potential have been tested extensively using molecular simulation. Notable exceptions are the hard-sphere, Lennard-Jones, and exp-6 potentials. Effective potentials for atoms are often incorporated into the molecular simulation of platonic molecules and increasingly, macromolecules. Therefore, the atomic pair potential is an important starting basis for predicting molecular properties.

### 3.6 Time integration algorithms

The engine of a MD program is its time integration algorithms, required to integrate the equation of motion of the interacting particles and follow their trajectories. The time integration algorithms are based on finite difference method, where time is discretized on a finite grid, the time step  $\Delta t$  being the distance between consecutive points on the grid. Knowing the positions and some of their time derivatives at time  $t$ , the integration scheme gives the same quantities at a later time  $t + \Delta t$ . By iterating the procedure, the time evolution of the system can be followed for long times. Two popular integration methods for MD calculations are the *Verlet algorithm* (Verlet, 1967) and *predictor-corrector algorithms* (Gear, 1971).

#### 3.6.1 Verlet algorithm

In MD, the most commonly used time integration algorithm is probably the so-called *Verlet algorithm*. The basic idea is to write two third-order Taylor expansions for the positions  $r(t)$ , one forward and one backward in time. Calling  $v$  the velocities,  $a$  the accelerations, and  $b$  the third derivatives of  $r$  with respect to  $t$ , one has,

$$\begin{aligned} r(t + \Delta t) &= r(t) + v(t)\Delta t + \frac{1}{2}a(t)\Delta t^2 + \frac{1}{6}b(t)\Delta t^3 + O(\Delta t^4) \\ r(t - \Delta t) &= r(t) - v(t)\Delta t + \frac{1}{2}a(t)\Delta t^2 - \frac{1}{6}b(t)\Delta t^3 + O(\Delta t^4), \end{aligned} \quad (3.8)$$

Adding these two equations give

$$r(t + \Delta t) = 2r(t) - r(t - \Delta t) + a(t)\Delta t^2 + O(\Delta t^4). \quad (3.9)$$

This is the basic form of the Verlet algorithm. Since the interest in Newton's equation,  $a(t)$ , is just the force divided by the mass, and the force is in turn a function of the position  $r(t)$ ,

$$a(t) = -\frac{1}{m}\Delta V(r(t)). \quad (3.10)$$

As one can clearly see, the truncation error of the algorithm when evolving the system by  $\Delta t$  is of the order of  $\Delta t^4$ , even if third derivatives do not appear explicitly. This algorithm is at the same time simple to implement, it is accurate and stable, thus explaining its great popularity among molecular dynamics simulations.

A problem with this version of Verlet algorithm is that velocities are not directly generated. While they are not required for the time evolution, knowledge of them is sometimes necessary. Moreover, they are used to compute the kinetic energy  $K$ , whose evaluation is necessary to test the conservation of the total energy ( $E = K + V$ ). This is one of the most important tests to verify that a MD simulation is proceeding correctly. In general, one could compute the velocities from the positions by using

$$v(t) = \frac{r(t + \Delta t) - r(t - \Delta t)}{2\Delta t}. \quad (3.11)$$

However, the error associated to this expression is in the order of  $\Delta t^2$  rather than  $\Delta t^4$ . To overcome this difficulty, some variants of the Verlet algorithm have been developed. They give rise to exactly the same trajectory, and differ in what variables are stored in memory and at what times. The *leap-frog* algorithm (Hockney, 1970) is a

common numerical approach to calculate trajectories based on Newton's equation.

The steps can be summarized as follows,

- |   |   |  |
|---|---|--|
| → | 1. solve for $a_i$ at $t$ using                   | $-\frac{dE}{dr_i} = F_i = m_i a_i(t)$  |
| → | 2. update $v_i$ at $t + \frac{\Delta t}{2}$ using | $v_i(t + \frac{\Delta t}{2}) = v_i(t - \frac{\Delta t}{2}) + a_i(t)\Delta t$ |
| → | 3. update $r_i$ at $t + \Delta t$ using           | $r_i(t + \Delta t) = r_i(t) + v_i(t + \frac{\Delta t}{2})\Delta t$           |

An even better implementation of the same basic algorithm is the so-called *velocity Verlet method* (Swope, Anderson, Berens and Wilson, 1982), where positions, velocities and accelerations at time  $t + \Delta t$  are obtained from the same quantities at time  $t$  in the following way,

$$\begin{aligned}
 r(t + \Delta t) &= r(t) + v(t)\Delta t + \frac{1}{2}a(t)\Delta t^2 \\
 v(t + \frac{\Delta t}{2}) &= v(t) + \frac{1}{2}a(t)\Delta t \\
 a(t + \Delta t) &= -\frac{1}{m}\nabla V(r(t + \Delta t)) \\
 v(t + \Delta t) &= v(t + \frac{\Delta t}{2}) + \frac{1}{2}a(t + \Delta t)\Delta t.
 \end{aligned}
 \tag{3.12}$$

### 3.6.2 Predictor-corrector algorithm

In mathematics, particularly numerical analysis, a predictor-corrector method is an algorithm that proceeds in two steps. First, the prediction step calculates a rough approximation of the desired quantity. Second, the corrector step refines the initial approximation using another means. In approximating the solution to a first-order ordinary differential equation, suppose one knows the solution points  $y_0$  and  $y_1$

at times  $t_0$  and  $t_1$ . By fitting a cubic polynomial to the points and their derivatives (obtained from the differential equation), one can predict a point  $\tilde{y}_2$  by extrapolating to a future time  $t_2$ . Using the new value  $\tilde{y}_2$  and its derivative there,  $\tilde{y}'_2$  along with the previous points and their derivatives, one can then better interpolate the derivative between  $t_1$  and  $t_2$  to get a better approximation  $y_1$ . The interpolation and subsequent integration of the differential equation constitute the corrector step. An example of an *Euler - trapezoidal* predictor-corrector method,

$$h = \Delta t, t_{i+1} = t_i + \Delta t = t_i + h. \quad (3.13)$$

$$y' = f(t, y), y(t_0) = y_0. \quad (3.14)$$

First, calculate an initial guess value  $\tilde{y}_0$  via Euler:

$$\tilde{y}_0 = y_i + h f(t_i, y_i). \quad (3.15)$$

Next, improve the initial guess through iteration of the *trapezoidal rule*. This iteration process normally converges quickly.

$$\begin{aligned} \tilde{y}_1 &= y_i + \frac{h}{2} \left( f(t_i, y_i) + f(t_{i+1}, \tilde{y}_0) \right) \\ \tilde{y}_2 &= y_i + \frac{h}{2} \left( f(t_i, y_i) + f(t_{i+1}, \tilde{y}_1) \right) \\ &\vdots \\ \tilde{y}_n &= y_i + \frac{h}{2} \left( f(t_i, y_i) + f(t_{i+1}, \tilde{y}_{n-1}) \right) \end{aligned} \quad (3.16)$$

This iteration process is repeated until some fixed value  $n$  or until the guesses converge to within some error tolerance  $e$ :

$$|\tilde{y}_n - \tilde{y}_{n-1}| \leq e. \quad (3.17)$$

Then use the final guess as the next step:

$$y_{i+1} = \tilde{y}_n. \quad (3.18)$$

Note that the overall error is unrelated to convergence in the algorithm but instead to the step size and the core method, which in this example is a trapezoidal (linear) approximation of the actual function. The step size  $h(\Delta t)$  needs to be relatively small in order to get a good approximation.

### 3.7 Periodic boundary conditions

Computer simulations using atomistic potentials are typically performed on small systems, usually of the order of a few hundred molecules. Assuming a simple cubic lattice, of 1,000 molecules, 488 lie on the surface. These molecules would experience different forces than the other molecules. To try and counteract this surface effect it is common to invoke *periodic boundary conditions*.

Here, the system is surrounded by an infinite number of identical systems, as shown in Figure 3.3. In the course of the simulation the molecules in each of the boxes move in the same way. Hence if a molecule leaves the simulation box at one side, an identical molecule enters the box at the other.

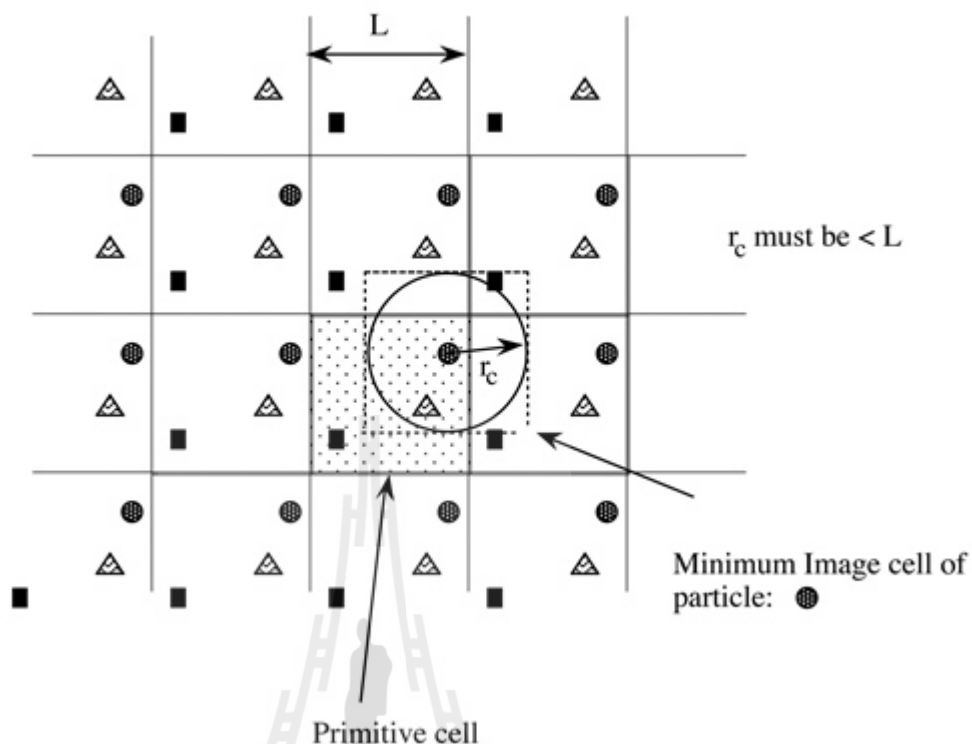


**Figure 3.3** Schematic representation of the idea of periodic boundary conditions.

Periodic boundary conditions are usually used in conjunction with the *minimum image convention* for short ranged forces, *i.e.*, only considering interactions between each molecule and the closest periodic image of its neighbors. Short ranged forces are often truncated to increase computational efficiency. For consistency with the minimum image convention, this cut-off distance must be less than or equal to half of the box length. Periodic boundary conditions can sometimes have an effect on the system under consideration. This is especially pronounced for small system sizes and for properties with a large long range contribution, such as light scattering factors. They also inhibit long wavelength fluctuations that are important near phase transitions. However, they have little effect on equilibrium properties.

### 3.8 Cut-off and potential at cut-off

According to Figure 3.3,  $r_c$  is the cut-off radius, which is commonly applied along with the minimum image criterion when calculating the energy and force between two atoms, *i.e.*, in order to reduce the number of non-bonded interactions that will be calculated in each MD step. In classical MD simulation, the non-bonded interactions are of the most time-consuming part of the energy and force calculations. For  $N$  atom system, the number of non-bonded interactions are  $N*(N-1)/2$ . Normally, the cut-off limit should be no more than half of the box length ( $\leq L/2$ ). On the other hand, only non-bonded interactions for  $r \leq r_c$  are taken into account for calculating energy or force, while the interactions for  $r > r_c$  are ignored.

According to cut-off, the most straightforward way is the simple truncation at  $r = r_c$ . This leads to a discontinuity in potential energy and force at the cut-off distance. In practice, the MD simulation cannot deal with such situation because of poor energy conservation. To solve this problem, a shifted potential is employed in order to modify the potential at the cut-off radius,

$$V_{(r)} = \begin{cases} \phi_{LJ}(r) - \phi_{LJ}(r_c) & \text{if } r < r_c \\ 0 & \text{if } r > r_c \end{cases}, \quad (3.19)$$

where  $\phi_{LJ}(r_c)$  is equal to the value of the potential at the cut-off distance. Another way is to switch off the potential between a chosen distance  $r$  and  $r_c$ , which may not affect the equilibrium structure due to applied switching function over a narrow range, which can be expressed as

$$V_{(r)}^{SF} = \begin{cases} \phi_{LJ}(r) - \phi_{LJ}(r_c) - \left(\frac{d\phi_{LJ}(r)}{dr}\right)_{r=r_c}(r - r_c) & r \leq r_c \\ 0 & r > r_c \end{cases} \quad (3.20)$$

### 3.9 Neighbor lists

Atom within the cutoff distance is quite time-consuming in MD simulation because the distance between every pair of atoms still has to be calculated in each simulation step. In practice, since most of atoms move within a time step of less than  $0.2 \text{ \AA}$ , the local neighbors of a given atom remain the same for many time steps.

To avoid wasteful recalculation for every single time, the *Verlet neighbor list* (see Figure 3.4) is employed, which creates lists of all atoms within a certain distance of every atom. In this respect, every atom only interacts in its neighbor list. That is, it stores all atoms within the cut-off distance ( $r_{cut}$ ) and all atoms that locate slightly further away from the cut-off distance ( $r_m$ ).

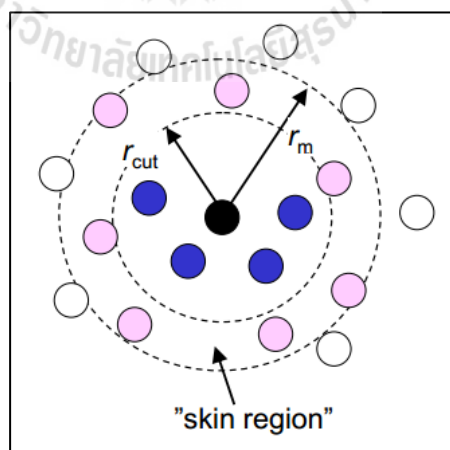


**Figure 3.4** Verlet neighbor list.

### 3.10 Long-range interactions

The neglect of interactions beyond the cut-off distance, especially for the strong interacting systems, may result in an incorrect description of molecular properties. One simple way to treat the long-range interactions is to use a large simulation cell, but this reflects in more time-consuming. There are many suitable methods for the treatment of long-range interactions. The first method is the Ewald summation method, which derived by Ewald in 1921 (Ewald, 1921). This method studies the energetic of ionic crystals, *i.e.*, a particle interacts with all the other particles in the simulation box and with all of their images in an infinite array of periodic cells. The charge-charge contribution to the potential energy of the Ewald summation method could be of the form

$$V = \frac{1}{2} \sum'_{|\mathbf{n}|=0} \sum_{i=1}^N \sum_{j=1}^N \frac{q_i q_j}{4\pi\epsilon_0 |r_{ij} + \mathbf{n}|}, \quad (3.21)$$

where the prime on the first summation indicates that the series does not include the interaction  $i = j$  for  $\mathbf{n} = 0$ ,  $q_i$  and  $q_j$  are charges and  $\mathbf{n}$  is a cubic lattice point. The Ewald summation method is the most correct way to accurately include all the effects of long-range forces in the computer simulation. However, this method is rather expensive to implement since the equation (3.21) converges extremely slowly.

Another method for the treatment of long-range interactions is the *reaction field method* (Foulkes and Haydock, 1989). This method constructs the sphere around the molecule with a radius equal to the cut-off distance. By this scheme, all interactions within the sphere are calculated explicitly, while those outside of the

sphere are modeled as a homogeneous medium of dielectric constant ( $\epsilon_s$ ). The electrostatic field due to the surrounding dielectric is given by

$$E_i = \frac{2(\epsilon_s - 1)}{\epsilon_s + 1} \left( \frac{1}{r_c^3} \right) \sum_{j:ij \leq r_c} \mu_j \quad (3.22)$$

where  $\mu_j$  are the dipoles of the neighboring molecules that are located within the cut-off distance ( $r_c$ ) of the molecules  $i$ . The interaction between molecule  $i$  and the reaction field equals to  $E_i \cdot \mu_i$ .

### 3.11 Temperature scaling

Temperature scaling is one of the “tricks of the trade” employed in MD to drive a simulation towards the desired system temperature.

If it turns out that system’s temperature is not the temperature required, it is simply to multiply the velocity of every atom by

$$\text{Temperature scaling} = \sqrt{\frac{T_0}{T}} . \quad (3.23)$$

where  $T_0$  is the required temperature. This technique can be applied at regular intervals during the equilibration period, and so drive the simulation consistently towards the desired temperature.

### 3.12 Conventional *ab initio* QM/MM MD technique

According to the conventional QM/MM technique, the system is partitioned into two parts, namely QM and MM regions. The QM region is the most interesting region which is treated by quantum mechanics, while the rest of the system, the MM region, is described by classical MM potentials.

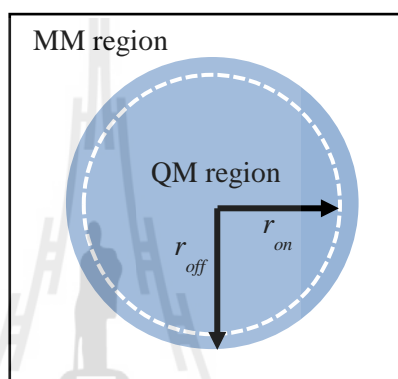


**Figure 3.5** System's partition.

According to Figure 3.4, the total energy ( $E_{tot}$ ) of the system can be obtained from the summation of three component parts, namely the interactions within the QM, in the MM and between the QM and MM regions;

$$E_{tot} = \left\langle \Psi_{QM} \left| \hat{H} \right| \Psi_{QM} \right\rangle + E_{MM} + E_{QM-MM}, \quad (3.24)$$

where  $\left\langle \Psi_{QM} \left| \hat{H} \right| \Psi_{QM} \right\rangle$  refers to the interactions within the QM region,  $E_{MM}$  is the interactions within the MM region and  $E_{QM-MM}$  is the interactions between the QM and MM regions.

By the conventional QM/MM MD technique, a thin switching layer located between the QM and MM regions is introduced to smooth the transition due to the solvent exchange, as show in Figure 3.5.

During the QM/MM MD simulation, exchanges of particles between the QM and MM regions can occur frequently. With regard to this point, the force acting on each particle in the system are switched according to which region the particle was entering or leaving the QM region and was defined as

$$F_i = S_m(r)F_{QM} + (1 - S_m(r))F_{MM}, \quad (3.25)$$

where  $F_i$  refers to force on each particle in the system,  $F_{QM}$  and  $F_{MM}$  are quantum mechanical and molecular mechanical forces, respectively.  $S_m(r)$  is a smoothing function,

$$S_m(r) = 1 \quad \text{for } r \leq r_1, \quad (3.26)$$

$$S_m(r) = \frac{(r_0^2 - r^2)(r_0^2 + 2r^2 - 3r_1^2)}{(r_0^2 - r_1^2)^3} \quad \text{for } r_1 < r < r_0, \quad (3.27)$$

$$S_m(r) = 0 \quad \text{for } r > r_0, \quad (3.28)$$

where  $r_1$  and  $r_0$  are the distances characterizing the start and the end of the QM region, applied within an interval of 0.2 Å to ensure a continuous change of forces at the transition between QM and MM regions.

### 3.13 ONIOM-XS MD technique

According to the conventional QM/MM MD technique, however, some unsolved problems have been demonstrated. First, only the exchanging particles which are crossings between the QM and MM regions are treated by a smoothing function, *i.e.*, not the whole particles in the QM region. With regards to this point, it is not reliable since immediate addition or deletion of a particle in the QM region due to the particle exchange also affects the forces acting on the remaining particles in the QM region. Thus, the conventional QM/MM MD simulation may provide numerical instability of forces whenever the particle exchange process occurs in the system. Second, the conventional scheme cannot clearly define the appropriate energy expression when particle exchange process occurs during the simulation.

To solve these problems, a more sophisticated QM/MM MD technique based on ONIOM-XS method has been proposed (Kerdcharoen and Morokuma, 2003). The ONIOM (Own N-layered Integrated molecular Orbital and molecular Mechanics) method was originally proposed by Morokuma *et al.* (Svensson *et al.*, 1996). The extension of the ONIOM method for the treatment of condensed-phase system was firstly applied by Kerdcharoen and co-worker, called ONIOM-XS (XS = eXtension to Solvation). Here, the term “ONIOM-XS MD” will be used throughout this work.

According to the ONIOM-XS MD technique, the system is comprised of a “high-level” QM sphere, *i.e.*, a sphere which contains the ion and its surrounding solvent molecules, and the remaining “low-level” MM bulk solvents. A thin switching shell located between the QM and MM regions is then introduced in order to smooth the transition due to the solvent exchange.

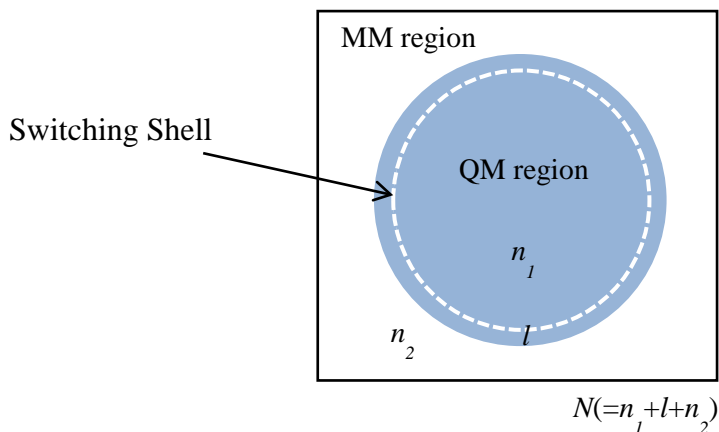


**Figure 3.6** Schematic diagram of the ONIOM-XS MD technique.

Given  $n_1$ ,  $l$  and  $n_2$  as number of particles in the QM sphere, the switching layer and the MM region, respectively, and  $N(= n_1+l+n_2)$  as the total number of particles, the potential energy of the system can be written in two ways based on the ONIOM extrapolation scheme (Svensson, Humbel, Froese, Matsubara, Sieber and Morokuma, 1996). If the switching layer is included into the high-level QM region, the energy expression is written as

$$E^{ONIOM}(n_1+l;N) = E^{QM}(n_1+l) - E^{MM}(n_1+l) + E^{MM}(N). \quad (3.29)$$

If the switching layer is considered as part of the “low-level” MM region, the energy expression is written as

$$E^{ONIOM}(n_1;N) = E^{QM}(n_1) - E^{MM}(n_1) + E^{MM}(N). \quad (3.30)$$

The potential energy of the entire system is taken as a hybrid between both energy terms (3.31) and (3.32),

$$E^{ONIOM-XS}(\{r_l\}) = (1 - \bar{s}(\{r_l\})) \cdot E^{ONIOM}(n_l + l; N) + \bar{s}(\{r_l\}) \cdot E^{ONIOM}(n_l; N), \quad (3.31)$$

where  $\bar{s}(\{r_l\})$  is an average over a set of switching functions for individual exchanging particle in the switching layer  $s_i(x_i)$ ,

$$\bar{s}(\{r_l\}) = \frac{1}{l} \sum_{i=1}^l s_i(x_i), \quad (3.32)$$

The switching function in equation (3.32) can have any form. In the present study, a polynomial form is employed,

$$s_i(x_i) = 6\left(x_i - \frac{1}{2}\right)^5 - 5\left(x_i - \frac{1}{2}\right)^3 + \frac{15}{8}\left(x_i - \frac{1}{2}\right) + \frac{1}{2}, \quad (3.33)$$

where  $x_i = ((r_i - r_0)/(r_1 - r_0))$ ,  $r_0$  and  $r_1$  are the radius of inner and outer surfaces of the switching shell, respectively, and  $r_i$  is the distance between the center of mass of the exchanging particle and the center of the QM sphere. The switching function has an S-shape and converges to 0 and 1 at  $r_0$  and  $r_1$ , respectively. The gradient of the energy can be written as

$$\begin{aligned} \nabla_R E^{ONIOM-XS}(\{r_l\}) &= (1 - \bar{s}(\{r_l\})) \cdot \nabla_R E^{ONIOM}(n_l + l; N) + \bar{s}(\{r_l\}) \\ &\quad \cdot \nabla_R E^{ONIOM}(n_l; N) + \frac{1}{(r_1 - r_0)} \nabla \bar{s}(\{r_l\}) \\ &\quad \cdot (E^{ONIOM}(n_l; N) - E^{ONIOM}(n_l + l; N)). \end{aligned} \quad (3.34)$$

### 3.14 Simulation details

All ONIOM-XS MD simulations have been performed in a canonical ensemble at 293 K with periodic boundary conditions. The system contains one  $\text{Li}^+$ , 163  $\text{H}_2\text{O}$  and 37  $\text{NH}_3$  molecules in a periodic box, with a box length of 18.56 Å. The QM size with diameter of 8.4 Å was chosen. All interactions inside the QM region were treated at Hartree-Fock (HF) level of accuracy using DZV (Part I) and DZP (Part II) basis sets. In this study, the HF method was selected since the correlated methods, even at the simple MP2 level, are still beyond our current computational facilities. Table A.2 summarizes the optimized geometries and stabilization energies of different  $\text{Li}^+(\text{H}_2\text{O})_m(\text{NH}_3)_n$  complexes, where  $m + n = 4$ , as obtained by various QM methods and basis sets. In addition, the comparisons of the stabilization energies, as well as the average Li-O and Li-N distances, of the optimized  $\text{Li}^+(\text{H}_2\text{O})_m(\text{NH}_3)_n$  complexes are also plotted in Figures 3.7-3.9. As compared to the results obtained by the B3LYP calculations, it is apparent that the HF method, although shows slightly weak ion-ligand interactions, produces the average ion-ligand distances in better agreement with those obtained by the correlated methods. In particular, the overestimations of the stabilization energies found in the B3LYP calculations clearly reflect in shortening of the Li-O and Li-N distances. Comparing the HF calculations using DZV and DZP basis sets, the observed differences could be expected due to the effect of polarization function in describing the structural and energetic properties of the  $\text{Li}^+(\text{H}_2\text{O})_m(\text{NH}_3)_n$  complexes. Thus, the effect of polarization function on the preferential solvation and dynamics of the  $\text{Li}^+$  ion in aqueous ammonia solution becomes another interesting subject in this study. Long-range interactions were treated using the reaction-field procedure (Adams, D.J., Adams, E.M. and Hill, 1979). The Newtonian

equations of motions were treated by a general predictor-corrector algorithm. The time step size was set to 0.2 fs. For each of the ONIOM-XS MD simulations, the system was initially equilibrated by performing the ONIOM-XS MD simulation for 20,000 time steps, followed by another 200,000 time steps to collect configurations every  $10^{\text{th}}$  step.

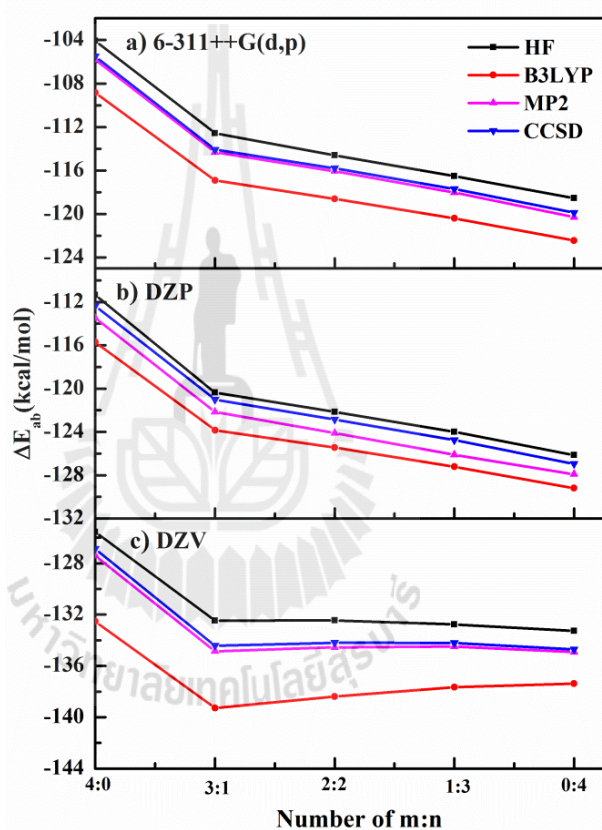


**Figure 3.7** Stabilization energies of different  $\text{Li}^+(\text{H}_2\text{O})_m(\text{NH}_3)_n$  complexes, where  $m + n = 4$ , as obtained by various QM levels of accuracy using a) 6-311++G(d,p), b) DZP and c) DZV basis sets, respectively.

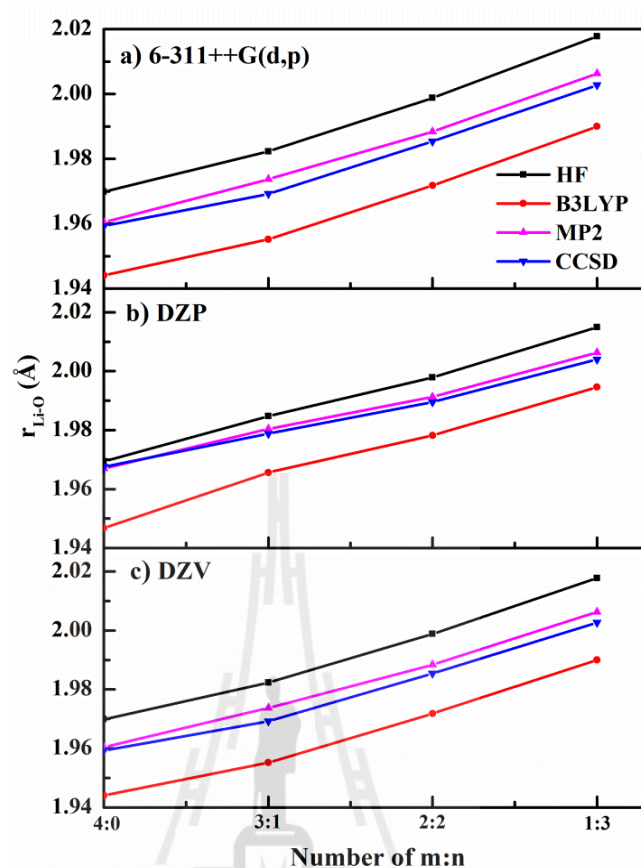


**Figure 3.8** Optimized Li-O distances of different  $\text{Li}^+(\text{H}_2\text{O})_m(\text{NH}_3)_n$  complexes, where  $m + n = 4$ , as obtained by various QM levels of accuracy using a) 6-311++G(d,p), b) DZP and c) DZV basis sets, respectively.

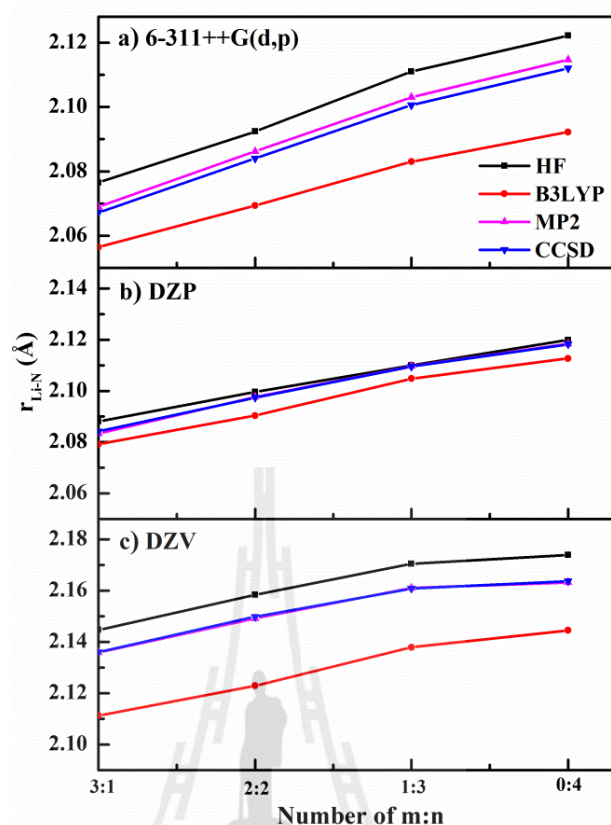


**Figure 3.9** Optimized Li-N distances of different  $\text{Li}^+(\text{H}_2\text{O})_m(\text{NH}_3)_n$  complexes, where  $m + n = 4$ , as obtained by various QM levels of accuracy using a) 6-311++G(d,p), b) DZP and c) DZV basis sets, respectively.

### 3.15 References

Ewald, P. P. (1921). Die berechnung optischer und elektrostatischer gitterpotentiale.

*Annalen der Physik.* 369: 253-287.

Foulkes, W. M. C. and Haydock, R. (1989). Tight-binding models and density-functional theory. *Physical Review B.* 39: 12520-12536.

Gear, C. W. (1971). **Numerical initial value problems in ordinary differential equations.** Englewood Cliffs, N.J.: Prentice-Hall.

Hockney, R. W. (1970). The potential calculation and some applications. *Methods in Computational Physics.* 9: 136-211.

- Kistenmacher, H., Popkie, H. and Clementi, E. (1974). Study of the structure of molecular complexes. VIII. Small clusters of water molecules surrounding  $\text{Li}^+$ ,  $\text{Na}^+$ ,  $\text{K}^+$ ,  $\text{F}^-$ , and  $\text{Cl}^-$  ions. **The Journal of Chemical Physics**. 61: 799-815.
- Svensson, M., Humbel, S., Froese, R. D. J., Matsubara, T., Sieber, S. and Morokuma, K. (1996). ONIOM: A multilayered integrated MO + MM method for geometry optimizations and single point energy predictions. A test for diels-alder reactions and  $\text{Pt}(\text{P}(t\text{-Bu})_3)_2 + \text{H}_2$  oxidative addition. **The Journal of Physical Chemistry**. 100: 19357-19363.
- Swope, W. C., Anderson, H. C., Berens, P. H. and Wilson, K. R. (1982). A computer simulation method for the calculation of equilibrium constants for the formation of physical clusters of molecules: Application to small water clusters. **Journal of Chemical Physics**. 53: 289-298.
- Verlet, L. (1967). Computer "experiments" on classical fluids. I. Thermodynamical properties of Lennard-Jones molecules. **Physical Review**. 159: 98-103.

## CHAPTER IV

# RESULTS AND DISCUSSION

According to the research objectives of this work, the results will be divided into two parts. First, the results obtained by the ONIOM-XS MD simulation will be compared to those derived by the conventional QM/MM MD scheme, and the observed discrepancies will be discussed with respect to the important treatment of the ONIOM-XS method in describing the behaviors of the solvated  $\text{Li}^+$  in aqueous ammonia solution. Second, the observed differences between the two ONIOM-XS MD simulations using the DZV and DZP basis sets will be discussed with respect to the effect of polarization function on the preferential solvation and dynamics of  $\text{Li}^+$  in such solvent mixture.

With regard to the present ONIOM-XS MD studies, it should be noted that the HF method and the DZV and DZP basis sets employed in the simulation were chosen as a compromise between the quality of the simulation results and the requirement of the CPU time. In general, it is known that the instantaneous electron correlation and the charge transfer effects are not typically well-described by the HF theory, and that the use of DZV and DZP basis sets could result in high basis set superposition error and an exaggeration of ligand-to-metal charge transfer. In this respect, the ONIOM-XS MD results should be discussed with caution (*i.e.*, they should not be over-interpreted).

#### 4.1 Preferential solvation and dynamics of $\text{Li}^+$ in aqueous ammonia solution: New insights through an ONIOM-XS MD simulation (Part I)

The structural properties of the solvated  $\text{Li}^+$  can be analyzed through a set of ion-ligand radial distribution functions (RDFs) and their corresponding integration numbers, as depicted in Figure 4.1, comparing the results as obtained by the ONIOM-XS and conventional QM/MM MD (Tongraar and Rode, 2008) simulations. Looking at Figure 4.1a, it is apparent that the characteristics of the Li-(N+O) RDFs obtained by the two simulation techniques are significantly different. As compared to the conventional QM/MM MD study (Tongraar and Rode, 2008), which reported a strong pronounced first Li-(N+O) RDF at 1.98 Å and a recognizable second peak centered at around 3.25 Å, the ONIOM-XS MD simulation reveals a broader and less pronounced first Li-(N+O) peak with a maximum exhibited at a slightly longer distance of 2.05 Å, together with a rather broad second peak in the region from 3 to 5 Å. With regard to the ONIOM-XS MD results, the shape and height of the first Li-(N+O) peak clearly suggests a less “structure-making” ability of  $\text{Li}^+$ . In addition, the observed broad and less defined second Li-(N+O) peak also implies a small influence of  $\text{Li}^+$  in ordering the solvent molecules in this shell. Hence, according to a relatively loose second solvation shell of  $\text{Li}^+$ , the structural parameters with respect to this shell are considered as a rough estimate, *i.e.*, the second minimum of all ion-ligand RDFs is assumed to be 5 Å throughout this work. According to Figure 4.1a, integrations up to first and second minimum of the Li-(N+O) RDF yield about 4 and 14 ligands in the first and second solvation shells of  $\text{Li}^+$ , respectively, compared to the corresponding values of 4 and ~4 ligands observed in the conventional QM/MM MD study

(Tongraar and Rode, 2008). Figures 4.1b and c separately plot the Li-O and Li-N RDFs and their corresponding integration numbers. In the conventional QM/MM MD study (Tongraar and Rode, 2008), since the first and second solvation shells of  $\text{Li}^+$  contain only water molecules, the characteristics of the first and second peaks in the Li-O RDF coincide with the respective peaks in the Li-(N+O) RDF. On the basis of the ONIOM-XS MD simulation, the characteristics of the Li-(N+O) RDF is regarded as a combination of the Li-O and Li-N RDFs. As can be seen in Figures 4.1b and c, the combination of rather well-defined first Li-O and Li-N peaks, with their maxima exhibited at slightly different distances of 1.95 and 2.10 Å, respectively, leads to a slightly broader and less pronounced first Li-(N+O) peak (cf. Figure 4.1a). Likewise, the observed broad second peak in the Li-(N+O) RDF can be ascribed to the combination of a broad second Li-O peak, with maximum at around 3.75 Å, and a recognizable second Li-N peak, with maximum at about 4.35 Å. According to the ONIOM-XS MD's Li-O and Li-N RDFs, it is obvious that  $\text{Li}^+$  can order both water and ammonia molecules to form its specific first and second solvation shells, with the water-to-ammonia ratios (*i.e.*, numbers of ligands according to integrations within the first and second peaks of the Li-O and Li-N RDFs) of about 3:1 and 11:3, respectively. In this work, the observed favorable  $\text{Li}^+[(\text{H}_2\text{O})_3\text{NH}_3][(\text{H}_2\text{O})_{11}(\text{NH}_3)_3]$  complex is in contrast to a clear water preference with the arrangement of the  $\text{Li}^+[(\text{H}_2\text{O})_4][(\text{H}_2\text{O})_4]$  type reported in the previous QM/MM MD study (Tongraar and Rode, 2008). These observed differences clearly point out that a more accurate simulation technique, like the ONIOM-XS MD, can provide more insights into the characteristics of  $\text{Li}^+$  in such a solvent mixture. Note that the results obtained by the ONIOM-XS MD simulation are also significantly different to the recent CP-MD

study, which reported a well-defined first solvation shell that contains only water molecules (Pratihari and Chandra, 2011). With regard to the CP-MD results, however, it should be realized that the simulation has been carried out in a relatively small system size, *i.e.*, in a cubic box with a box length of 9.95 Å, using a simple BLYP functional. In several cases, it has been shown that the results obtained by this technique are quite sensitive to the density functionals chosen, *i.e.*, several of them were found to overestimate the intermolecular interactions (Yoo, Zeng and Xantheas, 2009; VandeVondele, Mohamed, Krack, Hutter, Sprik and Parrinello, 2005; Lee and Tuckerman, 2007; Marx, Chandra and Tuckerman, 2010; Vuilleumier and Borgis, 1999). Consequently, the use of B3LYP functional is known to underestimate the diffusion values of species in aqueous media (Rode, Schwenk and Tongraar, 2004; VandeVondele, Mohamed, Krack, Hutter, Sprik and Parrinello, 2005).



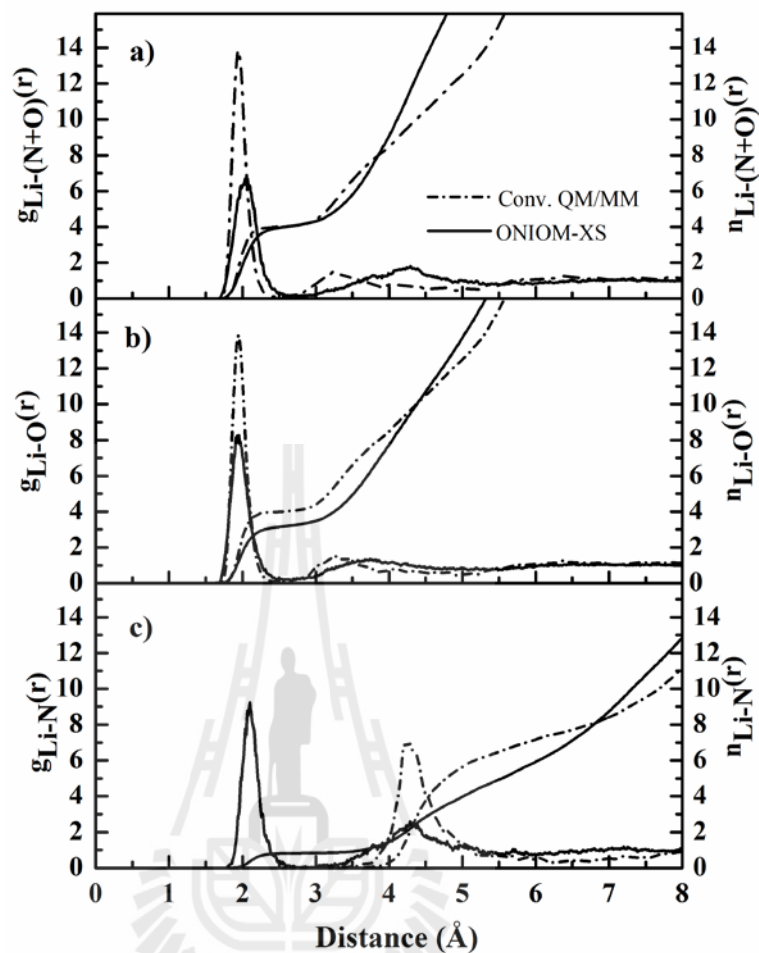


**Figure 4.1** a) Li-(N+O), b) Li-O and c) Li-N radial distribution functions and their corresponding integration numbers, as obtained by the conventional QM/MM and ONIOM-XS MD simulations.

The distributions of the number of ligands in the first solvation shell of  $\text{Li}^+$  are displayed in Figure 4.2. Based on the ONIOM-XS MD simulation, it is apparent that this ion favors a sole coordination number of 4 (cf. Figure 4.2a, with the probability distribution up to 86%), followed by 3 and 5 in small amounts. This implies a well-defined tetrahedral geometry of the first solvation shell of  $\text{Li}^+$ . According to Figures 4.2b and c, it could be demonstrated that ligand composition in the preferred 4-fold

coordinated complex favors a water-to-ammonia ratio of 3:1, which corresponds to a favorable  $\text{Li}^+(\text{H}_2\text{O})_3\text{NH}_3$  complex. Nevertheless, the distributions of the numbers of water and ammonia ligands that participated in the 4-fold coordinated complex of  $\text{Li}^+$  are found to deviate significantly from the ratio of 3:1. As can be seen in Figures 4.2b and c, the probability densities of finding 2 and 4 waters as well as 0 and 2 ammonia ligands become more visible, *i.e.*, compared to the observed deviations from the dominant number of 4 in Figure 2a. This supplies information that, although this ion strongly prefers a sole coordination number of 4, water and ammonia molecules in the first solvation shell of  $\text{Li}^+$  are somewhat labile, and that other different 4-fold coordinated complexes, such as  $\text{Li}^+(\text{H}_2\text{O})_4$  and  $\text{Li}^+(\text{H}_2\text{O})_2(\text{NH}_3)_2$ , can frequently be formed during the ONIOM-XS MD simulation.

According to Figure 4.2, the distributions of the number of ligands were obtained from the integrations up to first minimum of the Li-(N+O), Li-O and Li-N RDFs, respectively. In situation where the ion-ligand interactions are not too strong, *i.e.*, when compare to the interactions among solvent molecules, these distributions could be attributed partially to exchanges of solvent molecules (water and ammonia) between the nearest environment of the ion and the bulk solvents (cf. see Figures 4.5 and 4.6 in the next section). In the recent CP-MD study (Pratihari and Chandra, 2011), it has been reported that the water-ammonia interactions are quite strong when ammonia acts as an acceptor, *i.e.*, these HBs are found to live longer than water-water HBs.

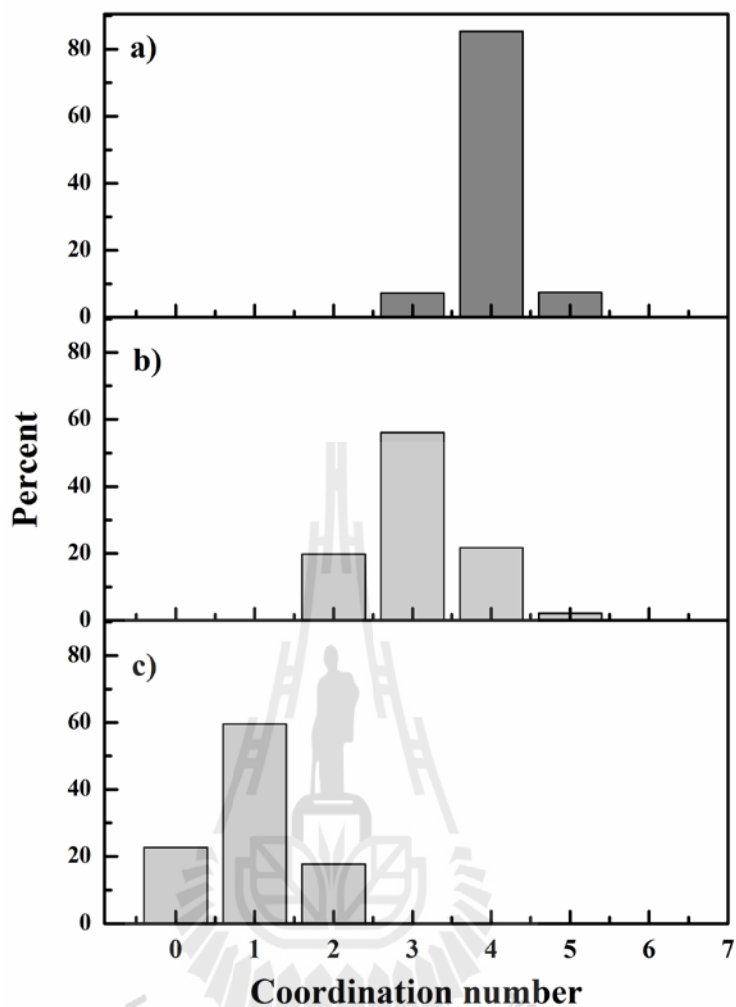


**Figure 4.2** Coordination number distributions, calculated up to first minimum of the  $\text{Li}^+$ -ligand RDFs: a)  $\text{Li}^+$ -( $\text{H}_2\text{O}+\text{NH}_3$ ), b)  $\text{Li}^+$ - $\text{H}_2\text{O}$  and c)  $\text{Li}^+$ - $\text{NH}_3$ .

The arrangement of ligands in the first solvation shell of  $\text{Li}^+$  can be analyzed from the plots of O-Li-N, O-Li-O and N-Li-N angular distributions, as shown in Figure 4.3. It is apparent that ligands in the first solvation shell of  $\text{Li}^+$  are arranged with respect to the preferred tetrahedral geometry, and with some degrees of flexibility, as can be seen from the broad peaks between  $80^\circ$  and  $140^\circ$ . Comparing to the distributions of the O-Li-O and O-Li-N angles, the observed narrower N-Li-N

angle between  $100^\circ$  and  $150^\circ$  can be described due to the stronger repulsion between the first-shell ammonia molecules, *i.e.*, a considerable amount of repulsive three-body effects at a short Li-N distance was found in the *ab initio* calculations of the  $\text{NH}_3\text{-Li}^+\text{-NH}_3$  complex (Tongraar, Hannongbua and Rode, 1997).

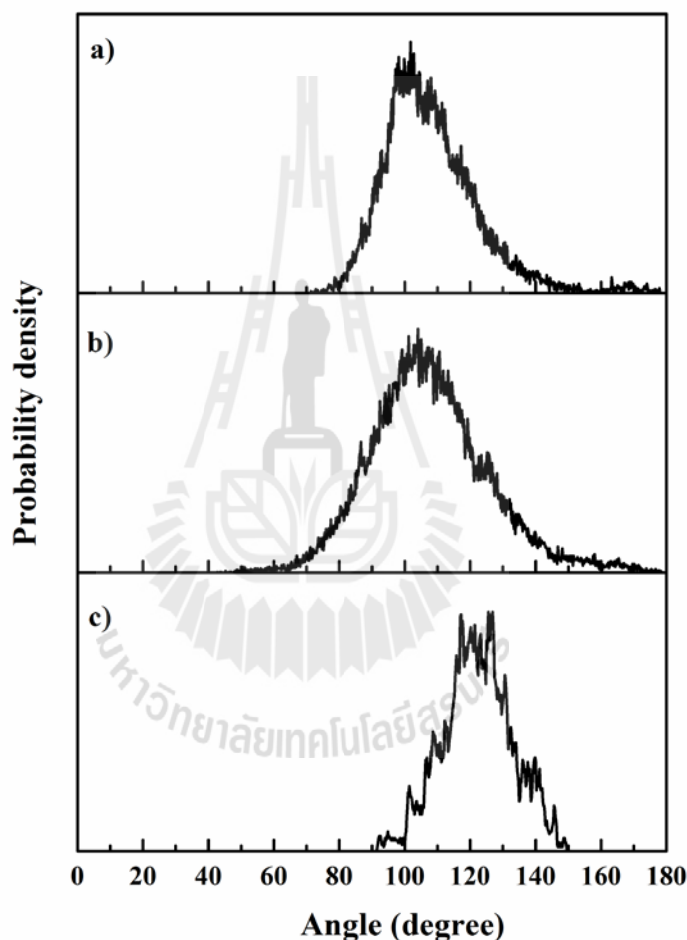


**Figure 4.3** Distributions of a) O-Li-N, b) O-Li-O and c) N-Li-N angles, calculated up to first minimum of the Li-(N+O) RDF.

Additional information on the arrangement of first-shell ligands can be gained from the plots of the  $\theta$  angle, defined by the dipole vector of the ligand molecules and

the Li---O and Li---N vectors, as depicted in Figure 4.4. Looking at Figure 4.4a, a broad peak between  $90^\circ$  and  $180^\circ$  clearly shows a high flexibility of the first-shell water's orientations. In contrast, the shape of the distribution peak in Figure 4.4b clearly reveals that ammonia molecules in the first solvation shell of  $\text{Li}^+$  stick more rigidly to their dipole-oriented configuration. According to Figure 4.4b, a recognizable shoulder between  $100^\circ$  and  $120^\circ$  suggests a higher flexibility of the first-shell ammonia's orientation, most probably influenced by their binding to solvent molecules in the second solvation shell.

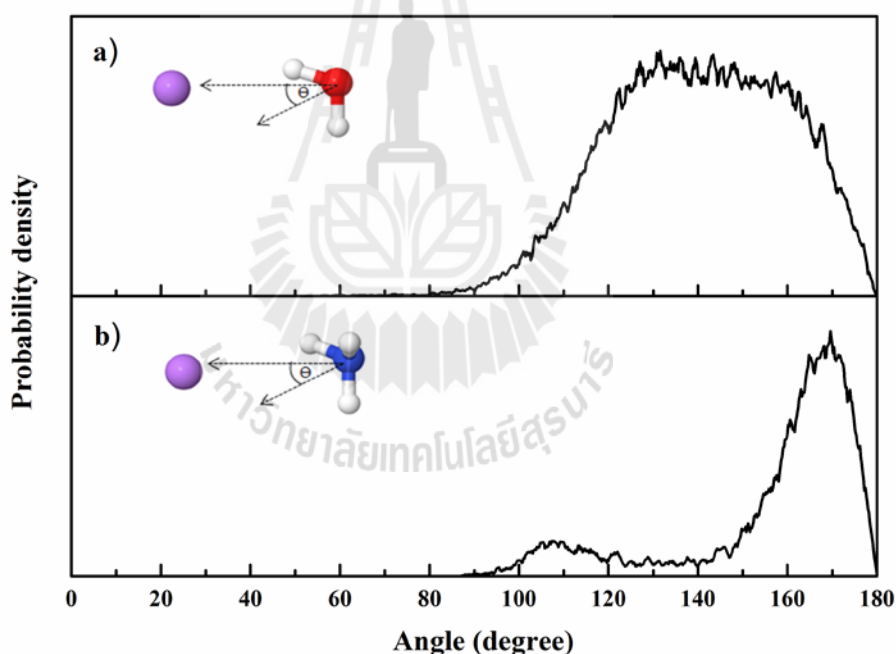


**Figure 4.4** Distributions of  $\theta$  angle in the first solvation shell of  $\text{Li}^+$ , calculated up to the first minimum of the Li-(N+O) RDF: a)  $\text{H}_2\text{O}$  and b)  $\text{NH}_3$ .

With regard to the qualitative expectation according to a hard and soft acid/base (HSAB) concept (Pearson, 1993; Komorowski, 1993),  $\text{Li}^+$  is classified as a

“hard” ion and it would prefer the “harder” water molecules over the “softer” ammonia ligands. In the course of the ONIOM-XS MD simulation, the favorable  $\text{Li}^+[(\text{H}_2\text{O})_3\text{NH}_3][(\text{H}_2\text{O})_{11}(\text{NH}_3)_3]$  complex is in good accord with the HSAB concept. In *ab initio* calculations of the  $\text{Li}^+\text{-H}_2\text{O}$  and  $\text{Li}^+\text{-NH}_3$  interactions, it has been shown that the global minima are not much different, namely 44.1 and 46.2 kcal.mol<sup>-1</sup>, respectively (Gao and Truhlar, 2002). This implies that an increase of ammonia ligands would result in an increase of the stabilization energy of the ion-ligand complexes. However, it should be realized that the larger ammonia ligands will experience more steric hindrance and thus will locate farther away from the ion than the smaller water molecules, *i.e.*, deviations from the dipole-oriented arrangement lead to much stronger repulsion forces in the case of ammonia than for water molecules (Gao and Truhlar, 2002).

By means of the ONIOM-XS MD simulation, the observed differences in the structural properties, *i.e.*, compared to those obtained by the conventional QM/MM MD study (Tongraar and Rode, 2008), can further be expected to reflect in different dynamics details of this solvated ion. With regard to the distributions of the ligand composition in the first solvation shell of  $\text{Li}^+$  (cf. Figures 4.2b and c), the arrangement of the preferred 4-fold coordinated complexes and the ligand exchange processes at the ion can be visualized through the plots of the Li-O and Li-N distances, as depicted in Figure 4.5.

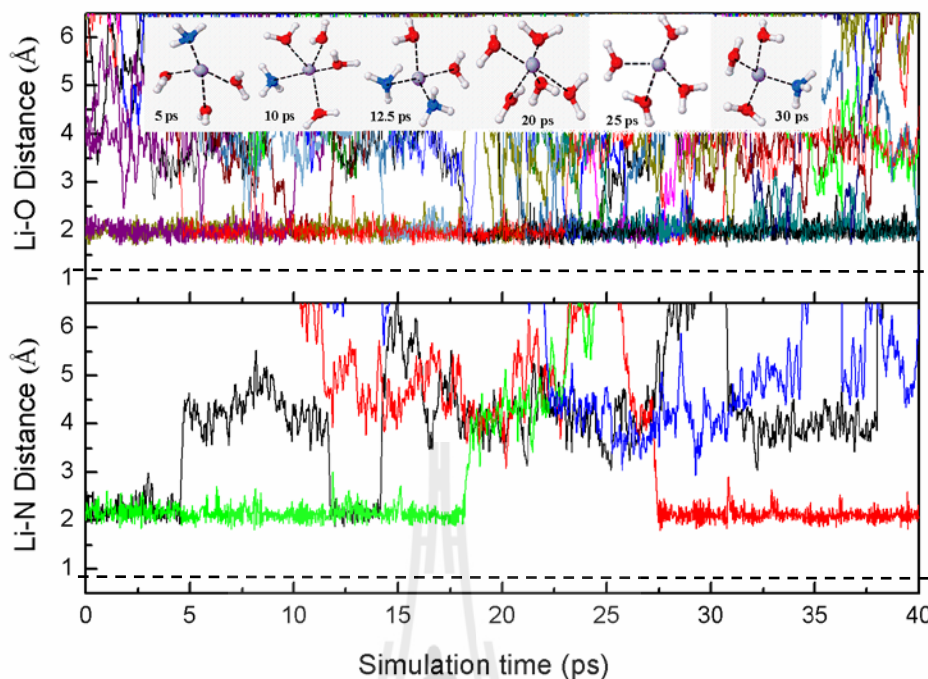


**Figure 4.5** Time dependence of Li-O (top) and Li-N (down) distances, as obtained from the 40 ps of the ONIOM-XS MD simulation.

In addition, the distributions of the numbers of first-shell ligands, calculated with respect to the first minimum of the Li-(N+O) RDF, are also plotted in Figure 4.6. Within the 40 ps of the ONIOM-XS MD data collection, it is apparent that the first solvation shell of  $\text{Li}^+$  is somewhat flexible and that this ion can order both water and ammonia molecules to form several 4-fold coordinated species, such as  $\text{Li}^+(\text{H}_2\text{O})_4$ ,  $\text{Li}^+(\text{H}_2\text{O})_3\text{NH}_3$  and  $\text{Li}^+(\text{H}_2\text{O})_2(\text{NH}_3)_2$ . In this respect, the arrangement of the 4-fold coordinated complexes with respect to the  $\text{Li}^+(\text{H}_2\text{O})_3\text{NH}_3$  structure is found to dominate over the  $\text{Li}^+(\text{H}_2\text{O})_4$  and  $\text{Li}^+(\text{H}_2\text{O})_2(\text{NH}_3)_2$  configurations, with the probability distributions of about 60%, 24% and 16%, respectively. Interestingly, as can be seen in Figures 4.5 and 4.6, it is observed that water molecules surrounding the

$\text{Li}^+$  ion are more labile than ammonia molecules, showing more frequency of water exchange processes during the 40 ps of the ONIOM-XS MD simulation.

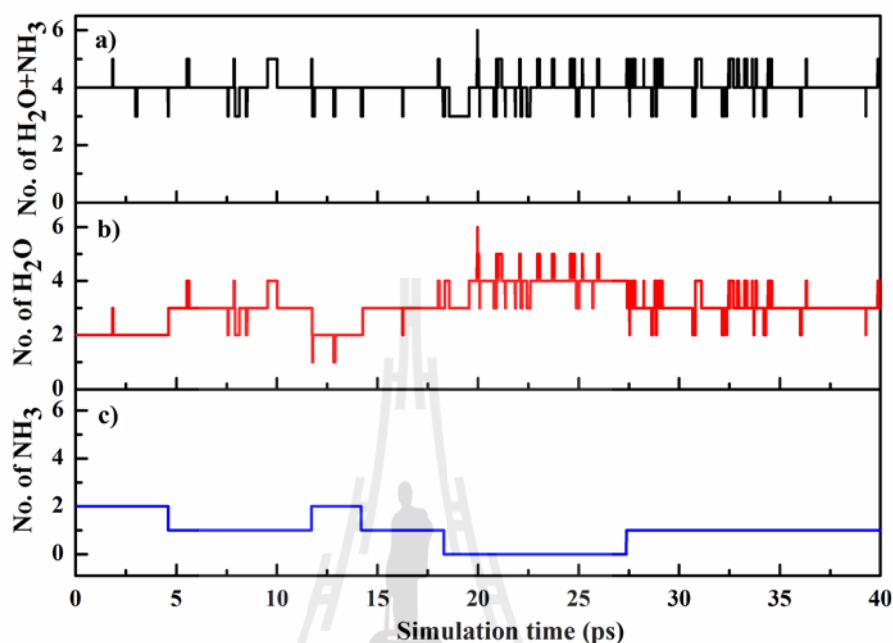


**Figure 4.6** Distributions of the number of first-shell ligands: a)  $\text{H}_2\text{O}+\text{NH}_3$ , b)  $\text{H}_2\text{O}$  and c)  $\text{NH}_3$ , calculated up to first minimum of the  $\text{Li}-(\text{N}+\text{O})$  RDF.

Regarding the ONIOM-XS MD results, it should be emphasized that the correct degree of lability of ligands in the solvation shells of  $\text{Li}^+$  is essential in order to understand the reactivity of  $\text{Li}^+$  in such a solvent mixture. The rates of ligand exchange processes in the first and second solvation spheres of  $\text{Li}^+$  were evaluated via the ligand mean residence times (MRTs), which were calculated using the “direct” method (Hofer, Tran, Schwenk and Rode, 2004), as the product of the average number of ligand molecules in the solvation sphere of ion with the duration of the simulation, divided by the observed number of exchange events lasting a given time interval  $t^*$ . In general, a  $t^*$  value of 0.0 ps is recommended as a good choice for the

estimation of H-bond lifetimes, and a value of 0.5 ps is proposed as a good measure for ligand exchange processes (Hofer, Tran, Schwenk and Rode, 2004). The calculated MRT data of ligand molecules in the first and second solvation shells of  $\text{Li}^+$  are summarized in Table 4.1, comparing the results to those obtained by the conventional QM/MM MD simulation (Tongraar and Rode, 2008). In addition, to provide useful discussion with respect to the “structure-making” ability of  $\text{Li}^+$ , the available MRT data for liquid water and ammonia obtained by the compatible ONIOM-XS and conventional QM/MM MD simulations were also given for comparison. With regard to both the conventional QM/MM (Tongraar and Rode, 2008) and ONIOM-XS MD simulations,  $\text{Li}^+$  clearly acts as a “structure-maker”, *i.e.*, the MRT values for ligands in the first solvation shell of  $\text{Li}^+$  are higher than the corresponding values observed in the pure solvent environments. However, it should be demonstrated that the ability of  $\text{Li}^+$  in ordering the structure of its surrounding ligands is much less than other stronger “structure-makers”, like  $\text{Mg}^{2+}$  or  $\text{Ca}^{2+}$  (Kerdcharoen, Liedl and Rode, 1996; Wanprakhon, Tongraar and Kerdcharoen, 2011). For example, according to the recent QM/MM MD studies of  $\text{Li}^+$ ,  $\text{Na}^+$ ,  $\text{K}^+$  and  $\text{Ca}^{2+}$  in aqueous solution (Rode, Schwenk and Tongraar, 2004; Hofer, Pribil and Randolph, 2008), the MRT values for first-shell waters were reported to be of 11, 2.4, 2.1 and 40 ps, respectively. In our previous ONIOM-XS MD studies (Wanprakhon, Tongraar and Kerdcharoen, 2011), the MRT values for water molecules in the first hydration shell of  $\text{K}^+$  and  $\text{Ca}^{2+}$  were reported to be of 1.80 and 21.7 ps, respectively. With regard to the QM/MM and ONIOM-XS MD results, since such simulations have been performed only for 30-40 ps (not many exchange processes can be observed) and only for one ion (assuming a very dilute solution), these data could be considered

as rough estimates for relative comparison, *i.e.*, they cannot be directly compared to the experimental observations. Note, for example, that the experimental estimation for MRT of first-shell water ligands at  $\text{Ca}^{2+}$  is  $\sim 10^{-7}$ - $10^{-9}$  s (Helm and Merbach, 1999; Lincoln and Merbach, 1995), while the QM/MM and ONIOM-XS MD simulations deliver  $0.04 \times 10^{-9}$  and  $0.02 \times 10^{-9}$  s, respectively. On the basis of the ONIOM-XS MD simulation,  $\text{Li}^+$  is able to order both water and ammonia molecules in its surrounding to form its specific complexes, and the MRT values for first-shell ligands reveal a clear order of  $t_{\text{NH}_3} > t_{\text{H}_2\text{O}}$ , *i.e.*, by about 4 and 2 times for  $t^* = 0.0$  and 0.5 ps, respectively. This can be ascribed to the higher binding energy of  $\text{Li}^+$  to ammonia ligands than to waters, *i.e.*, when  $\text{Li}^+$  is located near the global minimum of the corresponding interaction energy surface. According to the data in Table 4.1, it is apparent that the MRT data for water and ammonia ligands in the second solvation shell of  $\text{Li}^+$  are not much different to those for pure solvents, indicating a small influence of  $\text{Li}^+$  in ordering its surrounding ligands beyond the first solvation shell. Overall, as compared to the conventional QM/MM MD study (Tongraar and Rode, 2008), the observed differences in both the preferential solvation and the dynamical details of the solvated  $\text{Li}^+$  clearly confirm the elegant treatment of the ONIOM-XS MD technique in providing more detailed knowledge of such a complicated system.

**Table 4.1** Mean residence times (MRTs) of solvated ligands and of pure solvents, as obtained by the conventional QM/MM and ONIOM-XS MD simulations.

System	$t_{\text{sim}}$	ligand	CN	$t^* = 0.0$ ps		$t^* = 0.5$ ps	
				$N_{\text{ex}}^{0.0}$	$\tau^{0.0}$	$N_{\text{ex}}^{0.5}$	$\tau^{0.5}$
<b>Conv. QM/MM MD</b>							
Li <sup>+</sup> in H <sub>2</sub> O+NH <sub>3</sub> <sup>a</sup>	20.0	H <sub>2</sub> O (1 <sup>st</sup> shell)		58	1.38	19	4.21
4.0				382	0.22	41	2.05
		H <sub>2</sub> O (2 <sup>nd</sup> shell)	4.2	-	0.19	-	1.78
Liq. H <sub>2</sub> O <sup>b</sup>				-	0.33	-	1.62
Liq. NH <sub>3</sub> <sup>c</sup>							
<b>ONIOM-XS MD</b>							
Li <sup>+</sup> in H <sub>2</sub> O+NH <sub>3</sub> <sup>d</sup>	40.0	H <sub>2</sub> O (1 <sup>st</sup> shell)		151	0.82	33	3.76
3.1				2109	0.20	273	1.57
				11	3.27	5	7.20
		H <sub>2</sub> O (2 <sup>nd</sup> shell)	10.7	585	0.20	59	1.97
		NH <sub>3</sub> (1 <sup>st</sup> shell)	0.9	-	0.23	-	2.17
		NH <sub>3</sub> (2 <sup>nd</sup> shell)	2.9				
Liq. H <sub>2</sub> O <sup>e</sup>							

<sup>a</sup> (Tongraar and Rode, 2008)

<sup>b</sup> (Hofer, Tran, Schwenk and Rode, 2004)

<sup>c</sup> (Rode, Schwenk and Tongraar, 2004)

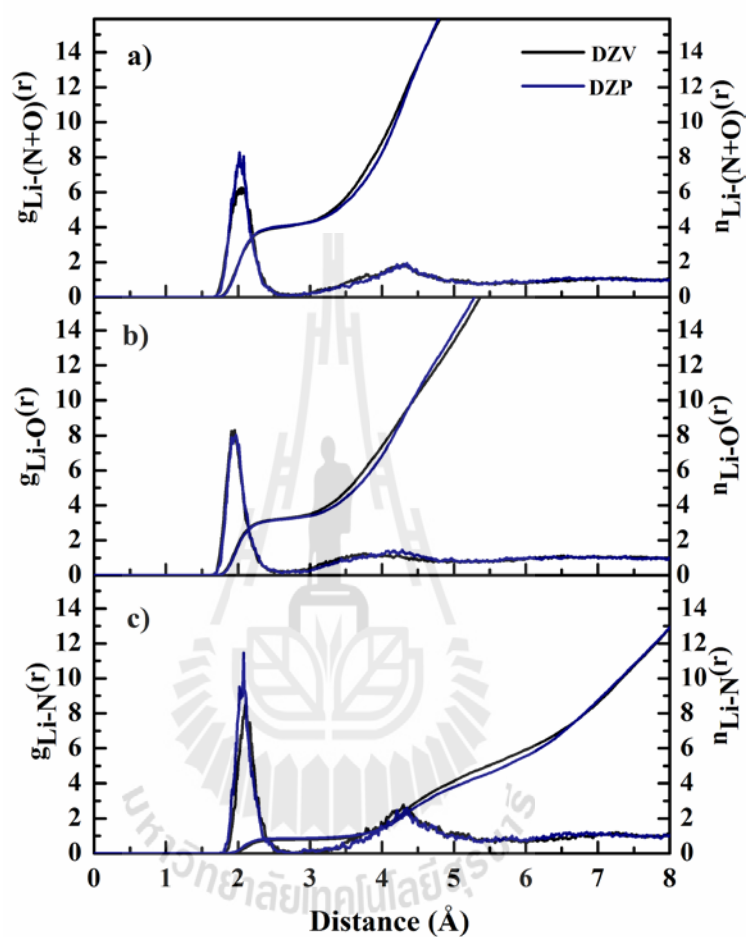
<sup>d</sup> (Present study)

<sup>e</sup> (Thaomola, Tongraar and Kerdcharoen, 2012)

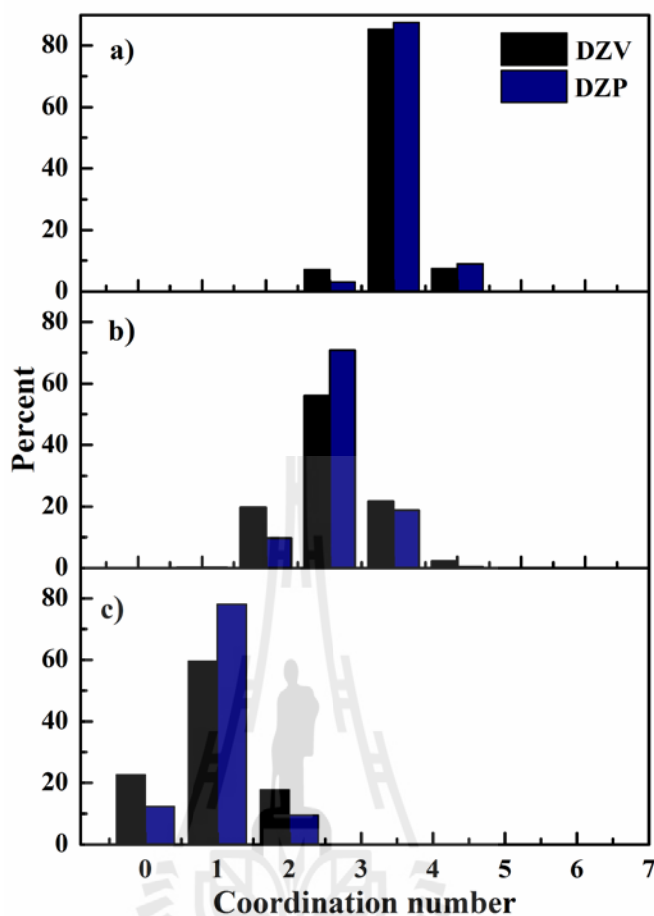
## 4.2 The effect of polarization function on the preferential solvation and dynamics of $\text{Li}^+$ in aqueous ammonia solution (Part II)

In this part, another ONIOM-XS MD simulation has been performed with the same simulation protocol as employed in the part I. A significant change is made by using a larger DZP basis set, *i.e.*, instead of the DZV. The objective of this part is to investigate the effect of polarization function on the preferential solvation and dynamics of  $\text{Li}^+$  in aqueous ammonia solution. Figure 4.7 displays the ion-ligand RDFs and their corresponding integration numbers, comparing the results as obtained by the ONIOM-XS MD simulations using the DZV and DZP basis sets. According to the plots in Figure 4.7, it is apparent that the structural properties of the solvated  $\text{Li}^+$  obtained by the two ONIOM-XS MD simulations are not much different, *i.e.*, in terms of the coordination number and the ligand composition within the first solvation shell. As compared to the ONIOM-XS MD simulation using the DZV basis set, however, the later one suggests that the use of DZP basis set reflects in slightly more pronounced first Li-(N+O) and Li-N peaks. In this respect, it could be demonstrated that the inclusion of polarization function enhances the  $\text{Li}^+$ - $\text{NH}_3$  interactions, leading to a slightly more structured of the ion-ligand complexes. The distributions of the number of ligands in the first solvation shell of  $\text{Li}^+$ , as obtained by the two ONIOM-XS MD simulations are displayed in Figure. 4.8. Obviously, the use of DZP basis set also predicts the similar ligand composition in the preferred 4-fold coordinated complex, *i.e.*, with the water-to-ammonia ratio of 3:1. However, as can be seen in Figure 4.8, the probability densities of finding 2 and 4 waters as well as 0 and 2 ammonia ligands become less visible, *i.e.*, compared to the ONIOM-XS MD

simulation using the DZV basis set. This corresponds to the observed more pronounced first peaks of the Li-(N+O) and Li-N RDFs (cf. Figure 4.7).



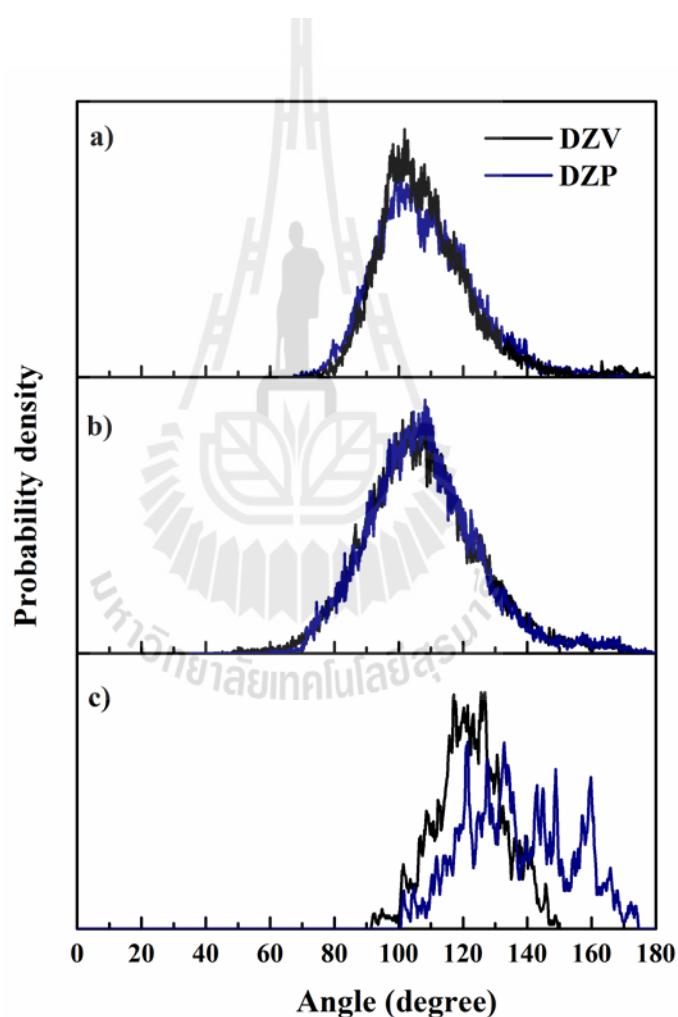
**Figure 4.7** a) Li-(N+O), b) Li-O and c) Li-N radial distribution functions and their corresponding integration numbers, as obtained by the ONIOM-XS MD simulations using the DZV and DZP basis sets.



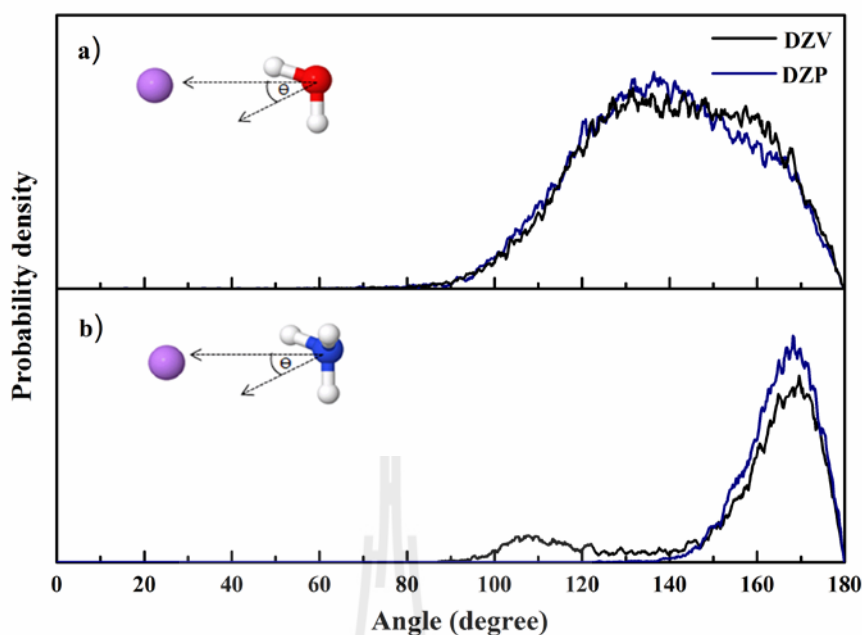
**Figure 4.8** Coordination number distributions, calculated up to first minimum of the  $\text{Li}^+$ -ligand RDFs: a)  $\text{Li}^+$ -( $\text{H}_2\text{O}+\text{NH}_3$ ), b)  $\text{Li}^+$ -( $\text{H}_2\text{O}$ ) and c)  $\text{Li}^+$ -( $\text{NH}_3$ ), as obtained by the ONIOM-XS MD simulations using the DZV and DZP basis sets.

Figure 4.9 shows the arrangement of ligands in the first solvation shell of  $\text{Li}^+$ , *i.e.*, in terms of O-Li-N, O-Li-O and N-Li-N angular distributions, comparing the results as obtained by the ONIOM-XS MD simulations using the DZV and DZP basis sets. In addition, the distributions of the  $\theta$  angle, defined by the dipole vector of the ligand molecules and the Li---O and Li---N vectors, are also plotted in Figure 4.10. Overall, it is apparent that the results obtained by the ONIOM-XS MD simulations using the DZV and DZP basis sets are not much different. With regard to Figure 4.9c,

the observed broader N-Li-N peak in the ONIOM-XS MD simulation using the DZP basis set is in accord with the observed less visible of the probability of finding 2 ammonia molecules (cf. Figure 4.8c). In Figure 4.10b, the ONIOM-XS MD simulation using the DZP basis set clearly reveals that ammonia molecules in the first solvation shell of  $\text{Li}^+$  stick more rigidly to the dipole-oriented arrangement than those obtained in the ONIOM-XS MD simulation using the DZV basis set.



**Figure 4.9** Distributions of a) O-Li-N, b) O-Li-O and N-Li-N angles, calculated up to first minimum of the Li-(N+O) RDFs, as obtained by the ONIOM-XS MD simulations using the DZV and DZP basis sets.



**Figure 4.10** Distributions of  $\theta$  angle in the first solvation shell of  $\text{Li}^+$ , calculated up to the first minimum of the Li-(N+O) RDF: a)  $\text{H}_2\text{O}$  and b)  $\text{NH}_3$ , as obtained by the ONIOM-XS MD simulations using the DZV and DZP basis sets.

The calculated MRT data of ligand molecules in the first and second solvation shells of  $\text{Li}^+$ , comparing the results as obtained by the ONIOM-XS MD simulations using the DZV and DZP basis sets, are summarized in Table 4.2. Comparing the two ONIOM-XS MD results, it is apparent that the inclusion of the polarization function, *i.e.*, regarding the ONIOM-XS MD simulation using the DZP basis set, results in slight differences of the MRT data. In this respect, it could be demonstrated that the effect of the polarization function is marginal (negligible) in obtaining the detailed descriptions of  $\text{Li}^+$  in aqueous ammonia solution. Consequently, in situation where the computational facilities are rather limited, the selection of the DZV basis set can be considered as an acceptable choice for the study of this particular system.

**Table 4.2** Mean residence times (MRTs) of solvated ligands, as obtained by the ONIOM-XS MD simulations using the DZV and DZP basis sets.

System	$t_{\text{sim}}$	ligand	CN	$t^* = 0.0$ ps		$t^* = 0.5$ ps	
				$N_{\text{ex}}^{0.0}$	$\tau^{0.0}$	$N_{\text{ex}}^{0.5}$	$\tau^{0.5}$
<b>ONIOM-XS MD (DZV)</b>							
Li <sup>+</sup> in H <sub>2</sub> O+NH <sub>3</sub>	40.0	H <sub>2</sub> O (1 <sup>st</sup> shell)		151	0.82	33	3.76
3.1				2109	0.20	273	1.57
		H <sub>2</sub> O (2 <sup>nd</sup> shell)	10.7	11	3.27	5	7.20
		NH <sub>3</sub> (1 <sup>st</sup> shell)	0.9	585	0.20	59	1.97
		NH <sub>3</sub> (2 <sup>nd</sup> shell)	2.9				
<b>ONIOM-XS MD (DZP)</b>							
Li <sup>+</sup> in H <sub>2</sub> O+NH <sub>3</sub>	32.8	H <sub>2</sub> O (1 <sup>st</sup> shell)		115	0.88	25	3.06
3.1				1677	0.22	263	1.38
		H <sub>2</sub> O (2 <sup>nd</sup> shell)	11.0	9	3.50	5	6.31
		NH <sub>3</sub> (1 <sup>st</sup> shell)	1.0	392	0.30	60	1.93
		NH <sub>3</sub> (2 <sup>nd</sup> shell)	3.5				

### 4.3 References

- Bopp, P. (1986). A study of the vibrational motions of water in an aqueous CaCl<sub>2</sub> solution. **The Journal of Chemical Physics**. 106: 205-212.
- Clementi, E., Kistenmacher, H., Kołos, W. and Romano, S. (1980). Non-additivity in water-ion-water interactions. **Theoretica Chimica Acta**. 55: 257-266.
- Gao, J. L. and Truhlar, D. G. (2002). **Annual Review of Physical Chemistry**. 53: 467.
- Helm, L. and Merbach, A. E. (1999). **Coordination Chemistry Reviews**. 187: 151.

- Hofer, T. S., Tran, H. T., Schwenk, C. F. and Rode, B. M. (2004). Characterization of dynamics and reactivities of solvated ions by *ab initio* simulations. **Journal of Computational Chemistry**. 25: 211-217.
- Hofer, T. S., Pribil, A. B. and Randolph, B. R. (2008). Capabilities of chemical simulation methods in the elucidation of structure and dynamics of solutions. **Pure and Applied Chemistry**. 80: 1195-1210.
- Kerdcharoen, T. and Hannongbua, S. (1999). *Ab initio* study of ion-ammonia complexes: Geometry and many-body interactions. **Chemical Physics Letters**. 310: 333.
- Kerdcharoen, T., Liedl, K. R. and Rode, B. M. (1996). A QM/MM simulation method applied to the solution of  $\text{Li}^+$  in liquid ammonia. **The Journal of Chemical Physics**. 211: 313-323.
- Kistenmacher, H., Popkie, H. and Clementi, E. (1974). Study of the structure of molecular complexes. VIII. Small clusters of water molecules surrounding  $\text{Li}^+$ ,  $\text{Na}^+$ ,  $\text{K}^+$ ,  $\text{F}^-$ , and  $\text{Cl}^-$  ions. **The Journal of Chemical Physics**. 61:799-815.
- Kollman, P. A. and Kuntz, I. D., (1974). Hydration number of lithium(1+) ion. **Journal of the American Chemical Society**. 96: 4766-4769.
- Komorowski, L. (1993). Structure and bonding. **Springer-Verlag**. Berlin-Heidelberg, Germany. 80: 45.
- Lee, H.-S. and Tuckerman, M. E. (2007). Dynamical properties of liquid water from *ab initio* molecular dynamics performed in the complete basis set limit. **The Journal of Chemical Physics**. 126: 164501-164516.
- Lincoln, S. F. and Merbach, A. E. (1995). **Advances in Inorganic Chemistry**, Academic Press Inc. 42: P.1.

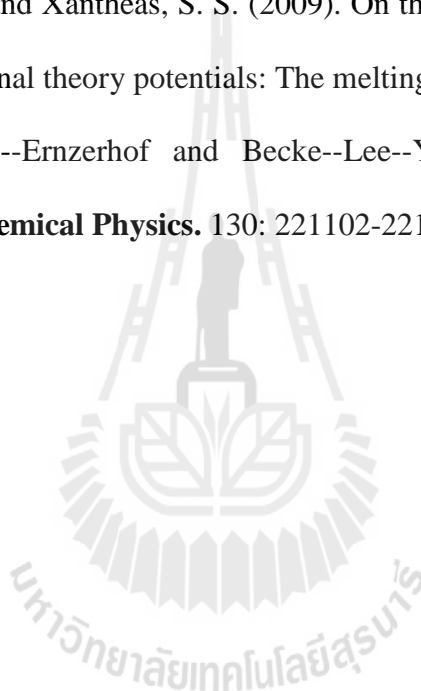
- Lybrand, T. P. and Kollman, P. A. (1985). Water-water and water-ion potential functions including terms for many body effects. **The Journal of Chemical Physics**. 83: 2923-2933.
- Marx, D., Chandra, A. and Tuckerman M. E. (2010). Aqueous basic solutions: Hydroxide solvation, structural diffusion, and comparison to the hydrated proton. **Chemical Reviews**. 110: 2174.
- Ortega-Blake, I., Novaro, O., Les, A. and Rybak, S., (1982). A molecular orbital study of the hydration of ions. The role of nonadditive effects in the hydration shells around  $Mg^{2+}$  and  $Ca^{2+}$  **The Journal of Chemical Physics**. 76: 5405.
- Pearson, R. G. (1993). Chemical hardness: A historical introduction. **Springer-Verlag**, Berlin, Heidelberg. Vol.80 : p.1.
- Probst, M. M., Spohr, E., Heinzinger, K. and Bopp, P. (1991). A molecular dynamics simulation of an aqueous beryllium chloride solution. **Molecular Simulation**. 7: 43-57.
- Pratihari, S. and Chandra, A. (2011). A first principles molecular dynamics study of lithium atom solvation in binary liquid mixture of water and ammonia: Structural, electronic, and dynamical properties. **The Journal of Chemical Physics**. 134: 024519.
- Rode, B. M., Schwenk, C. F. and Tongraar, A. (2004). Structure and dynamics of hydrated ions—new insights through quantum mechanical simulations. **Journal of Molecular Liquids**. 110: 105-122.
- Thaomola, S., Tongraar, A. and Kerdcharoen, T. (2012). Insights into the structure and dynamics of liquid water: A comparative study of conventional QM/MM

- and ONIOM-XS MD simulations. **Journal of Molecular Liquids**. 174: 26-33.
- Tongraar, A., Liedl, K. R. and Rode, B. M. (1997). Solvation of  $\text{Ca}^{2+}$  in water studied by Born-Oppenheimer *ab initio* QM/MM dynamics. **The Journal of Physical Chemistry A**. 101: 6299-6309.
- Tongraar, A., Liedl, K. R. and Rode, B. M. (1998). Born–Oppenheimer *ab initio* QM/MM dynamics simulations of  $\text{Na}^+$  and  $\text{K}^+$  in water: From structure making to structure breaking effects. **The Journal of Physical Chemistry A**. 102: 10340-10347.
- Tongraar, A. and Rode, B. M. (2008). The role of second shell quantum effects on the preferential solvation of  $\text{Li}^+$  in aqueous ammonia: An extended *ab initio* QM/MM MD simulation with enlarged QM region. **Chemical Physics Letters**. 466: 61-64.
- Tuckerman, M. E., Marx, D., Klein, M. L. and Parrinello, M. (1997). On the quantum nature of the shared proton in hydrogen bonds. **Science**. 275: 817-820.
- VandeVondele, J., Mohamed, F., Krack, M., Hutter, J., Sprik, M., and Parrinello, M. (2005). The influence of temperature and density functional models in *ab initio* molecular dynamics simulation of liquid water. **The Journal of Chemical Physics**. 122: 014515.
- Vuilleumier, R. and Borgis, D. (1999). Transport and spectroscopy of the hydrated proton: A molecular dynamics study. **The Journal of Chemical Physics**. 111: 4251-4266.
- Wanprakhon, S., Tongraar, A. and Kerdcharoen, T. (2011). Hydration structure and dynamics of  $\text{K}^+$  and  $\text{Ca}^{2+}$  in aqueous solution: Comparison of conventional

QM/MM and ONIOM-XS MD simulations. **Chemical Physics Letters**. 517: 171-175.

Xenides, D., Randolf, B. R. and Rode, B. M. (2005). Structure and ultrafast dynamics of liquid water: A quantum mechanics/molecular mechanics molecular dynamics simulations study. **The Journal of Chemical Physics**. 122:174506-174516.

Yoo, S., Zeng, X. C. and Xantheas, S. S. (2009). On the phase diagram of water with density functional theory potentials: The melting temperature of ice  $I_h$  with the Perdew--Burke--Ernzerhof and Becke--Lee--Yang—Parr functionals. **The Journal of Chemical Physics**. 130: 221102-221104.



## CHAPTER V

### CONCLUSION

In this work, more sophisticated ONIOM-XS MD simulations have been performed to investigate the preferential solvation and dynamics of  $\text{Li}^+$  in aqueous ammonia solution. In part I, an ONIOM-XS MD simulation was applied with the same simulation protocol as employed in the recent conventional QM/MM MD study. The main objective of this part was to test the validity of the conventional QM/MM MD scheme for obtaining the detailed descriptions of  $\text{Li}^+$  solvated in such a solvent mixture, *i.e.*, by comparing the ONIOM-XS MD results with those obtained by the conventional ONIOM-XS MD framework. As compared to the conventional QM/MM MD study, which predicted that the first and second solvation shells of  $\text{Li}^+$  consist exclusively of water molecules with the arrangement of the  $\text{Li}^+[(\text{H}_2\text{O})_4][(\text{H}_2\text{O})_4]$  type, the ONIOM-XS MD simulation clearly indicated that this ion can order both water and ammonia molecules to form a favorable  $\text{Li}^+[(\text{H}_2\text{O})_3\text{NH}_3][(\text{H}_2\text{O})_{11}(\text{NH}_3)_3]$  configuration. Of particular interest was that the “structure-making” ability of  $\text{Li}^+$  is not too strong and that the first solvation shell of  $\text{Li}^+$  is somewhat flexible, so that different 4-fold coordinated species, such as  $\text{Li}^+(\text{H}_2\text{O})_4$ ,  $\text{Li}^+(\text{H}_2\text{O})_3\text{NH}_3$  and  $\text{Li}^+(\text{H}_2\text{O})_2(\text{NH}_3)_2$ , could be converted back and forth. In addition, evidence was gained that the second solvation shell of  $\text{Li}^+$  is less structured, indicating a small influence of  $\text{Li}^+$  in ordering the ligand molecules in this shell. The observed discrepancy between the conventional QM/MM and ONIOM-XS MD result clearly confirmed that the more sophisticated simulation techniques, such

as the ONIOM-XS MD, offer advanced performance for the study of such a condensed-phase system.

In the second part of this study, another ONIOM-XS MD simulation has been performed with the same simulation protocol as employed in part I. A significant change was made by using a larger DZP basis set, *i.e.*, instead of the DZV. The objective here was to investigate the effect of polarization function on the preferential solvation and dynamics of  $\text{Li}^+$  in aqueous ammonia solution. It was observed that the results obtained by the ONIOM-XS MD simulations using the DZV and DZP basis sets are quite similar. This suggested that the effect of polarization function is marginal (negligible) for this particular system, *i.e.*, the use of the DZV basis set (in part I) is a promising choice in order to reduce the CPU time. In this context, it should be noted that, when the computational facilities become more powerful, further improvement of the ONIOM-XS MD results can be achieved by using higher *ab initio* correlated methods, such as MP2, together with the use of a larger QM size and basis set.



**APPENDICES**

## APPENDIX A

### THEORETICAL OBSERVATIONS

**Table A.1** Comparison of some structural parameters for  $\text{Li}^+$  solvation in aqueous ammonia solution

Methods	$R_{\text{Li-O}}$ (Å)	$R_{\text{Li-N}}$ (Å)	Number of $\text{H}_2\text{O} : \text{NH}_3$	CN	Year	Reference
Pair potential MC	1.95	2.50	4 : 2	6.0	1989	Kheawsrikul <i>et al.</i>
Pair potential MD	2.00	2.10	3 : 3	6.0	1999	Tongraar <i>et al.</i>
QM/MM MD (Small QM)	1.94	2.08	3 : 1	4.0	1999	Tongraar <i>et al.</i>
QM/MM MD (Larger QM)	1.98	-	4 : 0	4.0	2008	Tongraar <i>et al.</i>
CP-MD	1.96	-	4 : 0	4.0	2011	Pratihari <i>et al.</i>

**Table A.2** Optimized geometries and stabilization energies of  $\text{Li}^+(\text{H}_2\text{O})_m(\text{NH}_3)_n$  complexes, where  $m + n = 4$ , as obtained by various QM methods and basis sets.

Methods	Complex	$R_{\text{Li-O}} (\text{\AA})$			$R_{\text{Li-N}} (\text{\AA})$			$\Delta E_{\text{ab}}(\text{kcal.mol}^{-1})$		
		6-311++G(d,p)	DZP	DZV	6-311++G(d,p)	DZP	DZV	6-311++G(d,p)	DZP	DZV
HF	$\text{Li}^+\text{-w}_4$	1.9699	1.9694	1.9699	-	-	-	-104.08	-111.35	-125.57
	$\text{Li}^+\text{-w}_3\text{-am}_1$	1.9823	1.9847	1.9823	2.0765	2.0881	2.1447	-112.57	-120.37	-132.46
	$\text{Li}^+\text{-w}_2\text{-am}_2$	1.9988	1.9979	1.9988	2.0924	2.0996	2.1584	-114.60	-122.14	-132.46
	$\text{Li}^+\text{-w}_1\text{-am}_3$	2.0178	2.0149	2.0178	2.1110	2.1100	2.1705	-116.51	-123.99	-132.76
	$\text{Li}^+\text{-am}_4$	-	-	-	2.1222	2.1199	2.1739	-118.55	-126.14	-133.28
B3LYP	$\text{Li}^+\text{-w}_4$	1.9441	1.9468	1.9441	-	-	-	-108.85	-115.71	-132.53
	$\text{Li}^+\text{-w}_3\text{-am}_1$	1.9552	1.9656	1.9552	2.0565	2.0792	2.1113	-116.92	-123.84	-139.27
	$\text{Li}^+\text{-w}_2\text{-am}_2$	1.9718	1.9782	1.9718	2.0694	2.0904	2.1229	-118.61	-125.45	-138.39
	$\text{Li}^+\text{-w}_1\text{-am}_3$	1.9900	1.9946	1.9900	2.0830	2.1048	2.1379	-120.40	-127.22	-137.65
	$\text{Li}^+\text{-am}_4$	-	-	-	2.0922	2.1127	2.1245	-122.43	-129.20	-137.39
MP2	$\text{Li}^+\text{-w}_4$	1.9604	1.9670	1.9604	-	-	-	-105.81	-113.50	-127.42
	$\text{Li}^+\text{-w}_3\text{-am}_1$	1.9737	1.9804	1.9737	2.0690	2.0834	2.1359	-114.32	-122.16	-134.86
	$\text{Li}^+\text{-w}_2\text{-am}_2$	1.9884	1.9913	1.9884	2.0862	2.0976	2.1491	-116.06	-124.11	-134.54
	$\text{Li}^+\text{-w}_1\text{-am}_3$	2.0063	2.0063	2.0063	2.1030	2.1097	2.1611	-118.02	-126.12	-134.49
	$\text{Li}^+\text{-am}_4$	-	-	-	2.1147	2.1184	2.1632	-120.29	-127.91	-134.93
CCSD	$\text{Li}^+\text{-w}_4$	1.9593	1.9675	1.9593	-	-	-	-105.51	-112.37	-126.87
	$\text{Li}^+\text{-w}_3\text{-am}_1$	1.9692	1.9788	1.9692	2.0672	2.0842	2.1360	-114.08	-121.00	-134.42
	$\text{Li}^+\text{-w}_2\text{-am}_2$	1.9854	1.9895	1.9854	2.0840	2.0974	2.1498	-115.79	-122.85	-134.20
	$\text{Li}^+\text{-w}_1\text{-am}_3$	2.0027	2.0040	2.0027	2.1006	2.1095	2.1608	-117.70	-124.75	-134.22
	$\text{Li}^+\text{-am}_4$	-	-	-	2.1120	2.1182	2.1637	-119.89	-126.95	-134.70

## APPENDIX B

### LIST OF PRESENTATIONS

1. Pilailuk Kabbalee and Anan Tongraar. (March 27-29, 2013). The role of many-body interactions in  $\text{Li}^+(\text{H}_2\text{O})_M(\text{NH}_3)_N$  complexes, where  $M+N = 4$ , and the preferential solvation of  $\text{Li}^+$  in water+ammonia mixture (Oral presentation). **The 17<sup>th</sup> International Annual Symposium on Computational Science and Engineering (ANSCSE17)**. Khon Kaen University, Khon Kaen, Thailand.
2. Pilailuk Kabbalee and Anan Tongraar. (July 23-28, 2013). Solvation structure and dynamics of  $\text{Li}^+$  in water + ammonia mixture studied by ab initio QM/MM MD simulation based on ONIOM-XS method (Poster presentation). **7<sup>th</sup> Conference of the Asian Consortium on Computational Materials Science (ACCMS-7)**. Suranaree University of Technology, Nakhonratchasima, Thailand.
3. Pilailuk Kabbalee and Anan Tongraar. (January 8-10, 2014). Characteristics of  $\text{Li}^+$  and  $\text{Na}^+$  in aqueous ammonia solutions studied by ab initio QM/MM MD Simulations based on ONIOM-XS Method (Poster presentation). **Pure and Applied Chemistry International Conference 2014 (PACCON2014)**. Centara hotel and Convention Centre, Khon Kaen, Thailand.

# APPENDIX C

## PUBLICATION

Chemical Physics 446 (2015) 70–75



Contents lists available at ScienceDirect

Chemical Physics

journal homepage: [www.elsevier.com/locate/chemphys](http://www.elsevier.com/locate/chemphys)



### Preferential solvation and dynamics of $\text{Li}^+$ in aqueous ammonia solution: An ONIOM-XS MD simulation study



Pilailuk Kabbalee<sup>a</sup>, Anan Tongraar<sup>a,\*</sup>, Teerakiat Kerdcharoen<sup>b</sup>

<sup>a</sup>School of Chemistry, Institute of Science, Suranaree University of Technology and NANOTEC-SUT Center of Excellence on Advanced Functional Nanomaterials, Nakhon Ratchasima 30000, Thailand

<sup>b</sup>Department of Physics and NANOTEC Center of Excellence, Faculty of Science, Mahidol University, Bangkok 10400, Thailand

#### ARTICLE INFO

Article history:  
Received 7 June 2014  
In final form 13 November 2014  
Available online 18 November 2014

Keywords:  
Preferential solvation  
ONIOM-XS  
Molecular dynamics  
QM/MM

#### ABSTRACT

A more sophisticated quantum mechanics/molecular mechanics (QM/MM) molecular dynamics (MD) technique based on the ONIOM-XS method, called the ONIOM-XS MD, has been applied for studying the characteristics of  $\text{Li}^+$  in an aqueous ammonia solution. As compared to the conventional QM/MM MD study, which predicts a clear water preference with the arrangement of the  $\text{Li}^+[(\text{H}_2\text{O})_4][(\text{H}_2\text{O})_4]$  type, the ONIOM-XS MD simulation clearly reveals that this ion can order both water and ammonia molecules to form the preferred  $\text{Li}^+[(\text{H}_2\text{O})_3\text{NH}_3][(\text{H}_2\text{O})_{11}(\text{NH}_3)_3]$  complex. Of particular interest, it is observed that the “structure-making” ability of  $\text{Li}^+$  is not too strong and that the first solvation shell of  $\text{Li}^+$  is somewhat flexible, in which other different 4-fold coordinated species, such as  $\text{Li}^+(\text{H}_2\text{O})_4$  and  $\text{Li}^+(\text{H}_2\text{O})_2(\text{NH}_3)_2$ , can frequently be formed. In addition, it is found that the second solvation shell of  $\text{Li}^+$  is less structured, implying a small influence of  $\text{Li}^+$  in ordering the solvent molecules in this shell.

© 2014 Elsevier B.V. All rights reserved.

#### 1. Introduction

During the past decades, a so-called combined quantum mechanics/molecular mechanics (QM/MM) molecular dynamics (MD) technique has been successfully applied for studying various systems [1–15]. This technique partitions the system into a part described by quantum mechanics (QM) and another part treated by means of classical molecular mechanical (MM) force fields. By this scheme, the complicated many-body interactions as well as the polarization effects, i.e., at least within the defined QM region, can be reliably included. In the course of QM/MM MD simulations of condensed phase systems [5–15], since the exchange of solvent molecules between the QM and MM regions can occur frequently, a smoothing function [16] is employed to ensure a smooth change of forces at the transition between the QM and MM regions. Here, a term “conventional QM/MM MD” will refer to the MD simulation technique based on this QM/MM approach. With regard to the conventional QM/MM MD technique, however, the smoothing function is applied only for the exchanging particles that are crossing the QM/MM boundary. Of course, this is not satisfactory since an interchange of particles between the QM and MM regions will also affect the forces acting on the remaining QM particles. In

addition, the conventional QM/MM MD framework cannot clearly define the system's energy expression during the solvent exchange process [17,18].

To improve these methodical weaknesses, a more sophisticated QM/MM MD technique based on the ONIOM-XS (Own N-layered Integrated molecular Orbital and molecular Mechanics – eXtension to Solvation) method, called briefly the ONIOM-XS MD, has been proposed [17,18]. By the ONIOM-XS MD technique, the forces on all QM particles will be smoothed during the particle exchanges and, thus, it better defines the system's energy expression. In particular, it is worth noting that this technique allows both energies and forces to be smoothed, whereas only forces were taken into account through the conventional QM/MM MD scheme. The ONIOM-XS MD technique has been applied, firstly, for the systems of  $\text{Li}^+$  and  $\text{Ca}^{2+}$  in liquid ammonia [17,18], and, later, for the systems of aqueous  $\text{Na}^+$ ,  $\text{K}^+$  and  $\text{Ca}^{2+}$  solutions [19,20] and pure water [21]. In all cases, as compared to the conventional QM/MM MD studies, the ONIOM-XS MD technique clearly reveals its capability in providing more reliable results which are in better agreement with experiments. For example, according to a comparative study of the conventional QM/MM and ONIOM-XS MD simulations of pure water [21], the ONIOM-XS MD results clearly pointed out that the structural arrangement of liquid water with respect to 4 HBs decreases significantly and that the distributions of 2- and 3-fold HB species becomes more visible. These observed phenomena are in good accord with recent experimental observations [22,23],

\* Corresponding author. Fax: +66 44 224017.  
E-mail address: [anan\\_tongraar@yahoo.com](mailto:anan_tongraar@yahoo.com) (A. Tongraar).

which reported considerable amounts of 2- and 3-fold HB clusters in liquid water. In the cases of Na<sup>+</sup> and K<sup>+</sup> in aqueous solutions [19,20], the results obtained by the ONIOM-XS MD simulations have provided more insights into the contrasting behaviors of these two ions with respect to their “structure-making” and “structure-breaking” abilities.

Besides the study of ions in pure solvents, the investigations of ions solvated in solvent mixtures have also been a topic of special interest since detailed knowledge of such systems has been utilized for many chemical and biological processes [24]. Under the environment of multiple solvent species, the ability of ions to preferentially order their solvent components, i.e., in order to form their specific solvation complexes, depends crucially on the strength of the binding energies between the ions and the solvent molecules, and is usually discussed in terms of preferential solvation. In this work, the ONIOM-XS MD technique will be employed for studying the preferential solvation and dynamics of Li<sup>+</sup> in an aqueous ammonia solution. In fact, the details with respect to the preferential solvation of this ion have been explored by both Monte Carlo (MC) and MD simulations using either classical MM, combined QM/MM or purely QM models. Regarding the prior MC simulation [25], it has been shown that the use of pair potentials (which neglects the effects of many-body contributions) had led to wrong prediction on the solvation structure of Li<sup>+</sup>, as well as on the ligand composition of the first and second solvation shells [8,26]. On the basis of the QM/MM MD approach, an early attempt has been made by using a small QM size (i.e., a QM region not comprising the second solvation shell), supplying information that Li<sup>+</sup> prefers to order its surrounding ligands to form a Li<sup>+</sup>[(H<sub>2</sub>O)<sub>2</sub>NH<sub>3</sub>][(H<sub>2</sub>O)<sub>4</sub>(NH<sub>3</sub>)<sub>2</sub>] complex [8]. Later, an extended QM/MM MD simulation using a relatively larger QM size has been revisited, which predicted a clear water preference with an arrangement of the Li<sup>+</sup>[(H<sub>2</sub>O)<sub>4</sub>][(H<sub>2</sub>O)<sub>4</sub>] type [26]. Recently, a Car–Parrinello (CP) MD simulation of Li<sup>+</sup> in a water–ammonia mixture has been carried out, which also reported the preference of only water molecules in a nearly tetrahedral arrangement of the first solvation shell of Li<sup>+</sup> [27]. By means of the CP-MD technique, however, it is widely known that some methodical drawbacks come from the use of simple generalized gradient approximation (GGA) functionals, such as BLYP and PBE, and of the relatively small system size [28,29]. With regard to the aforementioned limits of both the conventional QM/MM and CP-MD approaches, it is of particular interest, therefore, to apply the ONIOM-XS MD technique in order to provide more detailed description of this system. In this study, we focus on a comparative study between the conventional QM/MM and ONIOM-XS MD simulations, i.e., the observed differences derived by means of the ONIOM-XS MD technique will be shown and discussed with respect to the validity of the conventional QM/MM MD scheme.

## 2. Methods

By the ONIOM-XS MD technique [17–21], the system is divided into a “high-level” QM region, i.e., a sphere which includes the central Li<sup>+</sup> and its nearest-neighbor ligands, and the remaining “low-level” MM subsystem. A thin switching layer inserted between the QM and MM regions is employed to check the exchanging particles and help in smoothing the energy and forces of the combined system. In this respect, three parameters, namely  $n_1$ ,  $l$  and  $n_2$ , are defined as the number of particles involved in the QM region, the switching layer and the MM region, respectively, and  $N$  is set as the total number of particles (i.e.,  $N = n_1 + l + n_2$ ). Based on the ONIOM extrapolation scheme [30], the potential energy of the system can be written in two ways. First, if the switching layer is included into the high-level QM region, the energy expression is written as

$$E^{\text{ONIOM}}(n_1 + l; N) = E^{\text{QM}}(n_1 + l) - E^{\text{MM}}(n_1 + l) + E^{\text{MM}}(N). \quad (1)$$

Otherwise, if the switching layer is considered as part of the “low-level” MM subsystem, the energy expression is

$$E^{\text{ONIOM}}(n_1; N) = E^{\text{QM}}(n_1) - E^{\text{MM}}(n_1) + E^{\text{MM}}(N). \quad (2)$$

According to Eqs. (1) and (2), the  $E^{\text{QM}}$  and  $E^{\text{MM}}$  terms represent the interactions derived by the QM calculations and by the classical MM force fields, respectively. In addition, it should be noted that the interactions between the QM and MM regions are also described by means of MM potentials, and thus, these contributions are already included in the  $E^{\text{MM}}(N)$ . In the course of the ONIOM-XS MD simulation, when a particle moves into the switching layer (either from the QM or MM region), both Eqs. (1) and (2) must be evaluated. Then, the potential energy of the entire system can be expressed as a hybrid between both energy terms (1) and (2),

$$E^{\text{ONIOM-XS}}(\{r_i\}) = (1 - \bar{s}(\{r_i\})) \cdot E^{\text{ONIOM}}(n_1 + l; N) + \bar{s}(\{r_i\}) \cdot E^{\text{ONIOM}}(n_1; N), \quad (3)$$

where  $\bar{s}(\{r_i\})$  is an average over a set of switching functions for individual exchanging particles in the switching layer  $s_i(x_i)$ ,

$$\bar{s}(\{r_i\}) = \frac{1}{l} \sum_{i=1}^l s_i(x_i), \quad (4)$$

In general, the switching function applied in Eq. (4) can be of any form. In this study, a polynomial expression is employed,

$$s_i(x_i) = 6 \left( x_i - \frac{1}{2} \right)^5 - 5 \left( x_i - \frac{1}{2} \right)^3 + \frac{15}{18} \left( x_i - \frac{1}{2} \right) + \frac{1}{2}, \quad (5)$$

where  $x_i = ((r_i - r_0)/(r_1 - r_0))$ , and  $r_0$  and  $r_1$  are the radius of the inner and outer surfaces of the switching shell, respectively, and  $r_i$  is the distance between the center of mass of the exchanging particle and the center of the QM sphere. Note that the above polynomial form and parameter sets were derived to have an S-shape that converges to 0 and 1 at  $r_0$  and  $r_1$ , respectively [17]. Finally, the gradient of the energy can be written as

$$\begin{aligned} \nabla_r E^{\text{ONIOM-XS}}(\{r_i\}) &= (1 - \bar{s}(\{r_i\})) \cdot \nabla_r E^{\text{ONIOM}}(n_1 + l; N) \\ &+ \bar{s}(\{r_i\}) \cdot \nabla_r E^{\text{ONIOM}}(n_1; N) \\ &+ \frac{1}{(r_1 - r_0)} \nabla \bar{s}(\{r_i\}) \\ &\cdot (E^{\text{ONIOM}}(n_1; N) - E^{\text{ONIOM}}(n_1 + l; N)). \end{aligned} \quad (6)$$

The ONIOM-XS MD technique does improve the methodical drawbacks of the conventional QM/MM MD framework, although it has been shown that this sophisticated treatment does not eliminate all smoothing errors [31]. In this respect, the postulated advantages of the ONIOM-XS method over the conventional QM/MM scheme can be described in terms of the quantitative differences of the simulation results. To reliably compare the results with those obtained by the conventional QM/MM MD scheme, the present ONIOM-XS MD simulation was performed with the same simulation conditions as employed in the previous QM/MM MD study [26]. Note that the details with respect to the QM/MM MD simulation protocols can be found in literature [5,6]. In this respect, a QM radius of 4.2 Å and a switching width of 0.2 Å were chosen, which correspond to the ONIOM-XS parameters  $r_0$  and  $r_1$  of 4.2 and 4.4 Å, respectively. As compared to the recent QM/MM MD study [26], these parameters correspond to the start and the end of the QM radius, i.e., a defined QM/MM boundary where the smoothing applies. Inside the QM region, all interactions were treated at the Hartree–Fock (HF) level of accuracy using double

zeta valence basis sets [32]. In this work, all QM calculations were carried out using the Gaussian03 program [33]. For interactions within the MM and between the QM and MM regions, flexible models, which describe inter- and intramolecular interactions, were employed for water [34,35] and ammonia [36]. The pair potential functions for describing water–ammonia interactions were adopted from Tanabe and Rode [37], and those for describing ion–water and ion–ammonia interactions were obtained from our previous works [1,38]. Long-range interactions were treated using the reaction-field procedure [39]. The ONIOM-XS MD simulation was performed in a canonical ensemble at 293 K with a time step of 0.2 fs. The system's temperature was kept constant using the Berendsen algorithm [40]. The periodic cubic box, with a box length of 18.56 Å, employed in the simulations contained one ion, 37 ammonia and 163 water molecules, assuming the experimental density of 18.4% aqueous ammonia at the given temperature. The initial system's configuration was taken from a classical MD simulation that was performed for 100 ps using MM potentials [5,34–38]. The ONIOM-XS MD simulation was performed with re-equilibration for 15 ps, followed by another 40 ps to collect configurations every 10th step.

### 3. Results and discussion

The structural properties of the solvated  $\text{Li}^+$  can be analyzed through a set of ion–ligand radial distribution functions (RDFs) and their corresponding integration numbers, as depicted in Fig. 1, comparing the results as obtained by the ONIOM-XS and conventional QM/MM MD [26] simulations. Looking at Fig. 1a, it is apparent that the characteristics of the Li–(N+O) RDFs obtained by the two simulation techniques are significantly different.

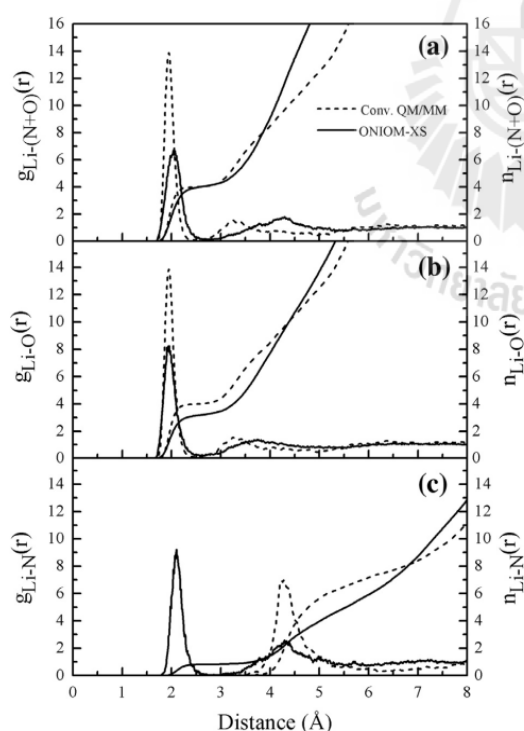
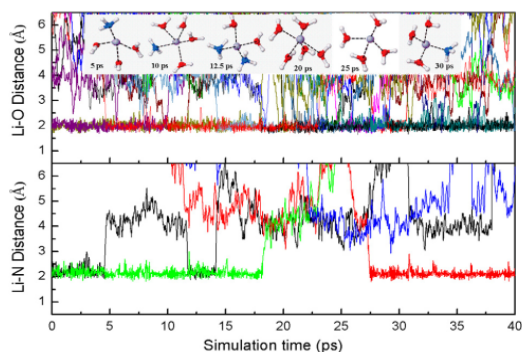


Fig. 1. (a) Li–(N+O), (b) Li–O and (c) Li–N radial distribution functions and their corresponding integration numbers, as obtained by the conventional QM/MM and ONIOM-XS MD simulations.

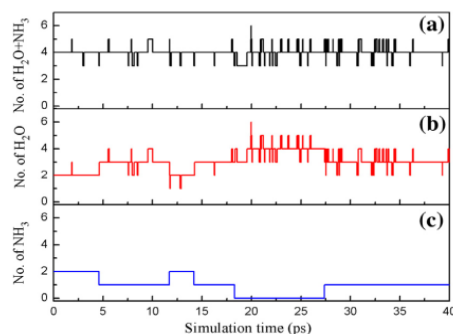
As compared to the conventional QM/MM MD study [26], which reported a strong pronounced first Li–(N+O) RDF at 1.98 Å and a recognizable second peak centered at around 3.25 Å, the ONIOM-XS MD simulation reveals a broader and less pronounced first Li–(N+O) peak with a maximum exhibited at a slightly longer distance of 2.05 Å, together with a rather broad second peak in the region from 3 to 5 Å. With regard to the ONIOM-XS MD results, the shape and height of the first Li–(N+O) peak clearly suggests a less “structure-making” ability of  $\text{Li}^+$ . In addition, the observed broad and less defined second Li–(N+O) peak also implies a small influence of  $\text{Li}^+$  in ordering the solvent molecules in this shell. Hence, according to a relatively loose second solvation shell of  $\text{Li}^+$ , the structural parameters with respect to this shell are considered as a rough estimate, i.e., the second minimum of all ion–ligand RDFs is assumed to be 5 Å throughout this work. According to Fig. 1a, integrations up to first and second minimum of the Li–(N+O) RDF yield about 4 and 14 ligands in the first and second solvation shells of  $\text{Li}^+$ , respectively, compared to the corresponding values of 4 and ~4 ligands observed in the conventional QM/MM MD study [26].

Fig. 1b and c separately plot the Li–O and Li–N RDFs and their corresponding integration numbers. In the conventional QM/MM MD study [26], since the first and second solvation shells of  $\text{Li}^+$  contain only water molecules, the characteristics of the first and second peaks in the Li–O RDF coincide with the respective peaks in the Li–(N+O) RDF. On the basis of the ONIOM-XS MD simulation, the characteristics of the Li–(N+O) RDF is regarded as a combination of the Li–O and Li–N RDFs. As can be seen in Fig. 1b and c, the combination of rather well-defined first Li–O and Li–N peaks, with their maxima exhibited at slightly different distances of 1.95 and 2.10 Å, respectively, leads to a slightly broader and less pronounced first Li–(N+O) peak (cf. Fig. 1a). Likewise, the observed broad second peak in the Li–(N+O) RDF can be ascribed to the combination of a broad second Li–O peak, with maximum at around 3.75 Å, and a recognizable second Li–N peak, with maximum at about 4.35 Å. According to the ONIOM-XS MD's Li–O and Li–N RDFs, it is obvious that  $\text{Li}^+$  can order both water and ammonia molecules to form its specific first and second solvation shells, with the water-to-ammonia ratios (i.e., numbers of ligands according to integrations within the first and second peaks of the Li–O and Li–N RDFs) of about 3:1 and 11:3, respectively. In this work, the observed favorable  $\text{Li}^+[(\text{H}_2\text{O})_3\text{NH}_3][(\text{H}_2\text{O})_{11}(\text{NH}_3)_3]$  complex is in contrast to a clear water preference with the arrangement of the  $\text{Li}^+[(\text{H}_2\text{O})_4][(\text{H}_2\text{O})_4]$  type reported in the previous QM/MM MD study [26]. These observed differences clearly point out that a more accurate simulation technique, like the ONIOM-XS MD, can provide more insights into the characteristics of  $\text{Li}^+$  in such a solvent mixture. Note that the results obtained by the ONIOM-XS MD simulation are also significantly different to the recent CP-MD study, which reported a well-defined first solvation shell that contains only water molecules [27]. With regard to the CP-MD results, however, it should be realized that the simulation has been carried out in a relatively small system size, i.e., in a cubic box with a box length of 9.95 Å, using a simple BLYP functional. In several cases, it has been shown that the results obtained by this technique are quite sensitive to the density functionals chosen, i.e., several of them were found to overestimate the intermolecular interactions [28,29,41–43]. Consequently, the use of B3LYP functional is known to underestimate the diffusion values of species in aqueous media [10,29].

The distributions of the number of ligands in the first solvation shell of  $\text{Li}^+$  are displayed in Fig. 2. Based on the ONIOM-XS MD simulation, it is apparent that this ion favors a sole coordination number of 4 (cf. Fig. 2a, with the probability distribution up to 86%), followed by 3 and 5 in small amounts. This implies a well-defined tetrahedral geometry of the first solvation shell of  $\text{Li}^+$ .



**Fig. 5.** Time dependence of Li–O (top) and Li–N (down) distances, as obtained from the 40 ps of the ONIOM-XS MD simulation.



**Fig. 6.** Distributions of the number of first-shell ligands: (a)  $\text{H}_2\text{O} + \text{NH}_3$ , (b)  $\text{H}_2\text{O}$  and (c)  $\text{NH}_3$ , calculated up to first minimum of the Li–(N + O) RDF.

exchange processes at the ion can be visualized through the plots of the Li–O and Li–N distances, as depicted in Fig. 5. In addition, the distributions of the numbers of first-shell ligands, calculated with respect to the first minimum of the Li–(N + O) RDF, are also plotted in Fig. 6. Within the 40 ps of the ONIOM-XS MD data collection, it is apparent that the first solvation shell of  $\text{Li}^+$  is somewhat flexible and that this ion can order both water and ammonia molecules to form several 4-fold coordinated species, such as  $\text{Li}^+(\text{H}_2\text{O})_4$ ,  $\text{Li}^+(\text{H}_2\text{O})_3\text{NH}_3$  and  $\text{Li}^+(\text{H}_2\text{O})_2(\text{NH}_3)_2$ . In this respect, the arrangement of the 4-fold coordinated complexes with respect to the  $\text{Li}^+(\text{H}_2\text{O})_3\text{NH}_3$  structure is found to dominate over the  $\text{Li}^+(\text{H}_2\text{O})_4$  and  $\text{Li}^+(\text{H}_2\text{O})_2(\text{NH}_3)_2$  configurations, with the probability distributions of about 60%, 24% and 16%, respectively. Interestingly, as can be seen in Figs. 5 and 6, it is observed that water molecules surrounding the  $\text{Li}^+$  ion are more labile than ammonia molecules, showing more frequency of water exchange processes during the 40 ps of the ONIOM-XS MD simulation.

Regarding the ONIOM-XS MD results, it should be emphasized that the correct degree of lability of ligands in the solvation shells of  $\text{Li}^+$  is essential in order to understand the reactivity of  $\text{Li}^+$  in such a solvent mixture. The rates of ligand exchange processes in the first and second solvation spheres of  $\text{Li}^+$  were evaluated via the ligand mean residence times (MRTs), which were calculated using the “direct” method [47], as the product of the average number of ligand molecules in the solvation sphere of ion with the duration of the simulation, divided by the observed number of exchange events lasting a given time interval  $t^*$ . In general, a  $t^*$  value of 0.0 ps is recommended as a good choice for the estimation of H-bond lifetimes, and a value of 0.5 ps is proposed as a good measure for ligand exchange processes [47]. The calculated MRT data of

ligand molecules in the first and second solvation shells of  $\text{Li}^+$  are summarized in Table 1, comparing the results to those obtained by the conventional QM/MM MD simulation [26]. In addition, to provide useful discussion with respect to the “structure-making” ability of  $\text{Li}^+$ , the available MRT data for liquid water and ammonia obtained by the compatible ONIOM-XS and conventional QM/MM MD simulations were also given for comparison. With regard to both the conventional QM/MM [26] and ONIOM-XS MD simulations,  $\text{Li}^+$  clearly acts as a “structure-maker”, i.e., the MRT values for ligands in the first solvation shell of  $\text{Li}^+$  are higher than the corresponding values observed in the pure solvent environments. However, it should be demonstrated that the ability of  $\text{Li}^+$  in ordering the structure of its surrounding ligands is much less than other stronger “structure-makers”, like  $\text{Mg}^{2+}$  or  $\text{Ca}^{2+}$  [5,19]. For example, according to the recent QM/MM MD studies of  $\text{Li}^+$ ,  $\text{Na}^+$ ,  $\text{K}^+$  and  $\text{Ca}^{2+}$  in aqueous solution [10,48], the MRT values for first-shell waters were reported to be of 11, 2.4, 2.1 and 40 ps, respectively. In our previous ONIOM-XS MD studies [19], the MRT values for water molecules in the first hydration shell of  $\text{K}^+$  and  $\text{Ca}^{2+}$  were reported to be of 1.80 and 21.7 ps, respectively. With regard to the QM/MM and ONIOM-XS MD results, since such simulations have been performed only for 30–40 ps (not many exchange processes can be observed) and only for one ion (assuming a very dilute solution), these data could be considered as rough estimates for relative comparison, i.e., they cannot be directly compared to the experimental observations. Note, for example, that the experimental estimation for MRT of first-shell water ligands at  $\text{Ca}^{2+}$  is  $\sim 10^{-7}$ – $10^{-9}$  s [49,50], while the QM/MM and ONIOM-XS MD simulations deliver  $0.04 \times 10^{-9}$  and  $0.02 \times 10^{-9}$  s, respectively. On the basis of the ONIOM-XS MD simulation,  $\text{Li}^+$  is able

**Table 1**

Mean residence times (MRTs) of solvated ligands and of pure solvents, as obtained by the ONIOM-XS and conventional QM/MM MD simulations.

System	$t_{\text{sim}}$	ligand	CN	$t^* = 0 \text{ ps}$		$t^* = 0.5 \text{ ps}$	
				$N_{\text{ex}}^{0.0}$	$\tau^{0.0}$	$N_{\text{ex}}^{0.5}$	$\tau^{0.5}$
<i>Conv. QM/MM MD</i>							
$\text{Li}^+$ in $\text{H}_2\text{O} + \text{NH}_3$ [26]	20.0	$\text{H}_2\text{O}$ (1st shell)	4.0	58	1.38	19	4.21
		$\text{H}_2\text{O}$ (2nd shell)	4.2	382	0.22	41	2.05
Liq. $\text{H}_2\text{O}$ [51]				–	0.19	–	1.78
Liq. $\text{NH}_3$ [10]				–	0.33	–	1.62
<i>ONIOM-XS MD</i>							
$\text{Li}^+$ in $\text{H}_2\text{O} + \text{NH}_3$	40.0	$\text{H}_2\text{O}$ (1st shell)	3.1	151	0.82	33	3.76
		$\text{H}_2\text{O}$ (2nd shell)	10.7	2109	0.20	273	1.57
		$\text{NH}_3$ (1st shell)	0.9	11	3.27	5	7.20
		$\text{NH}_3$ (2nd shell)	2.9	585	0.20	59	1.97
Liq. $\text{H}_2\text{O}$ [21]				–	0.23	–	2.17

to order both water and ammonia molecules in its surrounding to form its specific complexes, and the MRT values for first-shell ligands reveal a clear order of  $\tau_{\text{NH}_3} > \tau_{\text{H}_2\text{O}}$ , i.e., by about 4 and 2 times for  $t^* = 0.0$  and 0.5 ps, respectively. This can be ascribed to the higher binding energy of  $\text{Li}^+$  to ammonia ligands than to waters, i.e., when  $\text{Li}^+$  is located near the global minimum of the corresponding interaction energy surface. According to the data in Table 1, it is apparent that the MRT data for water and ammonia ligands in the second solvation shell of  $\text{Li}^+$  are not much different to those for pure solvents, indicating a small influence of  $\text{Li}^+$  in ordering its surrounding ligands beyond the first solvation shell. Overall, as compared to the conventional QM/MM MD study [26], the observed differences in both the preferential solvation and the dynamical details of the solvated  $\text{Li}^+$  clearly confirm the elegant treatment of the ONIOM-XS MD technique in providing more detailed knowledge of such a complicated system.

Regarding the ONIOM-XS MD study, it should be noted that the HF method and the double zeta valence basis set employed in the simulation were chosen as a compromise between the quality of the simulation results and the requirement of the CPU time. In general, it is known that the instantaneous electron correlation and the charge transfer effects are not typically well-described by the HF theory, and that the use of double zeta valence basis set could result in high basis set superposition error and an exaggeration of ligand-to-metal charge transfer. In this respect, the ONIOM-XS MD results should be discussed with caution (i.e., they should not be over-interpreted). When computational facilities become more feasible, further improvement of the ONIOM-XS MD results can be achieved by using higher *ab initio* correlated methods, such as MP2, together with the use of larger QM size and basis set.

#### 4. Conclusion

In this work, a more accurate ONIOM-XS MD simulation has been performed to investigate the preferential solvation and dynamics of  $\text{Li}^+$  in an aqueous ammonia solution. As compared to the conventional QM/MM MD study, which predicted that the first and second solvation shells of  $\text{Li}^+$  consist exclusively of water molecules with the arrangement of the  $\text{Li}^+[(\text{H}_2\text{O})_4][(\text{H}_2\text{O})_4]$  type, the ONIOM-XS MD simulation clearly indicates that this ion can order both water and ammonia molecules to form a favorable  $\text{Li}^+[(\text{H}_2\text{O})_3\text{NH}_3][(\text{H}_2\text{O})_{11}(\text{NH}_3)_3]$  configuration. Of particular interest, it is observed that the “structure-making” ability of  $\text{Li}^+$  is not too strong and that the first solvation shell of  $\text{Li}^+$  is somewhat flexible in which different 4-fold coordinated species, such as  $\text{Li}^+(\text{H}_2\text{O})_4$ ,  $\text{Li}^+(\text{H}_2\text{O})_3\text{NH}_3$  and  $\text{Li}^+(\text{H}_2\text{O})_2(\text{NH}_3)_2$ , could be converted back and forth. In addition, it is observed that the second solvation shell of  $\text{Li}^+$  is less structured, indicating a small influence of  $\text{Li}^+$  in ordering the ligand molecules in this shell. The observed discrepancy between the conventional QM/MM and ONIOM-XS MD results clearly confirms that more sophisticated simulation techniques, like the ONIOM-XS MD, are highly recommended for the study of such a condensed-phase system.

#### Conflict of interest

There is no conflict of interest for this work.

#### Acknowledgment

This work was supported by the Thailand Research Fund (TRF), under the Royal Golden Jubilee Ph.D. Program (Contract number PHD/0156/2551), and Suranaree University of Technology (SUT). A.T. also acknowledges support by the National Nanotechnology Center (NANOTEC), National Science and Technology Development Agency (NSTDA), Ministry of Science and Technology, Thailand, through its program of Center of Excellence Network. T.K.

acknowledges financial support from Mahidol University. High-performance computer facilities provided by the National e-Science Infrastructure Consortium are gratefully acknowledged.

#### References

- [1] U.C. Singh, P.A. Kollman, *J. Comput. Chem.* 7 (1986) 718.
- [2] M.J. Field, P.A. Bash, M. Karplus, *J. Comput. Chem.* 11 (1990) 700.
- [3] J. Gao, *Rev. Comput. Chem.* 7 (1996) 119.
- [4] J.L. Gao, D.G. Truhlar, *Annu. Rev. Phys. Chem.* 53 (2002) 467.
- [5] T. Kerdcharoen, K.R. Liedl, B.M. Rode, *Chem. Phys.* 211 (1996) 313.
- [6] A. Tongraar, K.R. Liedl, B.M. Rode, *J. Phys. Chem. A* 101 (1997) 6299.
- [7] A. Tongraar, K.R. Liedl, B.M. Rode, *J. Phys. Chem. A* 102 (1998) 10340.
- [8] A. Tongraar, B.M. Rode, *J. Phys. Chem. A* 103 (1999) 8524.
- [9] A. Tongraar, K. Sagarik, B.M. Rode, *J. Phys. Chem. B* 105 (2001) 10559.
- [10] B.M. Rode, C.F. Schwenk, A. Tongraar, *J. Mol. Liq.* 110 (2004) 105.
- [11] B.M. Rode, C.F. Schwenk, T.S. Hofer, B.R. Randolf, *Coord. Chem. Rev.* 249 (2005) 2993.
- [12] D. Xenides, B.R. Randolf, B.M. Rode, *J. Chem. Phys.* 122 (2005) 174506.
- [13] A. Tongraar, T. Kerdcharoen, S. Hannongbua, *J. Phys. Chem. A* 110 (2006) 4924.
- [14] A. Payaka, A. Tongraar, B.M. Rode, *J. Phys. Chem. A* 113 (2009) 885.
- [15] A. Tongraar, J.T. Theinprasert, S. Rujirawat, S. Limpjumnong, *Phys. Chem. Chem. Phys.* 12 (2010) 10876.
- [16] B.R. Brooks, R.E. Brucoleri, B.D. Olafson, D.J. States, S. Swaminathan, M. Karplus, *J. Comput. Chem.* 4 (1983) 187.
- [17] T. Kerdcharoen, K. Morokuma, *Chem. Phys. Lett.* 355 (2002) 257.
- [18] T. Kerdcharoen, K. Morokuma, *J. Chem. Phys.* 118 (2003) 8856.
- [19] S. Wanprakhon, A. Tongraar, T. Kerdcharoen, *Chem. Phys. Lett.* 517 (2011) 171.
- [20] P. Sripa, A. Tongraar, T. Kerdcharoen, *J. Phys. Chem. A* 117 (2013) 1826.
- [21] S. Thaumola, A. Tongraar, T. Kerdcharoen, *J. Mol. Liq.* 174 (2012) 26.
- [22] P. Wernet, D. Nordlund, U. Bergmann, M. Cavalleri, M. Odellius, H. Ogasawara, L.Å. Näslund, T.K. Hirsch, I. Ojamae, P. Glatzel, L.G.M. Pettersson, A. Nilsson, *Science* 304 (2004) 995.
- [23] T. Tokushima, Y. Harada, O. Takahashi, Y. Senba, H. Ohashi, L.G.M. Pettersson, A. Nilsson, S. Shin, *Chem. Phys. Lett.* 460 (2008) 387.
- [24] V. Gutmann, *The Donor-Acceptor Approach to Molecular Interactions*, Plenum Press, New York, 1978.
- [25] S. Kheawsrikul, S. Hannongbua, S. Kokpol, B.M. Rode, *J. Chem. Soc., Faraday Trans.* 85 (1989) 643.
- [26] A. Tongraar, B.M. Rode, *Chem. Phys. Lett.* 466 (2008) 61.
- [27] S. Pratihar, A. Chandra, *J. Chem. Phys.* 134 (2011) 024519.
- [28] S. Yoo, X.C. Zeng, S.S. Xantheas, *J. Chem. Phys.* 130 (2009) 221102.
- [29] J. VandeVondele, F. Mohamed, M. Krack, J. Hutter, M. Sprik, M. Parrinello, *J. Chem. Phys.* 122 (2005) 014515.
- [30] M. Svensson, S. Humbel, R.D.J. Froese, T. Mutsaers, S. Sieber, K. Morokuma, *J. Phys. Chem.* 100 (1996) 19357.
- [31] A. Heyden, H. Lin, D.G. Truhlar, *J. Phys. Chem. B* 111 (2007) 2231.
- [32] I.H. Dunning Jr., P.J. Hay, *Modern Theoretical Chemistry*, vol. III, Plenum, New York, 1976.
- [33] M.J. Frisch, G.W. Trucks, H.B. Schlegel, G.E. Scuseria, M.A. Robb, J.R. Cheeseman, J.A. Montgomery, T. Vreven, K.N. Kudin, J.C. Burant, J.M. Millam, S.S. Iyengar, J. Tomasi, V. Barone, B. Mennucci, M. Cossi, G. Scalmani, N. Rega, G.A. Petersson, H. Nakatsuji, M. Hada, M. Ehara, K. Toyota, R. Fukuda, J. Hasegawa, M. Ishida, T. Nakajima, Y. Honda, O. Kitao, H. Nakai, M. Klene, X. Li, J.E. Knox, H.P. Hratchian, J.B. Cross, V. Bakken, C. Adamo, J. Jaramillo, R. Gomperts, R.E. Stratmann, O. Yazyev, A.J. Austin, R. Cammi, C. Pomelli, J.W. Ochterski, P.Y. Ayala, K. Morokuma, G.A. Voth, P. Salvador, J.J. Dannenberg, V.G. Zakrzewski, S. Dapprich, A.D. Daniels, M.C. Strain, O. Farkas, D.K. Malick, A.D. Rabuck, K. Raghavachari, J.B. Foresman, J.V. Ortiz, Q. Cui, A.G. Baboul, S. Clifford, J. Cioslowski, B.B. Stefanov, G. Liu, A. Liashenko, P. Piskorz, I. Komaromi, R.L. Martin, D.J. Fox, T. Keith, M.A. Al-Laham, C.Y. Peng, A. Nanayakkara, M. Challacombe, P.M.W. Gill, B. Johnson, W. Chen, M.W. Wong, C. Gonzalez, J.A. Pople, *GAUSSIAN 03*, Revision D.1, Gaussian Inc., Wallingford, CT, 2005.
- [34] P. Bopp, G. Jancsó, K. Heinzinger, *Chem. Phys. Lett.* 98 (1983) 129.
- [35] F.H. Stillinger, A. Rahman, *J. Chem. Phys.* 68 (1978) 666.
- [36] S. Hannongbua, T. Ishida, E. Spohr, K. Heinzinger, *Z. Naturforsch.* 43a (1988) 572.
- [37] Y. Tanabe, B.M. Rode, *J. Chem. Soc., Faraday Trans.* 84 (1988) 679.
- [38] A. Tongraar, K.R. Liedl, B.M. Rode, *Chem. Phys. Lett.* 286 (1998) 56.
- [39] D.J. Adams, E.H. Adams, G.J. Hills, *Mol. Phys.* 38 (1979) 387.
- [40] H.J.C. Berendsen, J.P.M. Postma, W.F. van Gunsteren, A. DiNola, J.R. Haak, *J. Phys. Chem.* 81 (1984) 3684.
- [41] S. H. Lee, M.E. Tuckerman, *J. Chem. Phys.* 126 (2007) 164501.
- [42] D. Marx, A. Chandra, M.E. Tuckerman, *Chem. Rev.* 110 (2010) 2174.
- [43] R. Vuilleumier, D. Borgis, *J. Chem. Phys.* 111 (1999) 4251.
- [44] A. Tongraar, S. Hannongbua, B.M. Rode, *Chem. Phys.* 219 (1997) 279.
- [45] R.G. Pearson, *Structure and Bonding*, vol. 80, Springer-Verlag, Berlin, Heidelberg, 1993, p. 1.
- [46] L. Komorowski, *Structure and Bonding*, vol. 80, Springer-Verlag, Berlin, Heidelberg, 1993, p. 45.
- [47] T.S. Hofer, H.T. Tran, C.F. Schwenk, B.M. Rode, *J. Comput. Chem.* 25 (2004) 211.
- [48] T.S. Hofer, A.B. Pribil, B.R. Randolf, *Pure Appl. Chem.* 80 (2008) 1195.
- [49] L. Helm, A.E. Merbach, *Coord. Chem. Rev.* 187 (1999) 151.
- [50] S.F. Lincoln, A.E. Merbach, *Advances in Inorganic Chemistry*, vol. 42, Academic Press Inc., 1995, pp. 1.
- [51] A. Tongraar, B.M. Rode, *Chem. Phys. Lett.* 385 (2004) 378.

# CURRICULUM VITAE

## MISS PILAILUK KABBALEE

### Education Background:

- 2009            B.Sc. Second Class Honor (Chemistry), Ubon Ratchathani University,  
Ubonratchathani, Thailand
- 2009-2014      Ph.D. Candidate (Chemistry), Suranaree University of Technology,  
Nakhon Ratchasima, Thailand

### Experiences:

- 2010-2014      Teaching Assistant, School of Chemistry, Institute of Science,  
Suranaree University of Technology, Nakhon Ratchasima, Thailand
- 2014            Research exchange, The Gao group, University of Minnesota, USA

### Grant and Fellowships:

- 2010-2014      SUT Teaching Assistantship
- 2009-2014      The Royal Golden Jubilee (RGJ) Ph.D. Scholarship, Thailand  
Research Found (TRF)